MAX-PLANCK-INSTITUT
FÜR METEOROLOGIE

Dynamic Interaction between Climate, Lakes and Vegetation over North Africa

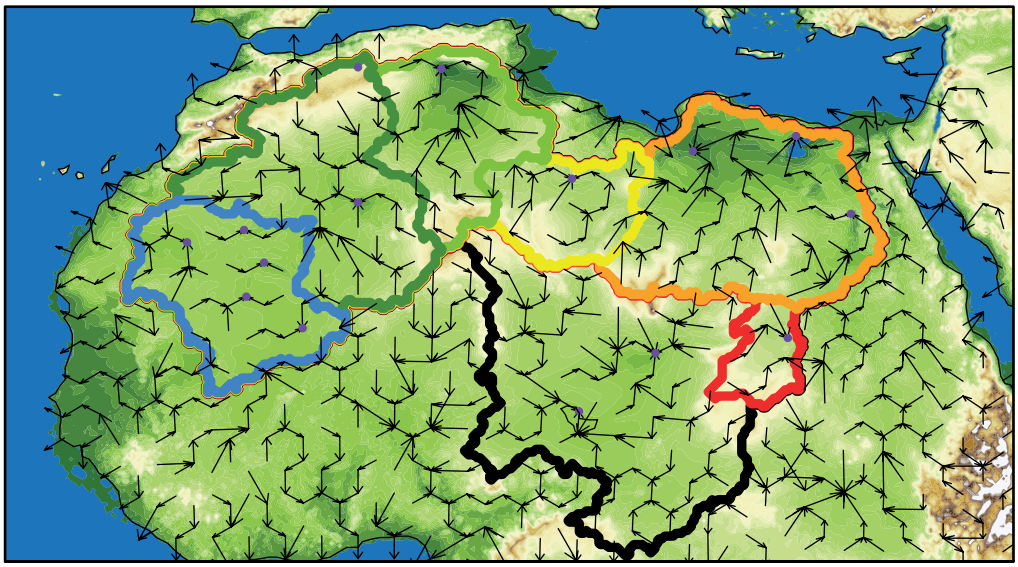

Nora Farina Specht

Hamburg 2023

Berichte zur Erdsystemforschung
Reports on Earth System Science

270
2023

Hinweis

Die Berichte zur Erdsystemforschung werden vom Max-Planck-Institut für Meteorologie in Hamburg in unregelmäßiger Abfolge herausgegeben.

Sie enthalten wissenschaftliche und technische Beiträge, inklusive Dissertationen.

Die Beiträge geben nicht notwendigerweise die Auffassung des Instituts wieder.

Die "Berichte zur Erdsystemforschung" führen die vorherigen Reihen "Reports" und "Examensarbeiten" weiter.

Anschrift / Address

Max-Planck-Institut für Meteorologie
Bundesstrasse 53
20146 Hamburg
Deutschland

Tel./Phone: +49 (0)40 4 11 73 - 0
Fax: +49 (0)40 4 11 73 - 298

name.surname@mpimet.mpg.de
www.mpimet.mpg.de

Notice

The Reports on Earth System Science are published by the Max Planck Institute for Meteorology in Hamburg. They appear in irregular intervals.

They contain scientific and technical contributions, including PhD theses.

The Reports do not necessarily reflect the opinion of the Institute.

The "Reports on Earth System Science" continue the former "Reports" and "Examensarbeiten" of the Max Planck Institute.

Layout

Bettina Diallo and Norbert P. Noreiks
Communication

Copyright

Dynamic Interaction between Climate, Lakes and Vegetation over North Africa

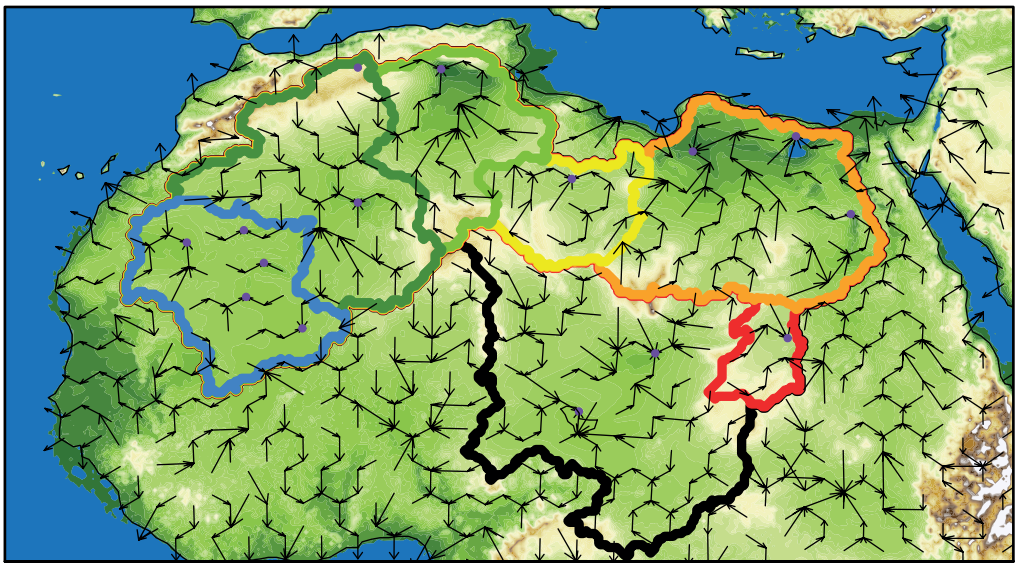

Nora Farina Specht

Hamburg 2023

Nora Farina Specht
aus Henstedt-Ulzburg, Deutschland

Max-Planck-Institut für Meteorologie
The International Max Planck Research School on Earth System Modelling
(IMPRS-ESM)
Bundesstrasse 53
20146 Hamburg

Tag der Disputation: 22. Juni 2023

Folgende Gutachter empfehlen die Annahme der Dissertation:
Prof. Dr. Martin Claußen
Dr. Thomas Kleinen

Vorsitzender des Promotionsausschusses:
Prof. Dr. Hermann Held

Dekan der MIN-Fakultät:
Prof. Dr.-Ing. Norbert Ritter

Titelgrafik: Nora Specht: *Outlines and drainage directions of the Sahelian and Saharan endorheic lake catchments*

Berichte zur Erdsystemforschung / Max-Planck-Institut für Meteorologie 270
Reports on Earth System Science / Max Planck Institute for Meteorology 2023

ISSN 1614-1199 - doi: 10.17617/2.3523251

Nora Farina Specht

Dynamic Interaction between Climate, Lakes and Vegetation over North Africa

dedicated to
my grandmother Lore Schwarz
(⋆ 1931 - † 2019)

This document was typeset using `classicthesis` developed by André Miede and Ivo Pletikosić available at https://bitbucket.org/amiede/classicthesis/.

ABSTRACT

During the early to mid-Holocene, about 11.500 to 5.500 years ago, increased summer monsoon precipitation caused an area-wide expansion of vegetation and lakes over the Sahel and Sahara. Model simulations show that this precipitation increase was triggered by changes in the orbital forcing and amplified by vegetation feedback. Little is known, though, about the effect of mid-Holocene lakes interacting with the West African summer monsoon and vegetation over the Sahel and Sahara. Previous simulation studies all prescribe mid-Holocene lakes and wetlands from reconstructions, which are subject to large uncertainties.

Therefore, I investigate the simulated range of precipitation changes that emerge from uncertainties in lake reconstructions and compare the effect of lakes to vegetated wetlands. Results show that prescribing a reconstructed maximum lake extent in the simulations shifts the monsoon rain belt about 2 to 7 ° farther north than prescribing a reconstructed small lake extent. This difference in the rain belt northward shift is mainly caused by lakes in the western Sahara that cause a stronger and prolonged monsoon rainfall season over northern Africa. Results show that the prescribed lakes increase the moisture transport from the Atlantic to the African inland south of the lakes. Therefore, the latitudinal position of the lakes influences the northward extent of the monsoon rain belt. A similar, but enhanced, response occurs when replacing the lakes with vegetated wetlands. Thus, lakes and wetlands cause a substantial precipitation increase. But is the prescribed lake and wetland extent consistent with the terrestrial water balance?

By prescribing the lakes, the terrestrial water cycle over northern Africa is not closed. Therefore, I construct a dynamic lake model that simulates the lake extent and the lake depth depending on the local moisture budget of the corresponding catchment. For the first time, this allows me to conduct mid-Holocene simulations, including dynamic lakes together with a dynamic vegetation. A pre-industrial control simulation shows that the lake model realistically simulates the lake extent over northern Africa. Comparison between the mid-Holocene experiments showed surprising effects. First, a pure deepening of Lake Chad causes an area-wide precipitation increase over the Sahel and western Sahara. This effect of lake depth changes was neglected in previous simulations studies. Second, the mid-Holocene vegetation expansion causes a higher precipitation increase over the Sahel and western Sahara than the mid-Holocene lakes and vegetation expansion together. The major reason for this is that the vegetation cools the land surface stronger than the simulated mid-Holocene

lakes. This reversal of the lake-land temperature gradient causes an area-wide drying response across the Sahel and western Sahara.

ZUSAMMENFASSUNG

Während des frühen bis mittleren Holozäns, vor etwa 11.500 bis 5.500 Jahren, führten vermehrte Sommermonsunniederschläge zu einer flächendeckende Ausdehnung von Vegetation und Seen in der Sahelzone und der Sahara. Modellsimulationen zeigen, dass diese Niederschlagszunahme durch Änderungen im Orbitalantrieb ausgelöst und durch eine Vegetationsrückkopplung verstärkt wurde. Jedoch ist nur wenig über den Einfluss der Seen im mittleren Holozän bekannt und wie diese mit dem westafrikanischen Sommermonsun und der Vegetation über der Sahelzone und der Sahara interagieren. Bisherige Simulationsstudien schreiben allesamt mittelholozänen Seen und Feuchtgebieten aus Rekonstruktionen vor, die mit großen Unsicherheiten behaftet sind.

Daher untersuche ich die simulierte Bandbreite der Niederschlagsänderungen, die sich aus den Unsicherheiten in den Rekonstruktionen der Seen ergeben und vergleiche die Auswirkungen von Seen mit denen von bewachsenen Feuchtgebieten. Die Ergebnisse zeigen, dass das Vorschreiben einer rekonstruierten maximalen Seeausdehnung den simulierten Monsunregengürtel etwa 2 bis 7 ° weiter nach Norden verschiebt als das Vorschreiben einer rekonstruierten kleinen Seeausdehnung. Dieser Unterschied in der Nordverschiebung des Regengürtels wird hauptsächlich durch Seen in der westlichen Sahara verursacht, die eine stärkere und längere Monsunregenzeit über Nordafrika bewirken. Die Ergebnisse zeigen, dass die vorgeschriebenen Seen den Feuchtetransport vom Atlantik ins afrikanische Binnenland südlich der Seen erhöhen. Daher beeinflusst die Breitengradposition der Seen die Ausdehnung des Monsunregengürtels nach Norden. Eine ähnliche, aber verstärkte Reaktion tritt auf, wenn die Seen durch bewachsene Feuchtgebiete ersetzt werden. Seen und Feuchtgebiete bewirken also eine erhebliche Niederschlagszunahme. Aber stimmt die vorgeschriebene Ausdehnung der Seen und Feuchtgebiete mit der terrestrischen Wasserbilanz überein?

Durch das Vorschreiben der Seen ist der terrestrische Wasserkreislauf über Nordafrika nicht geschlossen. Deshalb konstruiere ich ein dynamisches Seenmodell, das die Seeausdehnung und die Seentiefe in Abhängigkeit vom lokalen Wasserhaushalt des entsprechenden Einzugsgebietes berechnen. Damit ist es mir erstmals möglich, Simulationen für das mittlere Holozän durchzuführen, die dynamische Seen zusammen mit einer dynamischen Vegetation berücksichtigen. Eine vorindustrielle Kontrollsimulation zeigt, dass das Seenmodell eine realistische Seeausdehnung über Nordafrika simuliert. Der Vergleich zwischen den mittelholozänen Experimenten zeigte überraschende Effekte. Erstens führt eine reine Vertiefung des Tschadsees zu einer

flächendeckenden Niederschlagszunahme über der Sahelzone und der westlichen Sahara. Dieser Effekt der Seetiefenänderung wurde in früheren Simulationsstudien vernachlässigt. Zweitens verursacht die mittelholozäne Vegetationsausdehnung eine höhere Niederschlagszunahme über der Sahelzone und der westlichen Sahara als die mittelholozäne Seen- und Vegetationsausdehnung zusammen. Der Hauptgrund dafür ist, dass die Vegetation die Landoberfläche stärker abkühlt als die simulierten mittelholozänen Seen. Diese Umkehrung des Temperaturgradienten zwischen See und Land führt zu einer flächendeckenden Austrocknung in der Sahelzone und der westlichen Sahara.

ACKNOWLEDGMENTS

Many people have supported me on my way to completing the PhD. Thanks to these people, I have gained many valuable experiences and precious memories during my time as a PhD student. I would especially like to thank my supervisors Martin Claussen and Thomas Kleinen, who have always supported and encouraged me during various phases of my dissertation. Thank you for your valuable feedback and advice, which helped me in stressful situations and showed me creative ways to solve problems that occurred during my PhD studies.

I would also like to thank Reiner Schnur, Tobias Stacke, Veronika Gayler, and Tom Riddick for their excellent technical support on implementing the lake model and wetland surface type into the ICON-JSBACH4 model. Especially in the difficult times of the Corona lockdowns, Reiner helped me with his fast and problem-oriented solutions. Without this comprehensive support, I would have had a much harder time implementing the dynamic lake model. In addition, Tom helped me to create the flow directions for the HD model and Veronika and Tobias supported me in understanding the codes of the HD model.

My thanks also go to Jürgen Bader, Christian Reick and Thomas Raddatz, who always supported me with their expertise and valuable feedback when I had a question or a problem to solve. Especially during the final phase of my PhD thesis, the conversations with you were very helpful. I would like to thank Jürgen Bader, in particular, for the exciting discussions during the Thursday lunch breaks at Hanmi. These conversations helped me a lot to regain some normality after several Corona lockdowns.

A big thank you also goes to Sylvia Houston, Antje Weitz, Cornelia Kampmann and the whole IMPRS office for their help with administrative questions and for their constant support in coping with the bureaucratic tasks for my PhD thesis. Thanks to you, the planning of my PhD thesis became much easier, especially in the final phase.

Throughout my PhD studies, my family, my boyfriend and my friends have always supported me, particularly during the most difficult phases of my studies. Therefore, I want to say thank you to Sylvia Specht, Roger Schwarz, Nana Appelt, Akihiko Ito, Carla Rook, Zoé Rehder, Meike Schickhoff, and Pinhsin Hu for their great support. Thank you for always encouraging me in difficult times and calming me down in stressful moments. In particular, I would like to thank Zoé, Meike, Pinhsin and Akihiko for their emotional support during the final phase of my PhD study.

Finally, I would also like to thank all employees on the 17^{th} floor for the nice coffee breaks, conversations during the lunch breaks and

the sociable T-Days. I want to thank Matéo Duque and Constanze Reinken for organizing the social T-Day.

PUBLICATIONS RELATED TO THIS DISSERTATION
Teilveröffentlichungen dieser Dissertation

APPENDIX A:

Specht N.F., Claussen C., and Kleinen T. (2022). "Simulated range of mid-Holocene precipitation changes from extended lakes and wetlands over North Africa." In: *Clim. Past* 18. DOI: 10.5194/cp-18-1035-2022

APPENDIX B:

Specht N.F., Claussen C., and Kleinen T. (2023). "Dynamic interaction of Saharan lakes, climate and vegetation during the mid-Holocene." Manuscript in preparation.

CONTENTS

UNIFYING ESSAY

1 INTRODUCTION

Green Sahara

A Period [...] with a high number of lakes and wetlands and occurrence of tropical humid plants in a region that is nowadays arid.

— Watrin et al. (2009)[1]

green Saharan reconstructions

Paleo-environmental reconstructions show that the Sahara has undergone alternating phases of desertification and greening over the past 11 millennia (Crocker et al., 2022). While the Sahara is a desert today, the latest "green Sahara" existed about 11.500 to 5.500 years ago, during the early to mid-Holocene (e.g. Claussen et al., 2017). During that period, the North Africa[2] was widely covered with Savannah vegetation (e. g. Hély & Lézine, 2014). Additionally, some tropical gallery forests grew in the vicinity of the numerous rivers, lakes, and wetlands that formed in response to the enhanced summer monsoon precipitation over North Africa (Hély & Lézine, 2014; Holmes & Hoelzmann, 2017; Lézine et al., 2011b).

The West African summer monsoon produces most of the annual precipitation over the Sahel and Sahara. During the mid-Holocene, this rain-bringing circulation system extended further north than today. Paleo-climate reconstructions indicate that, due to this northward extent, the mean annual precipitation in the Central Sahara was about 200-600 mm year^{-1} higher during the mid-Holocene than today (Bartlein et al., 2011). These paleo-reconstructions provide an approximate picture of the North African climate during the mid-Holocene. But they give little inside into the mechanisms that contributed to this northward shift.

reconstructions vs. simulations

Model simulations show that changes in the orbital forcing triggered a northward shift of the West African summer monsoon (Kutzbach & Guetter, 1986). This initial northward shift was amplified by feedback from the ocean (Kutzbach & Liu, 1997), vegetation (Claussen & Gayler, 1997) and soil dynamics (Vamborg et al., 2011). But even when these feedback processes are included, present climate models fail to reproduce a large enough northward migration of the West African summer monsoon and systematically underestimate the precipitation over North Africa by about 20% to 50% (Braconnot et al., 2012).

knowledge gap

This gap between simulated and reconstructed precipitation over northern Africa indicates that crucial processes are neglected or misrepresented by present climate models. One of these missing processes

1 https://doi.org/10.1016/j.crte.2009.06.007, last accessed: 12.09.2022

2 the region that includes the Sahel (12 °N-18 °N) and Sahara (18 °N-38 °N)

might be the effect of lakes and wetlands interacting with the atmosphere and the vegetation over the Sahel and Sahara.

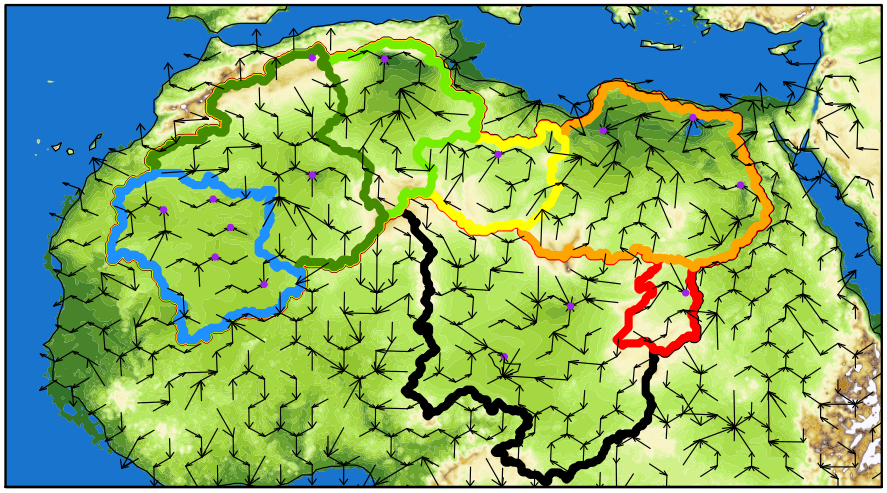

Figure 1.1: River flow directions (arrows) used as boundary conditions to simulate the down-slope water transport within each endorheic catchment (colored outlines) to the internal drainage points (purple dots). The colored background shows the topography of northern Africa.

1.1 MID-HOLOCENE LAKE RECONSTRUCTIONS

endorheic and exorheic lakes

The Sahel and Sahara mainly consists of endorheic catchments. This includes the Ahnet Catchment (Fig. 1.1: dark green), Chad Catchment (Fig. 1.1: black), Chotts Catchment (Fig. 1.1: light green), Dafur Catchment (Fig. 1.1: red), Fezzan Catchment (Fig. 1.1: yellow), Qattara Catchment (Fig. 1.1: orange) and Taoudeni Catchment (Fig. 1.1: blue). Endorheic catchments are watersheds that have no outlet to other external waters such as rivers or oceans. This means that the drainage water accumulates in an internal basin or in the underlying aquifer (Fig. 1.1: purple dots). An internal basin is that part of a catchment that can be inundated by a lake and that lies below the outlet height of the catchment. During the early to mid-Holocene, increased discharge water from precipitation accumulated in the aquifers below the internal basins (e. g. Lézine et al., 2011b). As the aquifers successively filled with water, the aquifer water level exceeded the elevation of the internal basins. As a result, lakes formed and expanded across North Africa during the mid-Holocene (Lézine et al., 2011b).

Reconstructions show that lakes also formed in some exorheic catchments. For example, Lake Timbuktu in the Niger River Inland Delta of Mali in the western Sahel (Drake et al., 2022). In contrast to endorheic lakes, exorheic lakes have an outlet to external waters and formed in

response to enhanced flooding from the increased summer monsoon precipitation.

paleo-lake features and reconstructions

During previous African Humid Periods, endorheic and exorheic lakes, both, caused the formation of shorelines and lake sediments in the Sahara and Sahel. But in the Sahara the strong eolian erosion removed large parts of the lake shorelines and the lake sediments of some former lake basins are largely covered by eolian depositions (e. g. Drake et al., 2022; Swezey, 2003). Accordingly, remote sensing data only provide information on lakes in the Sahel that have better preserved shorelines. Additionally, Saharan sediment records are spatially sparse (e. g. Drake et al., 2022) and most of these records are temporally discontinuous, which make it difficult to reliably date the sediment cores (Lézine et al., 2011a). Along with this issue, Drake et al. (2022) point out that some lake reconstructions are based on unreliable dating methods, like the reconstructions of Lake Ahnet and Lake Chotts. Thus, most Saharan lake records have a poor chronology and lake reconstructions only provide a fragmentary picture of the Saharan landscape. So, what do we know about mid-Holocene lakes over North Africa?

Mega-lakes

Several reconstruction studies investigated the existence of so-called mega-lakes (eg Drake et al., 2022; Quade et al., 2018). A mega-lake is defined as a lake with a surface area of >10.000 km^2 (Quade et al., 2018) or even >25.000 km^2 (Drake et al., 2022). Reconstructions show that Mega-lake Chad (Drake et al., 2022; Quade et al., 2018; Schneider, 1969) and Mega-lake Timbuktu (Drake et al., 2022; Petit-Maire & Riser, 1987) likely existed during the mid-Holocene. Mega-lake Chad had a surface area of about 330.000-361.000 km^2 (Drake & Bristow, 2006; Quade et al., 2018; Schneider, 1969) and Mega-lake Timbuktu had a surface area of about 24.000-27.000 km^2 (Drake et al., 2022; Petit-Maire & Riser, 1987).

smaller lakes

Beside these mega-lakes in the Sahel, several smaller but substantial lakes existed farther north in the Sahara. This includes lakes in the Dafur Catchment, Fezzan Catchment, and Taoudeni Catchment (e. g. Drake et al., 2022; Hoelzmann et al., 1998). Sediment reconstructions show that during the mid-Holocene Lake Dafur reached a size of about 5330 km^2 (Pachur & Hoelzmann, 1991) and Lake Fezzan covered an area of about 210 km^2 (Drake et al., 2018). In the Taoudeni Basin, lakes with an area of about 500 km^2 existed (Hoelzmann et al., 1998; Petit-Maire, 1991; Petit-Maire & Riser, 1983).

Sediment records also suggest that Lake Ahnet and Lake Chotts extended during previous African Humid Periods, but reliably dated mid-Holocene reconstructions are missing (Drake et al., 2022). Therefore, a large uncertainty range exists for the extent of these Saharan lakes. For example, Lake Chotts currently covers an area of about 620 km^2 (Swezey et al., 1999), while sediment reconstruction show that Lake Chotts covered an estimated area of about 30.000 km^2 dur-

ing African Humid Periods prior to the mid-Holocene (Drake et al., 2022). In comparison to the mid-Holocene, these prior African Humid Periods are associated with stronger orbital forcing and a stronger precipitation increase over North Africa. Therefore, the mid-Holocene extent of Lake Chotts likely lies somewhere between 620 km^2 and 30.000 km^2. Such large uncertainties in the lake reconstructions make it difficult to accurately map the mid-Holocene paleo-lakes across North African.

comprehensive lake landscape?

Hoelzmann et al. (1998) used a collection of lake reconstructions to derive a mid-Holocene lake map. This map includes Mega-lake Chad and some smaller lakes in the western Sahel and Sahara (Fig. 1.2a). Comparison between this sediment-based reconstruction map and a model-derived maximum lake map (Tegen et al. (2002); Fig. 1.2b) shows large differences in the lake extent over the western Sahara: in the Taoudeni Catchment, Ahnet Catchment and Chotts Catchment (Fig. 1.1c). The model-derived maximum lake area represent regions with highly productive dust sources. Egerer et al. (2018) showed that large part of these maximum lakes areas in the western Sahara must have been covered with lakes (or vegetation) during the mid-Holocene to explain a coherent decline in the simulated and observed mid-Holocene dust deposition at the west coast of North Africa. This reduced dust emission at the North African west coast during the mid-Holocene suggests the possible existence of larger lakes in western Sahara.

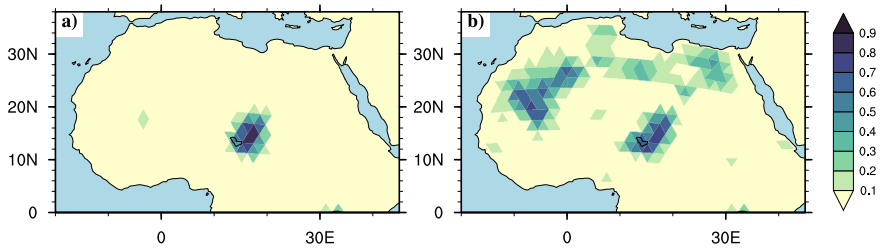

Figure 1.2: Mid-Holocene (a) small lake extent derived from sediment records (Hoelzmann et al., 1998) and (b) maximum lake extent derived with a hydrological routing algorithm (Tegen et al., 2002).

1.2 MID-HOLOCENE WETLAND RECONSTRUCTIONS

What is a wetland?

A uniform and consistent definition of the term wetland and its differentiation from lakes is currently missing in the literature (Hu et al., 2017). In general, wetlands represent transitional areas between terrestrial and aquatic systems (e. g. Lehner & Döll, 2004). But this definition is interpreted differently by individual reconstructions (Enzel et al., 2017). Hoelzmann et al. (1998), who derived a lake and wetland map from various sediment record, summarizes that, in contrast to lake deposits, wetlands deposits are characterized by high inputs of

fluvial material as in flooding regions of rivers, or by a high organic content as in shallow water (<2 m depth) with swamp or aquatic vegetation. For clarity, I provide my own definition of lakes and wetlands in this thesis. Following the definition by Hoelzmann et al. (1998), I distinguish between wetlands as vegetated moisture-saturated soils and lakes as inland waters without vegetation.

sediment-based and model-based reconstructions differ

Sediment-based and model-based wetland reconstructions substantially differ from each other in the western Sahara. The sediment-based reconstruction map by Hoelzmann et al. (1998) indicates that mid-Holocene wetlands primarily existed in the Sahel: in the vicinity of Mega-lake Timbuktu in the Niger River Inland Delta of Mali and in the vicinity of Mega-lake Chad. These reconstructed wetlands cover about 4.6% of North Africa (10 °N - 30 °N).

In contrast, the model-based reconstruction by Chen et al. (2021) suggests that wetlands covered about 18.9±4.0% of North Africa (0 °N - 35 °N). That is about 14.3% larger than the sediment-based wetland extent by Hoelzmann et al. (1998). This large difference between the sediment-based and model-based wetland reconstruction is mainly due to additional wetlands over the western Sahel and Sahara in the model-derived reconstruction. This includes wetlands in the Taoudeni and Ahnet Basin. Hoelzmann et al. (1998) point out that their sediment-based wetland map potentially underestimates the wetland extent in the western Sahel and Sahara because in this region information only exists on the major wetland basins, that is the Niger River Inland Delta and the lower course of the Senegal river.

1.3 PRESCRIBED SAHARAN LAKES AND WETLANDS

prescribing differing lake maps

To investigate the effect of lakes during the mid-Holocene, previous simulation studies prescribed different lake reconstructions from sediment records. While some studies use the reconstruction map by Hoelzmann et al. (1998) that only considers Mega-lake Chad and several smaller lakes in the southwestern Sahel (Broström et al., 1998; Krinner et al., 2012), other simulation studies primarily focused on the existence of potential Mega-lakes (Chandan & Peltier, 2020). None of these studies, though, considered a larger lake extent in the western Sahara as suggested by model-based lake maps (Broström et al., 1998; Chandan & Peltier, 2020; Coe & Bonan, 1997; Krinner et al., 2012).

little investigations of wetlands

Even less is known about the effect of vegetated wetlands. At present, the study by Carrington et al. (2001) is the only one that explicitly investigates the influence of vegetated wetlands on the mid-Holocene climate. In their study, they use the reconstruction map by (Hoelzmann et al., 1998) that suggests the existence of wetlands around Lake Chad and in the Niger River Inland Delta of Mali. But also in this study larger potential wetlands in the western Sahara, as

suggested by a model-based wetland reconstruction of Chen et al. (2021), is missing.

Thus, differences between these sediment-based reconstruction (Hoelzmann et al., 1998) and model-based reconstructions (Chen et al., 2021; Tegen et al., 2002) suggest large uncertainties in the lake and wetland reconstructions. Since the climate effect of these uncertainties in the mid-Holocene lake and wetland extent is unknown, I propose the following first research question:

1st research question

WHAT IS THE RANGE OF MID-HOLOCENE PRECIPITATION CHANGES FROM A SMALL AND POTENTIAL MAXIMUM LAKE AND WETLAND EXTENT OVER NORTH AFRICA?

This research question contributes to the debate on whether lakes and wetlands substantially influenced the mid-Holocene climate over northern Africa, and the corresponding results provide a first estimate on the range of precipitation changes caused by uncertainties in mid-Holocene lake and wetland reconstructions.

1.4 PRECIPITATION RESPONSE TO SAHARAN LAKES AND WETLANDS

precipitation response to prescribed mid-Holocene lakes

Previous simulations studies consistently show that mid-Holocene lakes and wetlands increased the precipitation over northern Africa (Broström et al., 1998; Carrington et al., 2001; Chandan & Peltier, 2020; Coe & Bonan, 1997; Krinner et al., 2012). But their results differ on whether the prescribed lakes and wetlands cause a localized precipitation increase only, (Broström et al., 1998; Carrington et al., 2001; Chandan & Peltier, 2020; Coe & Bonan, 1997) or whether they cause a wide-spread precipitation increase across northern Africa (Krinner et al., 2012). This difference in the precipitation response likely relates to whether the mid-Holocene vegetation is prescribed or a dynamic vegetation model is used. While those simulation studies that prescribe the mid-Holocene vegetation only show marginal precipitation changes across northern Africa in response to the extended Saharan lakes (Broström et al., 1998), the same lake extent causes a northward shift of the West African summer monsoon by about 1.5 ° when a dynamic vegetation is considered (Krinner et al., 2012).

a positive vegetation and lake feedback?

Thus, comparison between various simulations studies suggest that mid-Holocene lakes induce a positive vegetation feedback. But a robust evidence of a study that explicitly examine the vegetation feedback to a mid-Holocene lake extent is missing. Along with this, little is known about the dynamic interaction between Saharan lakes, vegetation and the West African summer monsoon during the mid-Holocene because previous simulation studies all prescribed static lakes from mid-Holocene reconstructions (Broström et al., 1998; Chandan & Peltier,

2020; Coe & Bonan, 1997; Krinner et al., 2012). By prescribing these lakes, the terrestrial water balance is not closed, and it remains unclear whether the prescribed lakes would be maintained under the simulated mid-Holocene climate. Additionally, no information is provided about the interactive effects between dynamic lakes, vegetation and the West African summer monsoon and to what extent this interaction contribute to closing the gap between simulated and reconstructed mid-Holocene precipitation increase over northern Africa. Therefore, I propose the following second research question:

2nd research question

HOW DOES THE DYNAMIC INTERACTION BETWEEN THE WEST AFRICAN SUMMER MONSOON, LAKES AND VEGETATION INFLUENCE THE MID-HOLOCENE PRECIPITATION OVER NORTHERN AFRICA?

complexity of interaction

Reconstructions indicate a complex interplay between the mid-Holocene precipitation increase of the West African summer monsoon and the extent of lakes and wetlands over northern Africa (Lézine et al., 2011b). Yet, the main mechanisms by which the climate, lakes, and vegetation interact over northern Africa during the mid-Holocene are only becoming apparent through simulations. This study is the first attempt to understand this complex interaction between mid-Holocene lakes, vegetation and the West African summer monsoon over northern Africa from a model point of view.

2 UNCERTAINTIES IN RECONSTRUCTIONS

reconstruction uncertainties

The first contribution of this thesis refers to the range of precipitation changes that emerge from uncertainties in mid-Holocene lake reconstructions (Specht et al., 2022; appendix A). Mid-Holocene lake and reconstruction from northern Africa are subject to large uncertainties (Drake et al., 2018). Therefore, the previous simulation studies used different sediment reconstructions to investigate the effect of mid-Holocene lakes on the West African summer monsoon precipitation over northern Africa (Broström et al., 1998; Carrington et al., 2001; Chandan & Peltier, 2020; Coe & Bonan, 1997; Krinner et al., 2012). Yet, it is unclear to what extent the uncertainties in sediment reconstructions affect the simulated precipitation response over northern Africa.

sensitivity experiments

Therefore, I investigate the range of precipitation changes that emerge from uncertainties in mid-Holocene lake reconstructions (Specht et al., 2022; appendix A). In a mid-Holocene simulation, I prescribe the present-day lakes, a small lake extent (Fig. 1.2b) derived from sediment reconstructions (Hoelzmann et al., 1998) and a maximum lake extent (Fig. 1.2c) derived from a model-based reconstruction (Tegen et al., 2002). The maximum lake extent map includes a large potential lake area in the western Sahara that is absent in the previous model studies (Tegen et al., 2002). In addition, I replace the maximum lakes with vegetated wetlands, which allows me to compare the climate effect of both land surface types.

In the simulations, lakes are represented by a mixed layer of 10 m depth. Wetlands are defined as moisture-saturated soils with an equal vegetation cover of C_3 and C_4 grasses, similar to Carrington et al. (2001). The fractional wetland type has been implemented into the atmosphere-land model ICON-JSBACH4 for the purpose of this study.

2.1 NORTHWARD SHIFT OF THE MONSOON RAIN BELT

small lake extent

My results confirm the findings of previous studies, which show that the mid-Holocene lake expansion generally enhanced the monsoon precipitation over northern Africa (Fig. 2.1). A prescribed small lake extent shifts the simulated rain belt about 1 ° northwards (Fig. 2.1a: black and green), which is relatively large compared to the rain belt displacement simulated by most simulation studies that assume a similar (Broström et al., 1998) or even larger lake extent (Chandan & Peltier, 2020). Only the study by Krinner et al. (2012) shows a

northward shift of 1.5 ° in response to the same lake extent. Unlike other studies, Krinner et al. (2012) uses a dynamic vegetation model, which presumably reinforces the precipitation response to the prescribed lakes. Since the vegetation is prescribed in my simulations, the precipitation response to the extended lakes is likely caused by other feedbacks, such as changes in the background albedo by litter production along with an evaporative feedback.

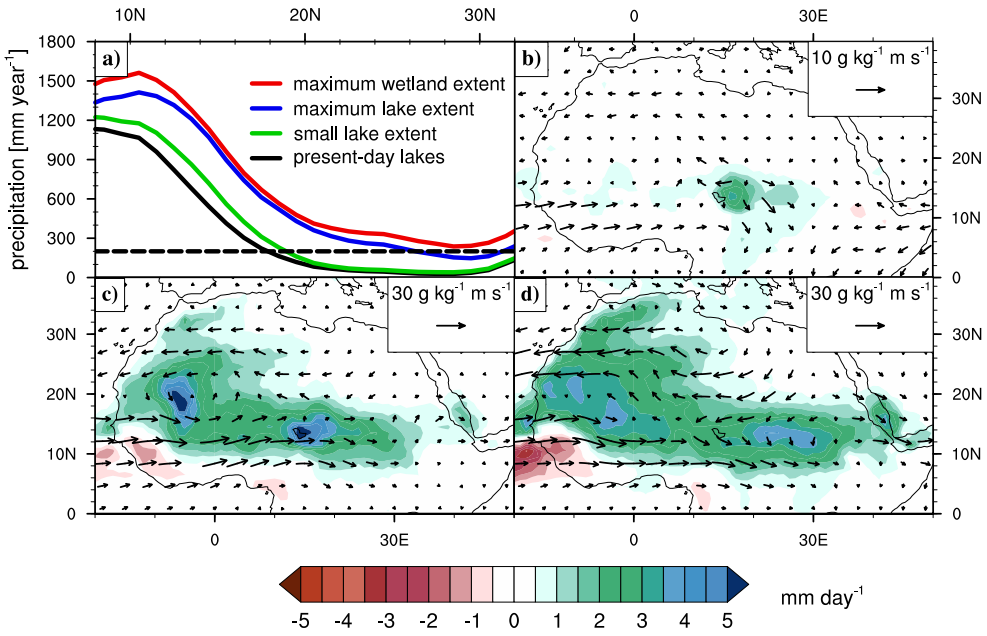

Figure 2.1: (a) Mid-Holocene 30-year mean annual precipitation zonally averaged over northern Africa (10 °E–30 °W). The black dashed line marks the 200 mm year^{-1} threshold, indicating the border between savanna and desert landscape. (b-c) Mid-Holocene 30-year mean JJAS precipitation response (colored shades) and moisture flux response at 850 hPa (arrows) to the (b) small lake extent, (c) maximum lake extent and (d) maximum wetland extent in comparison to the present-day lake simulation.

maximum lake extent

In the mid-Holocene simulations, the prescribed maximum lake extent shifts the margins of the simulated monsoon rain belt about 2 to 7 ° farther north than the prescribed small lake extent (Fig. 2.1a: green and blue). Since the size of Lake Chad is nearly the same in both mid-Holocene simulations (Fig. 1.2), the difference in the northward shift is primarily caused by lakes over the western Sahara (Fig. 2.1 b-c). These west Saharan lakes increase the monsoon precipitation over northern Africa by causing a stronger and prolonged rainfall season (Specht et al., 2022).

vegetated wetlands

When replacing the maximum lakes with vegetated wetlands, the precipitation over northern Africa is further enhanced, particularly over the northern Sahara (Fig. 2.1a: blue and red). This enhanced precipitation response is likely caused by a high surface roughness, which

is associated with an enhanced evaporation and enhanced surface cooling over the wetlands. Due to this strong surface cooling and, thus, local subsidence, wetlands cause a high precipitation increase in their warm vicinity (Fig. 2.1 d). In contrast, lakes which cool less show a local precipitation peak above their water surface (Fig. 2.1 c).

2.2 CIRCULATION RESPONSE TO LAKES AND WETLANDS

circulation response

The west Saharan lakes and wetlands increase the monsoon precipitation over northern Africa by causing a stronger and prolonged rainfall season (Specht et al., 2022). The monsoon precipitation is increased not only by enhancing the local evaporation, but also by increasing the moisture flux from the tropical Atlantic to the African inland south of the lakes and wetlands (Fig. 2.1 b-d: arrows). This increased inland moisture transport is associated with an overturning circulation response caused by the lakes and (Specht et al., 2022). Evaporative cooling causes descending motions above the lakes and wetlands and ascending motions in the warmer vicinity. This overturning lake-land circulation causes a low pressure response in the mid-troposphere, which, by Coriolis force, causes a westerly wind response to the south and an easterly wind response to the north of the lakes and wetlands (Fig. 2.1 b-d: indicated by arrows).

African Easterly Jet is shifted northward

This dipole-like zonal wind response to the lakes and wetlands, induces either a northward shift of the African Easterly Jet or a weakening of the African Easterly Jet, depending on the latitudinal position of the lakes and wetlands (Specht et al., 2022). E. g. the west Saharan lakes are located in the region of the Saharan heat low, which controls the African Easterly Jet. Since the overturning circulation associated with the Saharan heat low is revered to the circulation response caused by the lakes over northern Africa, the Saharan lakes primarily lead to a strong weakening of the African Easterly Jet. Since the position of the African Easterly Jet represents the northern border of the monsoon rain belt, a shift or weakening of the African Easterly Jet directly affect the northward extent of the monsoon rain belt.

2.3 THE POSITION OF THE LAKES AND WETLANDS MATTERS

My results suggest that the location of the prescribed lakes and wetlands likely plays a major role in the northward extent of the African summer monsoon (Specht et al., 2022). In contrast to my results, Chandan and Peltier (2020) found that prescribing several defined Saharan lakes in a mid-Holocene simulation causes a similar precipitation increase as when prescribing a homogeneous lake extent across the Sahara in a mid-Holocene simulation. This difference to my results likely relates to the fact that larger lakes in western Sahara are absent in the simulations of Chandan and Peltier (2020) and that the east

Saharan lakes prescribed by Chandan and Peltier (2020) generally cause a small precipitation increase.

Savannah extends northward?

Finally, my study shows that the border between Savannah and Sahara, marked by the 200 mm $year^{-1}$ isohyet, is shifted about 7 ° farther northward in the maximum-lake-extent simulation than in the small-lake-extent simulation (Fig. 2.1 a). This indicates that lakes might cause a positive vegetation feedback during the mid-Holocene, as suggested by Krinner et al. (2012).

3 EFFECT OF LAKES-VEGETATION INTERACTIONS

prescribing lakes vs simulating lakes

The second contribution of this thesis refers to the dynamic interaction between climate, lakes and vegetation over the Sahel and Sahara during the mid-Holocene (appendix B). Resent simulation studies show that mid-Holocene lakes substantially increase the precipitation over northern Africa (Krinner et al., 2012; Specht et al., 2022). But previous studies all prescribe the mid-Holocene lakes from reconstructions (Drake et al., 2018; Specht et al., 2022). By prescribing the mid-Holocene lakes the terrestrial water cycle is not closed, and the prescribed extent of the lakes is inconsistent with the terrestrial water balance.

Therefore, I construct a dynamic lake model that simulates the lake extent and lake depth depending on the local water budget of the corresponding catchment. For the first time, this allows me to simulate mid-Holocene lakes in interaction with the West African summer monsoon and the vegetation over the Sahel and Sahara. Additionally, I investigate the effect of lake depth changes on the mid-Holocene climate, which was neglected in previous simulation studies that only focus on the lake extent.

3.1 DYNAMIC ENDORHEIC LAKE MODEL

dynamic lake concept and implementation

The Sahara and Sahel mainly consists of endorheic catchment that have no outlet to other external waters such as rivers or oceans (Section 1.1: Fig. 1.1). Therefore, I construct an endorheic lake model, which I implement into the hydrological discharge model of the land model JSBACH4. The hydrological discharge model simulates the down-slope river flow of discharge water (D) from surface runoff and subsurface drainage. Within the endorheic catchments the discharge water is transported to internal drainage points (Section 1.1: Fig. 1.1) from where it enters the lake reservoir (V_{lake}):

$$\Delta V_{lake} = (D - O + f_{lake}(P - E_{lake}) + Fin_{lake} - Fout_{lake}) \cdot \Delta t \quad (3.1)$$

The water volume of the lake reservoir determines the lake extent and lake depth within each grid cell. The lake interacts with the atmosphere via its surface (f_{lake}) through precipitation (P) and evaporation (E_{lake}). As a lake grows larger, water flows from the current grid cell ($Fout_{lake}$) into the neighboring grid cell with the next highest elevation (Fin_{lake}). Thus, the lateral flow depends on the basin orography. This orography-dependent flow allows to simu-

late overflow processes, such as the overflow of Lake Chad into the adjacent Bodélé Depression.

equilibrium experiments

To evaluate the DEL model, I conduct a pre-industrial equilibrium simulation (pidVdL) with dynamic lakes and with a dynamic vegetation (Fig. 3.1 a). The lake extent in the pre-industrial equilibrium simulation is compared to an observation-based lake map (Fig. 3.1 b-c). The vegetation extent, lakes extent and lake depth from the pre-industrial simulation is used as static boundary conditions for a mid-Holocene reference simulation (mH). To investigate the influence of lake depth changes, I conduct a simulation similar to the mid-Holocene reference simulation, but with a prescribed constant 10-m lake depth (mH10L), as assumed in my previous study (Specht et al., 2022; appendix A). Additionally, I conduct a set of mid-Holocene simulation to investigate the individual and synergistic effects of dynamic lakes and a dynamic vegetation: (mHdV) with dynamic vegetation only, (mHdL) with dynamic lakes only, and (mHdVdL) with dynamic lake and dynamic vegetation. All simulations are run until a quasi-equilibrium state is reached and the last 100 to 150 years of the with a quasi-equilibrium state are used as evaluation period.

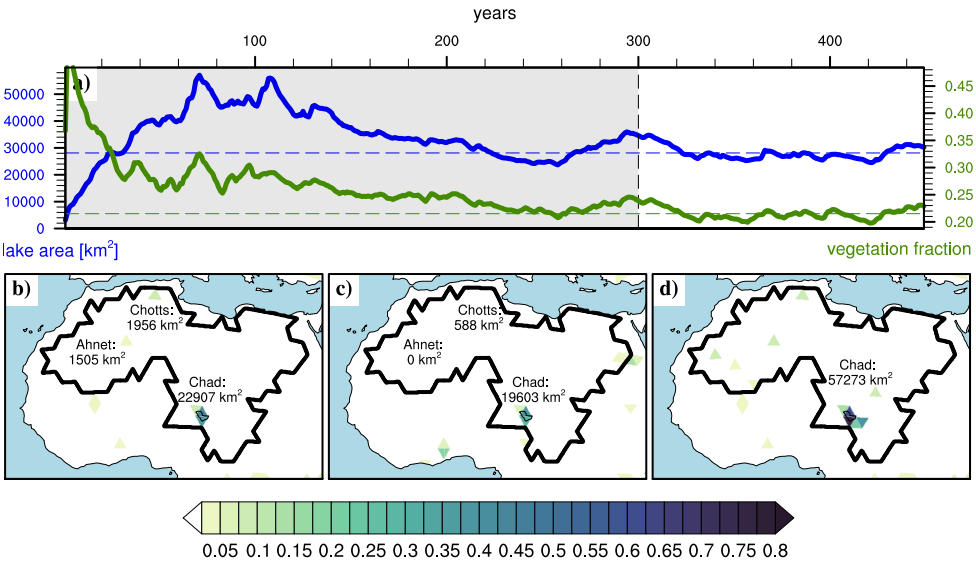

Figure 3.1: Time series of the simulated pre-industrial (a: blue line) lake area within the Saharan endorheic catchments and (a: green line) vegetation cover averaged over northern Africa (20 °W-35 °E,10 °N-35 °N). The lower panel shows the (b) pre-industrial 150-year mean lake extent of the piVdLd simulation, (c) the lake extent of the observation-based HydroLAKES data (Messager et al., 2016), and (d) the mid-Holocene 150-year mean lake extent of the mHdVdL simulation.

3.2 SIMULATED PRE-INDUSTRIAL AND MID-HOLOCENE LAKES

pre-industrial lakes

My results show that the DEL model realistically simulates the pre-industrial extent of Lake Chad and the presence of some dry basins over northern Africa (Fig. A.4 b-c). Only the extent of Lake Ahnet and Lake Chotts is overestimated by about 1.957 km^2 and 2.165 km^2. Both lakes receive most of their discharge water from the Atlas Mountains, mainly from orographic-forced precipitation (Specht et al., 2022). The overestimated water discharge from the Atlas Mountains likely relates to the coarse resolution of the simulation. The coarse resolution limits the accurate representation of the small-scale heterogeneous precipitation from orographic updrafts, as well as the accurate representation of the catchment boundaries.

too small and shallow mid-Holocene lakes

In the mid-Holocene simulation, the lake extent over northern Africa is generally underestimated. For example, Lake Chad only extends to a size of about 57.273 km^2, while reconstructions suggest an area of about 350.000 km^2 (Drake et al., 2022; Quade et al., 2018). Comparison between the pre-industrial and mid-Holocene simulation shows that Lake Chad extends mainly on its southern side, while the overflow into the Bodélé Depression causes only a small and isolated lake extent in the north (Fig. 3.1b, 3.1d). Sediment reconstructions indicate a much more profound northward extension of Lake Chad (Drake et al., 2022; Hoelzmann et al., 1998; Quade et al., 2018).

The underestimated mid-Holocene lake extent mainly relates to a known dry bias over northern Africa simulated by the ICON-ESM (Schneck et al., 2022), which becomes particularly obvious in the mid-Holocene simulation. This dry bias not only affect the lake extent, but also the depth of mid-Holocene lakes. As I show in the following section, such an underestimated lake depth might substantially influence the mid-Holocene precipitation over northern Africa.

3.3 EFFECT OF LAKE DEPTH CHANGES

precipitation response to lake deepening

An idealized mid-Holocene simulation shows that a pure deepening of the Lake Chad by about 1-5 m causes an area-wide precipitation increase across the Sahel and western Sahara (Fig. 3.2a-b). This sensitivity of the monsoon precipitation to changes in the lake depth was neglected by previous simulation studies, which only considered changes in the lake extent (Broström et al., 1998; Chandan & Peltier, 2020; Coe & Bonan, 1997; Krinner et al., 2012). Comparison between these simulation studies in terms of the lake depth is difficult because some of the studies do not provide an explicit description of how the lakes and their depth are represented in the model (Chandan & Peltier, 2020; Krinner et al., 2012).

circulation response to lake deepening

In this study, a deepening of Lake Chad increases the heat capacity and the surface cooling of the lake (Fig. 3.2e). The surface cooling of

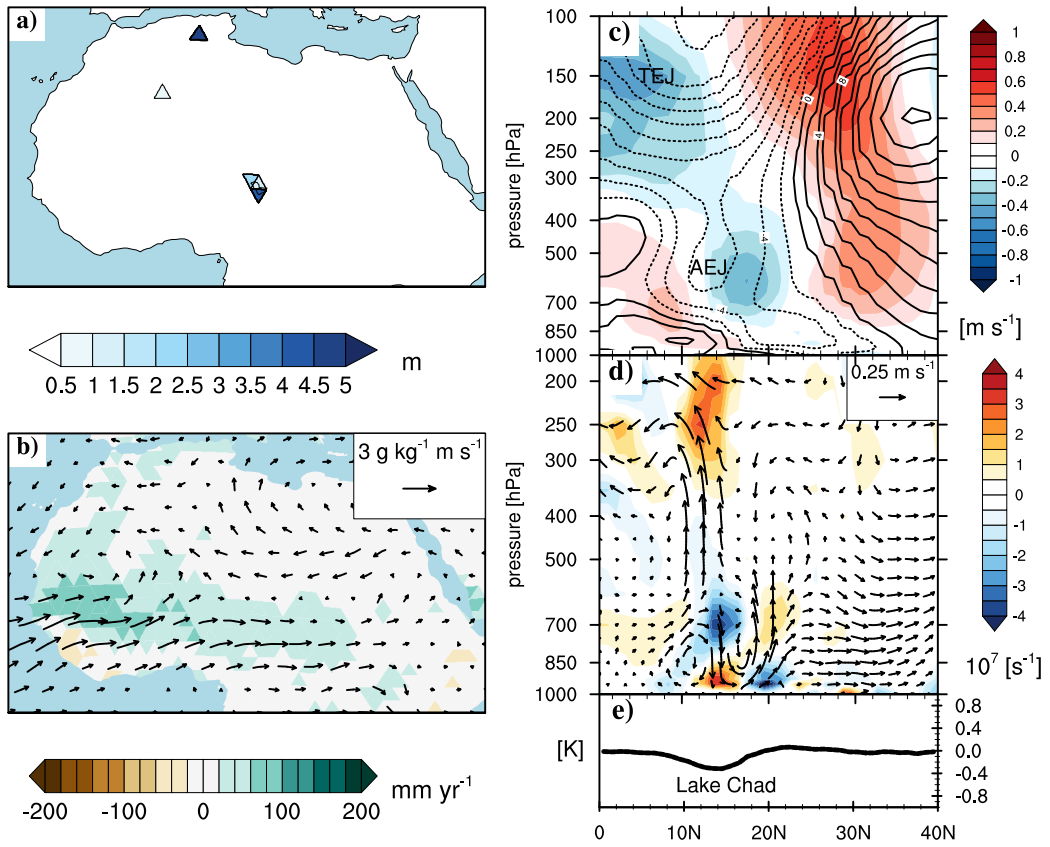

Figure 3.2: The left panel shows the differences in (a) the prescribed lake depth and (b) the simulated mid-Holocene precipitation (colored shades) and summer (JJAS) moisture flux response (arrows) to the lake depth increase (mH10L-mH). The right panel shows the zonally averaged (10 °N-20) summer (JJAS) response to a deepening of Lake Chad for (e) the surface temperature, (d) the vertical and meridional wind (arrows), the divergence (colored shades) and (c) the zonal wind (colored shades). The black contours in plot c) show the zonal wind climatology of the mid-Holocene reference simulation. The vertical wind component in plot d) was re-scaled (multiplied by 500) for visibility reasons.

Lake Chad induces an overturning lake-land circulation response in the lower to mid-troposphere (1000-600 hPa), with descending motions over the lake and ascending motions in its warmer vicinity (Fig. 3.2d: arrows). The descending motions over the lake cause a convergence response and, thus, low pressure response in the mid-troposphere (Fig. 3.2d: blue shade at 600 hPa). The low pressure response induces, by Coriolis force, a westerly wind acceleration to the south and an easterly wind acceleration to the north of Lake Chad (Fig. 3.2c: colored shades). This dipole-like response is associated with a northward shift

of the African Easterly Jet, which represents the northern boundary of the monsoon rain belt. Thus, the overturning lake-land circulation response induces a northward shift of the monsoon rain belt.

Additionally, near-surface convergence of moist air at the southern side of Lake Chad causes convection, which is associated with the release of latent heat. This release of latent heat increases the moist convection throughout the whole troposphere south of Lake Chad (Fig. 3.2d, arrows). This enhanced uplift motions together with the northward shift of the monsoon system enhances the near-surface moisture flux from the tropical Atlantic to the African inland (Fig. 3.2b: arrows). The northward shift of the monsoon system and the increased moisture availability over northern Africa explain the area-wide precipitation increased across the Sahel and western Sahara caused by a deepening of lake Chad.

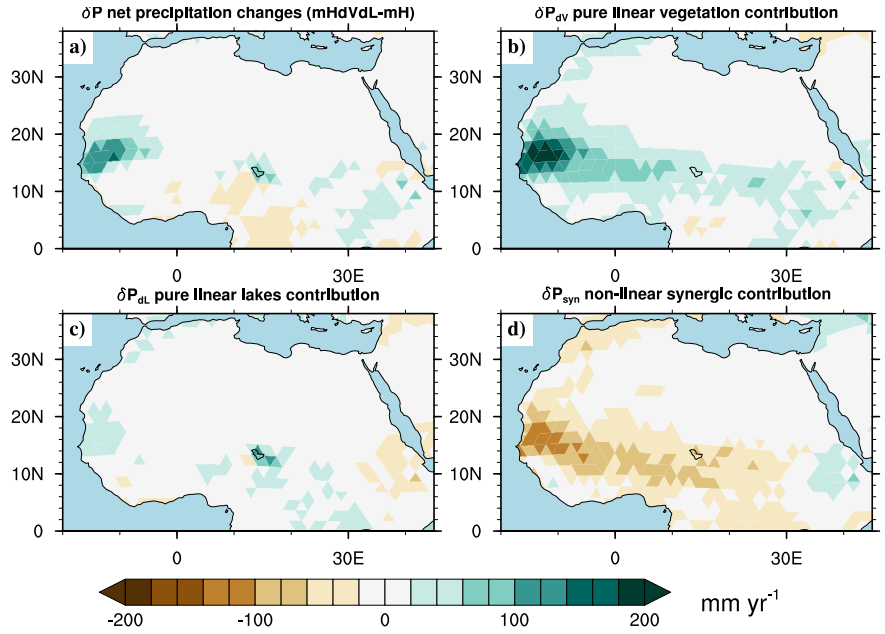

Figure 3.3: Simulated mid-Holocene (a) precipitation changes due to the influence of dynamic lakes and dynamic vegetation together (δP: mHdVdL-mH). Simulated mid-Holocene precipitation changes caused (b) by dynamic vegetation only (δP_{dV}: mHdV-mH), (c) by dynamic lakes only (δP_{dL}: mHdL-mH), and (d) by vegetation-lake synergies (δP_{syn}: mHdVdL+mH-mHdV-mHdL). The factor analysis of the mid-Holocene precipitation changes is given by: $\delta P = \delta P_{dV} + \delta P_{dL} + \delta P_{syn}$.

3.4 MID-HOLOCENE LAKE-VEGETATION INTERACTION

individual and synergistic effects

The dynamic interaction between lakes, vegetation and the West African summer monsoon contributes only little to the northward shift of the monsoon rain belt over northern Africa (Fig. 3.3 a). A

factor analysis shows that the dynamic vegetation alone (δP_{dV}) causes a broad precipitation increase over the Sahel and western Sahara (Fig. 3.3 b). The dynamic lakes alone (δP_{dL}) causes a precipitation increase mainly in the region of Lake Chad (Fig. 3.3 c). The sum of both, the pure vegetation contribution and the pure lake contribution (Fig. 3.3b-c: $\delta P_{dV} + \delta P_{dL}$) is higher than the net precipitation changes caused by dynamic lakes and a dynamic vegetation together (Fig. 3.3 a).

Accordingly, the synergistic effect of dynamic lakes and a dynamic vegetation causes an area-wide precipitation decrease over the Sahel and western Sahara (Fig. 3.3 d). The major reason for this precipitation decrease is that the mid-Holocene vegetation cools the land surface stronger than the simulated mid-Holocene Lake Chad (Specht et al., 2022). Instead of a cooling response, Lake Chad causes a warming response of the land surface in the presence of the mid-Holocene vegetation. Accordingly, the circulation and precipitation response associated with a surface cooling of Lake Chad (Fig. 3.2) is reversed (Specht et al., 2022). The resulting drying response from the lake-vegetation interaction is strong enough to almost compensate the precipitation increased caused by a vegetation expansion alone (Fig. 3.3b, 3.3d). This strong precipitation decrease explains why the net precipitation increase caused by the dynamic interaction between climate, lakes and vegetation is so weak.

vegetation response to mid-Holocene lakes?

In contrast to previous simulation studies (Krinner et al., 2012), my results suggest that the mid-Holocene lake extent does not cause a positive vegetation feedback. The simulated mid-Holocene lakes, though, generally show a too small northward extent and a too small deepening of the lakes over northern Africa, which might substantially influence the lake-land temperature contrast. A larger and deeper lake Chad, as suggested by reconstructions (Drake et al., 2022; Hoelzmann et al., 1998; Quade et al., 2018), might cool the land surface stronger than the mid-Holocene vegetation over northern Africa. But additional experiments are needed to investigate whether mid-Holocene lakes cool the land surface stronger than the mid-Holocene vegetation when reaching a certain lake depth.

4

SUMMARY AND CONCLUSIONS

4.1 MAIN FINDINGS

In this thesis, I investigate two aspects of mid-Holocene lakes over northern Africa. First, I examine the range of mid-Holocene precipitation changes from lakes and wetlands over northern Africa, considering uncertainties in mid-Holocene reconstructions. Second, I investigate the dynamic interaction between lakes, vegetation and the West African summer monsoon over northern Africa. In the following, I briefly summarize my main findings with regard to my proposed research questions.

1st research question

WHAT IS THE RANGE OF MID-HOLOCENE PRECIPITATION CHANGES FROM A SMALL AND POTENTIAL MAXIMUM LAKE AND WETLAND EXTENT OVER NORTH AFRICA?

- A small lake extent, mainly Mega-lake Chad, shifts the monsoon rain belt about 1 ° farther northward than the present-day lakes. A maximum lake extent shifts the rain belt about 2 to 7 ° farther north than the prescribed small lake extent. These large changes in the rain belt northwards shift are primarily caused by potential lake areas in the western Sahara.
- Vegetated wetlands cause an even larger precipitation increase than the same extent of lakes. This is likely due to the high surface roughness of the wetlands.
- The latitudinal positions of the lakes and wetlands influence the northward extent of West African summer monsoon. The African Easterly Jet, which is the northern boundary of the rain belt, is shifted northwards or is even strongly weakened depending on the position of the lakes and wetlands.

To answer the first research question, I prescribed static lakes and wetlands in a mid-Holocene simulation, similar to previous simulation studies (Broström et al., 1998; Carrington et al., 2001; Chandan & Peltier, 2020; Coe & Bonan, 1997; Krinner et al., 2012). By prescribing the lakes, the terrestrial water cycle is not closed, and the prescribed lake extent is inconsistent to the terrestrial water balance. To close the terrestrial water balance, I constructed and implemented a dynamic lake model into the atmosphere-land model ICON-JSBACH4. This allows me to investigate the following research question.

2nd research question

HOW DOES THE DYNAMIC INTERACTION BETWEEN THE WEST AFRICAN SUMMER MONSOON, LAKES AND VEGETATION INFLUENCE THE MID-HOLOCENE PRECIPITATION OVER NORTHERN AFRICA?

- An increase in the depth of Lake Chad causes an area-wide precipitation increase over the Sahel and western Sahara. The deepening of Lake Chad causes a surface cooling, which induces a lake-land circulation response that shifts the West African summer monsoon northwards and enhances the moisture transport from the tropical Atlantic to the dry African inland.
- The dynamic interaction between lakes, vegetation and the West African summer monsoon only contributes little to the mid-Holocene precipitation increase. While the mid-Holocene lake expansion and the mid-Holocene vegetation expansion individually cause an increase in precipitation over northern Africa, the simultaneous expansion of dynamic lakes and vegetation causes widespread drying over the Sahel and western Sahara.
- The major reason for the drying response is that the mid-Holocene vegetation cools the land surface stronger than the simulated mid-Holocene lakes. This causes a circulation and precipitation response inverted to the one associated with the deepening and surface cooling of Lake Chad.

My results provide first insights into the non-linear effects of lake-vegetation interaction on mid-Holocene climate. The temperature difference between mid-Holocene lakes and the surrounding environment plays an important role in this interaction. Yet, my study is also subject to limitations that I discuss in the following section.

4.2 OUTLOOK AND LIMITATIONS

limitations of the DEL model

In this thesis, I focus on endorheic lakes only and neglect the effect of exorheic lakes, like Mega-lake Timbuktu in the Niger River Inland Delta (Drake et al., 2022). Additionally, the DEL model only mimics the effect of an aquifer reservoir to avoid unrealistically high fluctuations in the extent and depth of lakes over northern Africa (Specht et al., 2022). Yet, reconstructions indicate a complex interplay between endorheic lakes and the underlying aquifers during the Holocene (Lézine et al., 2011a). For example, lake sediment records show a time-lag of roughly 3000 years between the orbital-forced summer insolation maximum over northern Africa and the maximum extent of Saharan lakes during the early to mid-Holocene (Lézine et al., 2011a). The delayed response in the lake extent is likely caused by the influence of the Saharan aquifers that filled with discharge water during the early

Holocene and recharge the overlying lakes towards the end of the African Humid Period. This lake-aquifer interaction is not explicitly simulated by the DEL model. Therefore, the DEL model potentially fails to realistically simulate the decline of lakes in the Sahara and Sahel towards the end of the African Humid Period. Beside these transitional phases, results indicate that the DEL model realistically simulates the lake extent and depth over northern Africa with respect to the terrestrial water balance.

interactive effects from wetlands?

In this PhD thesis, I also neglect the effect of dynamic wetlands over northern Africa, even though mid-Holocene reconstruction suggest the existence of wetlands in the vicinity of Lake Chad, Lake Timbuktu (Hoelzmann et al., 1998), and in the western Sahara (Chen et al., 2021). Vegetated wetlands potentially cool the land surface stronger than mid-Holocene lakes or the mid-Holocene vegetation because wetlands combine of the high surface roughness of the vegetation with the water saturated surface of the lakes. This resulting strong evaporation and surface cooling likely affects the interplay between West African summer monsoon and the land surface. However, constructing and implementing a suitable dynamic wetland model into JSBACH4, beside the DEL model, is beyond the scope of this thesis.

interactive effects in a wetter climate

Finally, the ICON-ESM simulates a too dry climate over northern Africa Schneck et al., 2022, particularly during the mid-Holocene. Therefore, the simulated mid-Holocene lake are too shallow, and their northward extent is too small. In a simulated wetter climate, the mid-Holocene lakes would become deeper and eventually cool the land surface stronger than the surrounding vegetated landscape, which could impose a positive vegetation-lake feedback. Such a wet climate could be simulated by tuning the atmospheric convection of the ICON-JSBACH4 model (Hopcroft & Valdes, 2021), or by using a state-of-the-art climate model that generally simulates a wetter mid-Holocene climate, like the MPI-ESM (Dallmeyer et al., 2021). Using different climate models to study the dynamic interaction between climate lakes and vegetation also provides more robust results.

BIBLIOGRAPHY

Bartlein, P. J., Harrison, S. P., Brewer, S., Connor, S., Davis, B. A. S., Gajewski, K., Guiot, J., Harrison-Prentice, T. I., Henderson, A., Peyron, O., Prentice, I. C., Scholze, M., Seppä, H., Shuman, B., Sugita, S., Thompson, R. S., Viau, A. E., Williams, J., & Wu, H. (2011). Pollen-based continental climate reconstructions at 6 and 21 ka: A global synthesis. *Climate Dynamics*, *37*(3-4), 775–802. https://doi.org/10.1007/s00382-010-0904-1

Braconnot, P., Harrison, S. P., Kageyama, M., Bartlein, P. J., Masson-Delmotte, V., Abe-Ouchi, A., Otto-Bliesner, B., & Zhao, Y. (2012). Evaluation of climate models using palaeoclimatic data. *Nature Climate Change*, *2*(6), 417–424. https://doi.org/10.1038/nclimate1456

Broström, A., Coe, M., Harrison, S. P., Gallimore, R., Kutzbach, J. E., Foley, J., Prentice, I. C., & Behling, P. (1998). Land surface feedbacks and palaeomonsoons in northern Africa. *Geophysical Research Letters*, *25*(19), 3615–3618. https://doi.org/10.1029/98GL02804

Carrington, D. P., Gallimore, R. G., & Kutzbach, J. E. (2001). Climate sensitivity to wetlands and wetland vegetation in mid-Holocene North Africa. *Climate Dynamics*, *17*(2-3), 151–157. https://doi.org/10.1007/s003820000099

Chandan, D., & Peltier, W. R. (2020). African Humid Period Precipitation Sustained by Robust Vegetation, Soil, and Lake Feedbacks. *Geophysical Research Letters*, *47*(21). https://doi.org/10.1029/2020GL088728

Chen, W., Ciais, P., Qiu, C., Ducharne, A., Zhu, D., Peng, S., Braconnot, P., & Huang, C. (2021). Wetlands of North Africa During the Mid-Holocene Were at Least Five Times the Area Today. *Geophysical Research Letters*, *48*(20), e2021GL094194. https://doi.org/10.1029/2021GL094194 e2021GL094194 2021GL094194

Claussen, M., Dallmeyer, A., & Bader, J. (2017). Theory and modeling of the African humid period and the green Sahara. *Oxford Research Encyclopedia of Climate Science*. https://doi.org/10.1093/acrefore/9780190228620.013.532

Claussen, M., & Gayler, V. (1997). The Greening of the Sahara during the Mid-Holocene: Results of an Interactive Atmosphere-Biome Model. *Global Ecology and Biogeography Letters*, *6*(5), 369–377. https://doi.org/10.2307/2997337

Coe, M. T., & Bonan, G. B. (1997). Feedbacks between climate and surface water in northern Africa during the middle Holocene. *Journal of Geophysical Research: Atmospheres*, *102*(D10), 11087–11101. https://doi.org/10.1029/97JD00343

Crocker, A. J., Naafs, B. D. A., Westerhold, T., James, R. H., Cooper, M. J., Röhl, U., Pancost, R. D., Xuan, C., Osborne, C. P., Beerling, D. J., & Wilson, P. A. (2022). Astronomically controlled aridity in the Sahara since at least 11 million years ago. *Nature Geoscience*, *15*(8), 671–676. https://doi.org/10.1038/s41561-022-00990-7

Dallmeyer, A., Claussen, M., Lorenz, S., Sigl, M., Toohey, M., & Herzschuh, U. (2021). Holocene vegetation transitions and their climatic drivers in MPI-ESM1.2. *Climate of the Past*, *17*, 2481–2513. https://doi.org/10.5194/cp-17-2481-2021

Drake, N., & Bristow, C. (2006). Shorelines in the Sahara: Geomorphological evidence for an enhanced monsoon from palaeolake Megachad. *The Holocene*, *16*(6), 901–911. https://doi.org/10.1191/0959683606hol981rr

Drake, N. A., Candy, I., Breeze, P., Armitage, S. J., Gasmi, N., Schwenninger, J. L., Peat, D., & Manning, K. (2022). Sedimentary and geomorphic evidence of Saharan megalakes: A synthesis. *Quaternary Science Reviews*, *276*, 107318. https://doi.org/10.1016/j.quascirev.2021.107318

Drake, N. A., Lem, R. E., Armitage, S. J., Breeze, P., Francke, J., El-Hawat, A. S., Salem, M. J., Hounslow, M. W., & White, K. (2018). Reconstructing palaeoclimate and hydrological fluctuations in the Fezzan Basin (southern Libya) since 130 ka: A catchment-based approach. *Quaternary Science Reviews*, *200*, 376–394. https://doi.org/10.1016/j.quascirev.2018.09.042

Egerer, S., Claussen, M., & Reick, C. (2018). Rapid increase in simulated North Atlantic dust deposition due to fast change of northwest African landscape during the Holocene. *Climate of the Past*, *14*(7), 1051–1066. https://doi.org/10.5194/cp-14-1051-2018

Enzel, Y., Quade, J., & Kushnir, Y. (2017). Response to Engel et al. (in press): Lakes or wetlands? A comment on "The middle Holocene climatic records from Arabia: Reassessing lacustrine environments, shift of ITCZ in Arabian Sea, and impacts of the southwest Indian and African monsoons" by Enzel et al. (2015). *Global and Planetary Change*, *148*, 268–271. https://doi.org/10.1016/j.gloplacha.2016.11.003

Hély, C., & Lézine, A.-M. (2014). Holocene changes in African vegetation: Tradeoff between climate and water availability. *Clim. Past*, *7*.

Hoelzmann, P., Jolly, D., Harrison, S. P., Laarif, F., Bonnefille, R., & Pachur, H.-J. (1998). Mid-Holocene land-surface conditions in northern Africa and the Arabian Peninsula: A data set for the analysis of biogeophysical feedbacks in the climate system. *Global Biogeochemical Cycles*, *12*(1), 35–51. https://doi.org/10.1029/97GB02733

Holmes, J., & Hoelzmann, P. (2017). The Late Pleistocene-Holocene African Humid Period as Evident in Lakes. *Oxford Research Encyclopedia of Climate Science*. https://doi.org/10.1093/acrefore/9780190228620.013.531

Hopcroft, P. O., & Valdes, P. J. (2021). Paleoclimate-conditioning reveals a North Africa land–atmosphere tipping point. *Proceedings of the National Academy of Sciences*, *118*(45), e2108783118. https://doi.org/10.1073/pnas.2108783118

Hu, S., Niu, Z., & Chen, Y. (2017). Global Wetland Datasets: A Review. *Wetlands*, *37*(5), 807–817. https://doi.org/10.1007/s13157-017-0927-z

Krinner, G., Lézine, A.-M., Braconnot, P., Sepulchre, P., Ramstein, G., Grenier, C., & Gouttevin, I. (2012). A reassessment of lake and wetland feedbacks on the North African Holocene climate. *Geophysical Research Letters*, *39*(7). https://doi.org/10.1029/2012GL050992

Kutzbach, J. E., & Liu, Z. (1997). Response of the African Monsoon to Orbital Forcing and Ocean Feedbacks in the Middle Holocene. *Science*, *278*(5337), 440–443. https://doi.org/10.1126/science.278.5337.440

Kutzbach, J. E., & Guetter, P. J. (1986). The Influence of Changing Orbital Parameters and Surface Boundary Conditions on Climate Simulations for the Past 18 000 Years. *Journal of the Atmospheric Sciences*, *43*(16), 1726–1759. https://doi.org/10.1175/1520-0469(1986)043<1726:TIOCOP>2.0.CO;2

Lehner, B., & Döll, P. (2004). Development and validation of a global database of lakes, reservoirs and wetlands. *Journal of Hydrology*, *296*(1-4), 1–22. https://doi.org/10.1016/j.jhydrol.2004.03.028

Lézine, A.-M., Zheng, W., Braconnot, P., & Krinner, G. (2011a). Late Holocene plant and climate evolution at Lake Yoa, northern Chad: Pollen data and climate simulations. *Climate of the Past*, *7*(4), 1351–1362. https://doi.org/10.5194/cp-7-1351-2011

Lézine, A.-M., Hély, C., Grenier, C., Braconnot, P., & Krinner, G. (2011b). Sahara and Sahel vulnerability to climate changes, lessons from Holocene hydrological data. *Quaternary Science Reviews*, *30*(21), 3001–3012. https://doi.org/10.1016/j.quascirev.2011.07.006

Messager, M., Lehner, B., Grill, G., Nedeva, I., & Schmitt, O. (2016). Estimating the volume and age of water stored in global lakes using a geo-statistical approach. *Nature Communications*, *7*, 13603. https://doi.org/10.1038/ncomms13603

Pachur, H.-J., & Hoelzmann, P. (1991). Paleoclimatic implications of late quaternary lacustrine sediments in Western Nubia, Sudan. *Quaternary Research*, *36*(3), 257–276. https://doi.org/10.1016/0033-5894(91)90002-M

Petit-Maire, N. (1991). *Paléoenvironnements du Sahara (lacs holocènes à Taoudenni (Mali))*. Editions du Centre national de la recherche scientifique.

Petit-Maire, N., & Riser, J. (1983). *Sahara ou Sahel? Quaternaire recent du Bassin de Taoudenni (Mali)* (tech. rep.). Paris (France) Librairie du Museum.

Petit-Maire, N., & Riser, J. (1987). Holocene palaeohydrography of the Niger. *Palaeoecology of Africa*, *18*, 135–141
Cited By :14.

Quade, J., Dente, E., Armon, M., Dor, Y. B., Morin, E., Adam, O., & Enzel, Y. (2018). Megalakes in the Sahara? A Review. *Quaternary Research*, *90*(2), 253–275. https://doi.org/10.1017/qua.2018.46

Schneck, R., Gayler, V., Nabel, J. E. M. S., Raddatz, T., Reick, C. H., & Schnur, R. (2022). Assessment of JSBACHv4.30 as land component of ICON-ESM-V1 in comparison to its predecessor JSBACHv3.2 of MPI-ESM1.2. *Geoscientific Model Development Discussions*, 1–45. https://doi.org/10.5194/gmd-2022-74

Schneider, J.-L. (1969). Evolution du demier lacustre et peuplements prthistorique aux Bas-Pays du Tchad. *Etudes et documents tchadiens*, 358–363.

Specht, N. F., Claussen, M., & Kleinen, T. (2022). Simulated range of mid-Holocene precipitation changes from extended lakes and wetlands over North Africa. *Climate of the Past*, *18*(5), 1035–1046. https://doi.org/10.5194/cp-18-1035-2022

Swezey, C., Lancaster, N., Kocurek, G., Deynoux, M., Blum, M., Price, D., & Pion, J. .-. (1999). Response of aeolian systems to Holocene climatic and hydrologic changes on the northern margin of the Sahara: A high-resolution record from the Chott Rharsa basin, Tunisia. *The Holocene*, *9*(2), 141–147. https://doi.org/10.1191/095968399670329816

Swezey, C. (2003). The role of climate in the creation and destruction of continental stratigraphic records: An example from the northern margin of the Sahara Desert. In *SEPM Spec Publ* (pp. 207–225). https://doi.org/10.2110/pec.03.77.0207

Tegen, I., Harrison, S. P., Kohfeld, K., Prentice, I. C., Coe, M., & Heimann, M. (2002). Impact of vegetation and preferential source areas on global dust aerosol: Results from a model study. *Journal of Geophysical Research: Atmospheres*, *107*(D21). https://doi.org/10.1029/2001JD000963

Vamborg, F. S. E., Brovkin, V., & Claussen, M. (2011). The effect of a dynamic background albedo scheme on Sahel/Sahara precipitation during the mid-Holocene. *Climate of the Past*, *7*(1), 117–131. https://doi.org/10.5194/cp-7-117-2011

Watrin, J., Lézine, A.-M., & Hély, C. (2009). Plant migration and plant communities at the time of the "green Sahara". *Comptes Rendus Geoscience*, *341*(8), 656–670. https://doi.org/10.1016/j.crte.2009.06.007

APPENDICES

A

SIMULATED RANGE OF MID-HOLOCENE PRECIPITATION CHANGES FROM EXTENDED LAKES AND WETLANDS OVER NORTH AFRICA

The attached paper has been published as:

Specht N.F., Claussen M. and Kleinen T. (2022). "Simulated range of mid-Holocene precipitation changes from extended lakes and wetlands over North Africa." In: *Climate of the Past* 18.5, pp. 1035–1046. DOI: https://doi.org/10.5194/cp-18-1035-2022

AUTHOR CONTRIBUTIONS

NFS and MC planned the study. NFS developed the model components, ran the simulations and analyzed the results. MC and TK contributed to the discussion of results and the paper.

DATA AVAILABILITY

Data has been published at https://doi.org/10.5194/cp-18-1035-2022 (Specht et al., 2022)

Simulated range of mid-Holocene precipitation changes from extended lakes and wetlands over North Africa

Specht Nora Farina [1], **Claussen Martin** [1,2] **and Kleinen Thomas** [1]

Received: 23 September 2021 – Accepted: 28 March 2022 – Published: 13 May 2022.

[1] Max Planck Institute for Meteorology, Bundesstrasse 53, 20146 Hamburg, Germany

[2] Meteorological Institute, Centrum für Erdsystemforschung und Nachhaltigkeit (CEN), Universität Hamburg, Bundesstrasse 55, 20146 Hamburg, Germany

ABSTRACT

Enhanced summer insolation over North Africa induced a monsoon precipitation increase during the mid-Holocene, about 6000 years ago, and led to a widespread expansion of lakes and wetlands in the present-day Sahara. This expansion of lakes and wetlands is documented in paleoenvironmental sediment records, but the spatially sparse and often discontinuous sediment records provide only a fragmentary picture. Previous simulation studies prescribed either a small lake and wetland extent from reconstructions or focused on documented mega-lakes only to investigate their effect on the mid-Holocene climate. In contrast to these studies, we investigate the possible range of mid-Holocene precipitation changes in response to a small-lake extent and a potential maximum lake and wetland extent.

Our study shows that during the summer monsoon season, the African rain belt is shifted about 2 to 7 ° farther north in simulations with a maximum lake or wetland extent than in simulations with a small lake extent. This northward extent is caused by a stronger and prolonged monsoon rainfall season over North Africa which is associated with an increased monsoon precipitation over the southern Sahara and an increased precipitation from tropical plumes over the northwestern Sahara. Replacing lakes with vegetated wetlands causes an enhanced precipitation increase, which is likely due to the high surface roughness of the wetlands. A moisture budget analysis reveals that both lakes and wetlands cause a local precipitation increase not only by enhanced evaporation but also by a stronger inland moisture transport and local moisture recycling to the south of Lake Chad and the west Saharan lakes. Analysis of the dynamic response shows that lakes and wetlands cause a circulation response inverse to the one associated with the Saharan heat low. Depending on the latitudinal position of the lakes and wetlands, they predominantly cause a northward shift or a decay of the African Easterly Jet. These results indicate that the latitudinal position of the lakes and wetlands strongly affects the northward extension of the African summer monsoon.

A.1 INTRODUCTION

Paleoenvironmental sediment records reveal that North African lakes and wetlands expanded spatially during the mid-Holocene, as a result of increased summer monsoon precipitation (Holmes & Hoelzmann, 2017; Lézine et al., 2011). This precipitation increase was initiated by changes in the orbital forcing (Kutzbach, 1981) but reinforced by surface changes such as the expansion of vegetation (Claussen & Gayler, 1997; Kutzbach & Guetter, 1986), the formation of soil (Levis et al., 2004; Vamborg et al., 2011), and the extent of lakes and wetlands (Broström et al., 1998; Carrington et al., 2001; Chandan & Peltier, 2020; Coe & Bonan, 1997; Krinner et al., 2012). Even though the extent of lakes and wetlands during the mid-Holocene is visible in sediment records, these records are spatially sparse and most of them are temporally discontinuous (Holmes & Hoelzmann, 2017; Lézine et al., 2011) . Additionally, reconstructions differ widely regarding the existence of mega-lakes (Quade et al., 2018). Given this spatially and temporally limited information from reconstructions, investigating the effect of lakes and wetlands on the mid-Holocene climate becomes a scientific challenge.

Previous simulation studies used different approaches to prescribe mid-Holocene lakes and wetlands to investigate their effect on the North African climate. The majority of these studies (Broström et al., 1998; Carrington et al., 2001; Krinner et al., 2012) prescribed a small lake and wetland extent using the reconstruction map by Hoelzmann et al. (1998). Results from these investigations show that a small lake and wetland extent only causes a marginal northward shift of the North African rain belt (Broström et al., 1998; Carrington et al., 2001; Coe & Bonan, 1997). A larger shift is caused, though, when this initial precipitation response is reinforced by vegetation feedback (Krinner et al., 2012). A more recent simulation study by Chandan and Peltier (2020) that considers several documented mega-lakes (e.g., Lake Ahnet, Chotts, Fezzan, Dafur and Chad) indicates that these large lakes only have a little impact on the northward penetration of the North African rain belt but induce a precipitation increase over the Sahel region. These prior simulation studies all follow the approach of prescribing lakes and wetlands that are documented by reconstructions.

Comparison between dust emission simulations and marine sediment cores indicate that mid-Holocene lakes and wetlands might have expanded much more strongly over the western Sahara (Egerer et al., 2018; Tegen et al., 2002) than prescribed in any mid-Holocene simulations (Chandan & Peltier, 2020; Hoelzmann et al., 1998). Moreover, little research has been done regarding the role of vegetated wetlands during the mid-Holocene. Vegetated wetlands have been prescribed in the vicinity of mega-lake Chad (Carrington et al., 2001; Hoelzmann et al., 1998), yet the existence of vegetated wetlands in the vicinity of other documented mega-lakes is also conceivable. In addition, vegetated wetlands may have formed as a result of seasonal flooding, as seen in the Okavango Delta in South Africa.

Thus, the limited availability of mid-Holocene sediment records entail interpretative uncertainties in the effect of lakes and wetlands on the mid-Holocene climate. Therefore, we investigate the possible range of mid-Holocene precipitation changes by exploring the effect of a small (Hoelzmann et al., 1998) and a potential

maximum lake and wetland extent (Tegen et al., 2002) rather than following the approach of prescribing lakes and wetlands documented in reconstructions. This includes larger lakes and wetlands over the western Sahara, which might strongly affect the Saharan heat low, a shallow low-pressure system, where near-surface monsoon southwesterlies and dry desert northeasterlies converge (Nicholson, 2009). The Saharan heat low controls the northward penetration of the monsoon winds (Claussen et al., 2017) and, thus, the West African monsoon precipitation itself.

A.2 MATERIALS AND METHODS

In order to investigate the potential range of mid-Holocene precipitation changes induced by extended lakes and wetlands, we conduct four mid-Holocene sensitivity experiments. The sensitivity experiments are performed using the atmosphere model ICON-A (Giorgetta et al., 2018) and the land model JSBACH4 (Reick et al., 2021; Schneck et al., 2022) at ˜160 km horizontal resolution and 47 vertical hybrid sigma levels. This coupled atmosphere–land model is forced with climatological 6 kyr BP orbital parameters (Berger, 1978) and greenhouse gas concentrations (Brovkin et al., 2019). The 6 kyr BP climatological vegetation distribution is prescribed based on a transient mid-Holocene MPI-ESM simulation (Dallmeyer et al., 2021).

The ICON-Earth System Model (ICON-ESM) simulates regional sea-surface temperature (SST) biases of up to 5 K (Jungclaus et al., 2021), which causes a latitudinal displacement of the North African summer monsoon (Zhao et al., 2007). In order to simulate the latitudinal position of the North African summer monsoon in better agreement with proxy data, we use observation-based Atmospheric Model Intercomparison Project II (AMIP2) data to prescribe the SST and sea-ice concentration (SIC) (Kanamitsu et al., 2002; Taylor et al., 2000). The SST and SIC boundary conditions are derived as follows: monthly climatological differences between a 6 kyr BP (Brierley et al., 2020; Jungclaus et al., 2019) and historical (1980–2014) (Wieners et al., 2019) MPI-ESM (Max Planck Institute Earth System Model) PMIP4-CMIP6 (Palaeoclimate Model Intercomparison Project 4 of the Coupled Model Intercomparison Project 4) simulation are superimposed onto an AMIP2 climatology (1980–2014). To take into account the seasonal SST and SIC variability, transient monthly SST and SIC anomalies from the 6 kyr BP simulation are added to the AMIP2-like mid-Holocene climatology. Since Sahel rainfall responds non-linearly to SST changes (Neupane & Cook, 2013), particularly over the tropical Atlantic (e.g., Rodríguez-Fonseca et al. (2015)), adding transient monthly anomalies to the climatological monthly mean SST affects the overall mean state of the North African monsoon system.

Using this setup, the individual sensitivity experiments are run for 35 years, in which only the last 30 years are used as the evaluation period. The individual sensitivity experiments differ only in their lake and wetland extent over North Africa: (1) present lakes, (2) small lake extent, (3) maximum lake extent, (4) maximum wetland extent. In the control simulation, the present lake map for standard ICON AMIP2 simulations is used (Fig. A.1a). The small lake extent is given by the reconstruction map from Hoelzmann et al. (1998), which is based on paleoenvironmental records (Fig. A.1b). The maximum lake extent is represented by the potential maximum

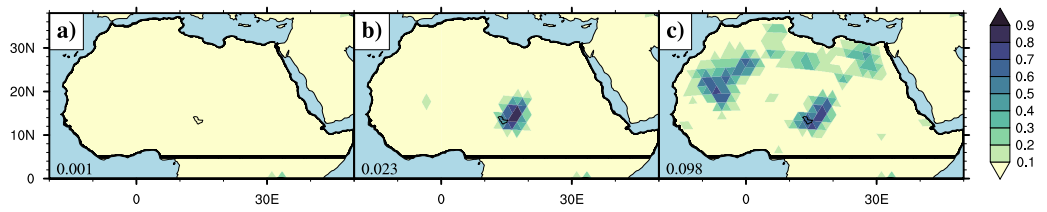

Figure A.1: (a) Standard AMIP2 present-day lake fraction from the JSBACH4-ICON model, (b) mid-Holocene small-lake fraction derived from paleoecological reconstructions (Hoelzmann et al., 1998) and (c) mid-Holocene maximum-lake fraction derived using the hydrological routing algorithm (HYDRA) (Tegen et al., 2002). The present-day lake fraction of Lake Chad is less than 10% per grid box, which falls into the lowest subsection of the plotting scale. The labels in the lower left corner of the plots indicate the lake fraction averaged over the North African region (5 °N (black line) to 38 °N and 20–50 °W).

lake extent simulated by Tegen et al. (2002) using the hydrological model HYDRA (hydrological routing algorithm) (Fig. A.1c). The same potential maximum-extent map is also used to prescribe the maximum extent of wetlands (Fig. A.1c).

The lakes and wetlands are treated as fractional grid cell types in the land model JSBACH4. The lakes are represented by a simple constant-depth mixed-layer (10 m) approach (Roeckner et al., 2003). The surface temperature of the lakes is uniquely dependent on the net surface heat flux, and the lake albedo is set to a constant value of 0.07 (Roeckner et al., 2003). The wetland surface cover type was implemented into JSBACH4 for the purpose of this study and is defined as moisture-saturated soil with an equal ratio of C3 and C4 grasses growing on it. This representation of wetlands is similar to the one used by (Carrington et al., 2001). In contrast to lakes, wetlands have a higher surface roughness and a dynamic background albedo that depends on the vegetation's net primary productivity.

As indicated in the previous section, the changes in the Saharan desert ground due to litter production from the vegetation is taken into account. Previous simulation studies showed that these changes in the background albedo (surface albedo without vegetation) substantially influence the mid-Holocene precipitation over the Sahel–Sahara region (Vamborg et al., 2011). To prescribe these background albedo changes, we use a parameterization scheme that is based on the concept by Egerer et al. (2018):

$$\alpha_{background} = \alpha_{mineral} - (\alpha_{mineral} - \alpha_{soil}) \times \mathrm{MIN}\left(\sum_{PFT}^{i=1} f_i \frac{\overline{NPP_i}}{NPP_{soil,i}}, 1.0\right) \quad \text{(A.1)}$$

The scheme by Egerer et al. (2018) prescribes the albedo changes in a mineral desert ground ($\alpha_{mineral}$) towards an organic soil ground α_{soil} due to the production of dead biomass from the vegetation in the mineral ground. The background albedo changes depend linearly on the 5-year mean net primary productivity, $\overline{NPP}$, of the vegetation relative to the fixed annual NPP needed to completely cover the

ground with one layer of dead organic material (NPP_{soil}). By considering this linear relation Eq. (A.1), the scheme by Egerer et al. (2018) neglects non-linear processes such as the overlapping of dead leaves and litter with increasing coverage of the ground with organic material. Therefore, we here use the following exponential function to describe the background albedo changes during the mid-Holocene:

$$\alpha_{background} = \alpha_{mineral} - (\alpha_{mineral} - \alpha_{soil}) \times \left(1 - e^{-\sum_{PFT}^{i=1} f_i \frac{\overline{NPP_i}}{\overline{NPP_{soil,i}}}}\right) \quad (A.2)$$

The soil albedo α_{soil} is set to a mean value of 0.13 for the visible range and a mean value of 0.22 for the near-infrared range as suggested by Egerer et al. (2018). $\alpha_{mineral}$ is derived by inverting Eq. (A.2) and then calculating $\alpha_{mineral}$ for each grid cell using $\overline{NPP}$ from a standard AMIP ICON simulation, and $\alpha_{background}$ is obtained from Moderate Resolution Imaging Spectroradiometer (MODIS) observation data (Otto et al., 2011). Since the background albedo scheme prescribed the transition from a mineral desert ground to a savanna landscape, this scheme is applied only in the North African Sahel–Sahara region (10–35 °N; 20–35 °W). Results reveal that the exponential parameterization scheme is able to capture the relation between background albedo and NPP (not shown).

In this study, the mid-Holocene climate response to the extended lakes and wetlands is calculated by the 30-year mean difference between the control simulation (present-day lakes) and the sensitivity simulations (extended lakes and wetlands):

$$\delta(\cdot) = (\cdot)_{sensitivity} - (\cdot)_{control}. \quad (A.3)$$

Under this stationary state, the moisture budget changes can be divided into

$$\delta P = \delta E + \delta(P - E), \quad (A.4)$$

where δP is the precipitation response, which consists of a local evaporation response δE and a moisture convergence response $\delta(P - E)$ that indicates local drying or wetting. Following Seager et al. (2010), the moisture convergence response can be separated into a dynamic δDY, a thermodynamic δTH, a transient eddy δTE, a non-linear δNL and a surface term δS. In this study, the δS is relatively small, so that the moisture convergence response can be expressed as

$$\delta(P - E) \approx \delta DY + \delta TH + \delta TE + \delta NL \quad (A.5)$$

$$\delta DY = -\frac{1}{g\rho_w} \int_0^{p_s} \nabla \cdot ([\delta\overline{u}]\overline{q}_{control}) dp \quad (A.6)$$

$$\delta TH = -\frac{1}{g\rho_w} \int_0^{p_s} \nabla \cdot (\overline{u}_{control}[\delta\overline{q}]) dp \quad (A.7)$$

$$\delta TE = -\frac{1}{g\rho_w}\int_0^{p_s} \nabla \cdot \delta(\overline{u'q'})dp \tag{A.8}$$

$$\delta NL = -\frac{1}{g\rho_w}\int_0^{p_s} \nabla \cdot (\delta\overline{u}\delta\overline{q})dp \tag{A.9}$$

where an overbar indicates a monthly mean and a primed variable deviation from the monthly mean. δDY (Eq. A.6) represents changes in the moisture convergence due to changes in the mean circulation $\delta\overline{u}$, and δTH (Eq. A.7) indicates changes in the moisture convergence due to changes in the mean specific humidity $\delta\overline{q}$. The δTE (Eq. A.8) and δNL (Eq. A.9) account for moisture convergence changes caused by coherent changes in the wind and specific humidity. The terms of the moisture budget equation provide information about the mechanisms that affect the simulated precipitation response induced by the prescribed extended lakes and wetlands.

A.3 RESULTS

SPATIAL AND TEMPORAL PRECIPITATION RESPONSE

The maximum lake extent shifts the North African rain belt about 2 to 3 ° farther north into the Sahel region (11–17 °N) than the small lake extent (Fig. A.2). The line between savanna and desert landscape, marked by the Sahel rainfall threshold (200 mm yr^{-1}), is shifted about 7 ° farther north in the simulation with the maximum lake extent than in the simulation with the small lake extent (Fig. A.2). Comparison of the maximum-lake and wetland experiments shows that replacing lakes with vegetated wetlands leads to an overall increase in precipitation over North Africa (Fig. A.2). The relative precipitation difference is particularly strong over the northern Sahara (22–30 °N).

The annual course of the zonally averaged daily precipitation shows that the expansion of lakes and wetlands prolongs the rainfall season over North Africa (Fig. A.3a–d). Hagos and Cook (2007) define the onset and offset of the rain season over North Africa as a jump of the precipitation maximum from 5 °N (near the Gulf of Guinea) to 10 °N. Accordingly, the duration of the North African rainfall season is marked by the period in which the core of maximum rainfall lies above 10 °N (black solid line in Fig. A.3a–d). Results show that, by this definition, the rainfall season is almost twice as long in the maximum-lake and wetland simulations than in the control simulation. Prescribing a small lake extent in the mid-Holocene simulation, however, only causes a marginally longer duration of the North African rainfall season.

In all sensitivity experiments, the earlier onset and later offset of the monsoon season are associated with an enhanced monsoon precipitation over the rain belt region between the Tropical Easterly Jet (TEJ) and the African Easterly Jet (AEJ) (Fig.

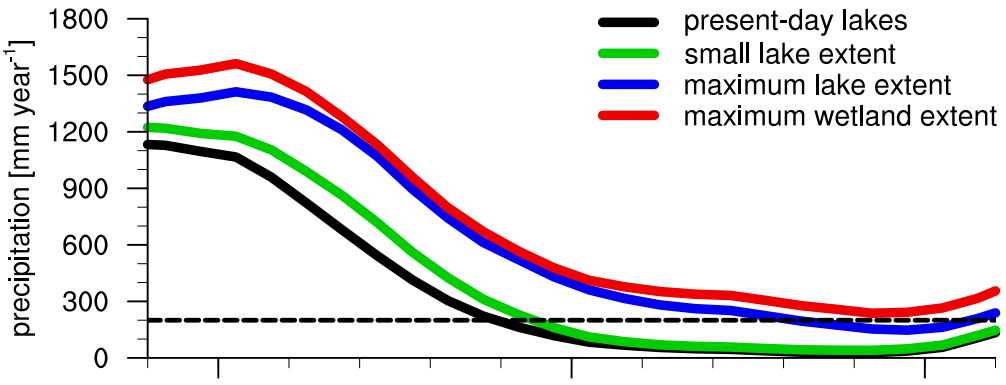

Figure A.2: Mid-Holocene 30-year mean annual precipitation zonally averaged over Africa (10 °E–30 °W). The black dashed line marks the 200 mm yr^{-1} threshold indicating the border between savanna and desert landscape.

A.3). In the maximum-lake and wetland experiments, the prolonged rainfall season is also associated with an increased rainfall over the northwestern Sahara (20-35 °N) during September (Fig. A.3c–d and g–h). In the maximum wetland experiment, this enhanced rainfall over the northwestern Sahara also occurs at the rain season onset in June (Fig. A.3h).

Beside seasonal changes, we also analyze the spatial precipitation response to the prescribed extended lakes and wetlands for the summer months (JJAS). Results show that the small and the maximum lake extent both cause a local precipitation increase over the southern Saharan (Fig. A.3f–g). The maximum lake extent, additionally, causes an enhanced monsoon precipitation increase over the rain belt region (between the AEJ and TEJ) as well as increased precipitation over the center of tropical–extratropical interaction in the northwestern Sahara (Fig. A.3e and g). Comparison of the maximum-lake and maximum-wetland experiments shows that replacing the lakes with vegetated wetland leads to an overall increase in the summer monsoon precipitation over North Africa. The vegetated wetlands cause a spatially broader precipitation increase compared to the local precipitation peak induced by the lakes (Fig. A.3g–f).

MOISTURE CONVERGENCE RESPONSE

In order to better understand the influences of the lakes and wetlands on mid-Holocene precipitation, changes in the moisture budget terms are analyzed. Changes in evaporation and moisture convergence both substantially contribute to the summer precipitation increase over North Africa (Fig. A.4). A local evaporation increase over the prescribed lakes and wetlands corresponds to an enhanced precipitation over the northern Sahara and Lake Chad (Fig. A.4a–c). The moisture convergence response shows a dipole pattern with a drying response over the northern Sahara and north of Lake Chad and a wetting response over the southern Sahara, the Sahel region and south of Lake Chad (Fig. A.4d–f). Results show that evaporation changes are the major cause for the precipitation increase over the northern Sahara and over

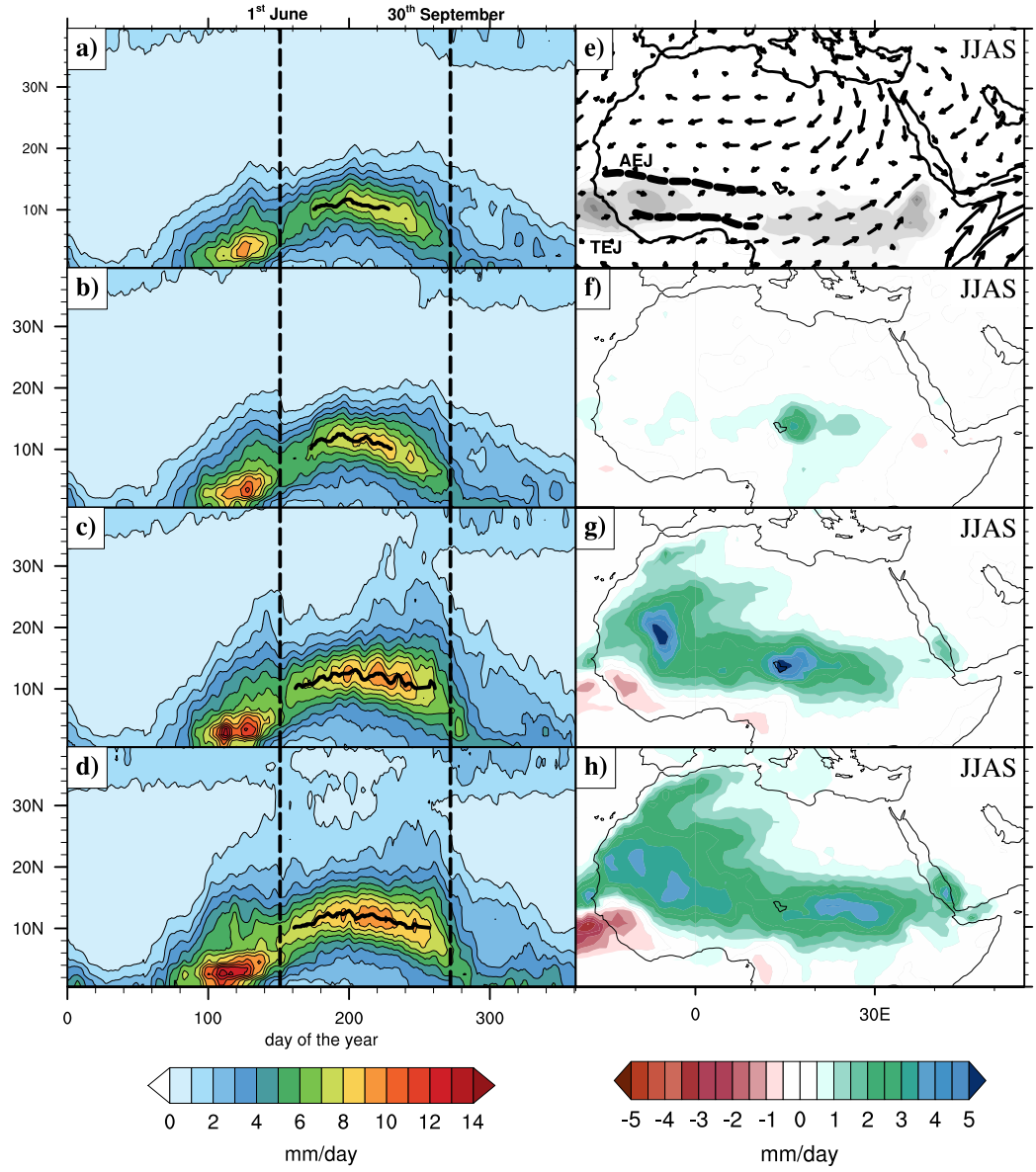

Figure A.3: (a-d) Mid-Holocene 30-year mean daily precipitation zonally averaged over Africa (10 °E – 30 °W) and smoothed with a 5-day running mean. The black lines represent the time period in which the core of maximum rainfall lies above 10 °N and, thus, indicates the duration of the rain season over the Sahel. (e) Schematics of 30-year mean JJAS African summer monsoon features from the present-day lake simulation: (arrows) the near-surface wind (at 850 hPa), the mid-troposphere African Easterly Jet (AEJ) (600 hPa), the Tropical Easterly Jet (TEJ) (150 hPa) and (grey shades) the rain belt region between both jets. (f-g) Mid-Holocene 30-year mean JJAS precipitation response to the (f) small lake extent, (g) maximum lake extent and (h) maximum wetland extent in comparison to the present-day lake simulation.

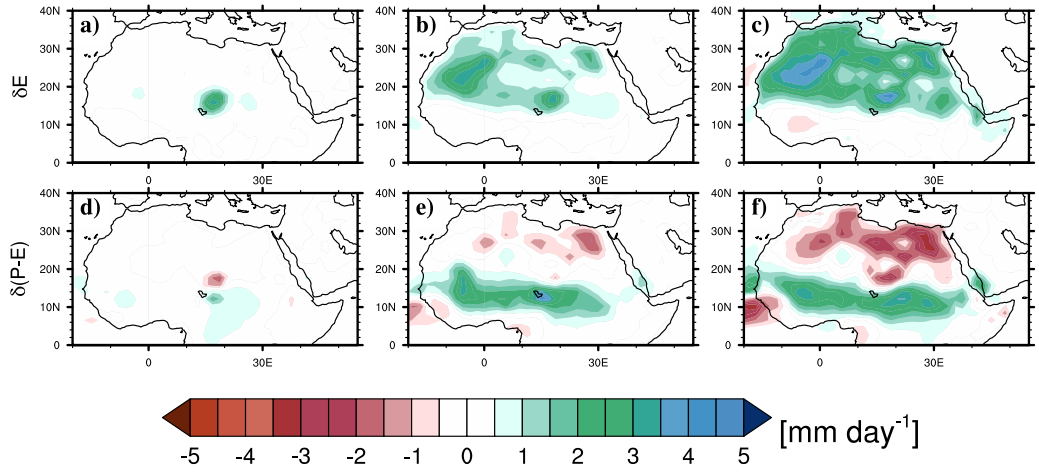

Figure A.4: Mid-Holocene 30-year mean summer (JJAS) (a–c) evaporation and (d–f) moisture convergence response to a (a, d) small lake extent, (b, e) maximum lake extent and (c, f) maximum wetland extent. The sum of the evaporation and moisture convergence response is equal to the precipitation response shown in Fig. A.3f–h.

Lake Chad, whereas enhanced moisture convergence primarily contributes to the rainfall increase over the southern Sahara and Sahel region.

The moisture divergence and, thus, drying response over the northern Sahara and north of Lake Chad counteract the effect of increased evaporation in this region (Fig. A.4). In the maximum-lake and wetland experiments, the drying response over the northeastern Sahara completely compensates for the local effect of increased evaporation (Fig. A.4b–c and e–f). Accordingly, the summer precipitation is unchanged over the northeast Saharan lakes and wetlands in the maximum-lake and wetland experiments (Fig. A.3g–h).

Results also show that the latitudinal position of the wet-south–dry-north dipole pattern differs between the small lake extent and the maximum-lake and wetland extent experiments. The boundaries between wetting and drying response are related to the latitudinal position of the prescribed lakes and wetlands over the western Sahara and the Chad region. In the maximum-lake and wetland experiments, the line between wet and dry response reaches up to 20 °N over the western Sahara, whereas this line is restricted to 15 °N by Lake Chad in the small-lake experiment.

In order to investigate the causes for this dipole-like moisture convergence response $\delta(P-E)$ over North Africa, $\delta(P-E)$ is split into a dynamic δDY, thermodynamic δTH, transient eddy δTE and non-linear term δNL following Seager et al. (2010). Results indicate that the dipole-like response is primarily caused by dynamic and thermodynamic changes that affect the moisture convergence (Fig. A.4d–i). Therefore, we only analyze the δDY and δTH in detail.

The thermodynamic response δTH reflects the near-surface convergence-divergence pattern associated with the mean summer monsoon circulation (Fig. A.5a–c). This response is associated with a general increase in the near-surface mean specific humidity caused by the prescribed lakes and wetlands. Increased moisture conver-

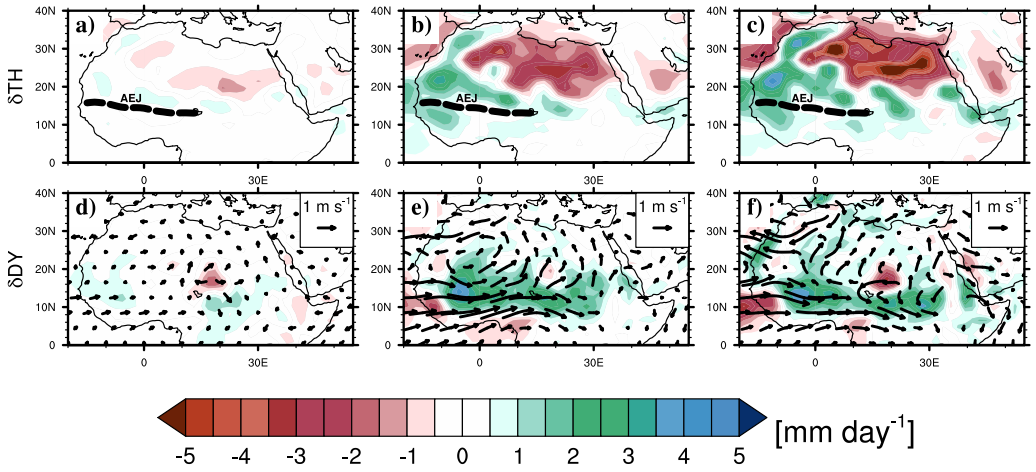

Figure A.5: Mid-Holocene 30-year mean summer (JJAS) (a–c) thermodynamic δTH and (d–f) dynamic moisture convergence response δDY to a (a, d) small lake extent, (b, e) maximum lake extent and (c, f) maximum wetland extent. Changes in the moisture convergence (precipitation response minus evaporation response) are primarily caused by changes in the dynamic component δDY and thermodynamic component δTH.

gence occurs to the south and north of the AEJ, particularly near the African west coast (Fig. A.5a–c). This region is associated with the southern and northern track of the African easterly waves (e.g Nicholson (2009)). Increased moisture convergence also occurs near the northwest Saharan coast (Fig. A.5b–c), where the cyclonic flow from the Saharan heat low and the anticyclonic flow from the extratropical Azores high converge (e.g Nicholson (2009)). Moisture divergence and, thus, a drying response is visible over the northeastern Sahara (Fig. A.5a–c), where hot and dry northeasterlies, known as Harmattan winds, likely transport moisture away from the lakes and wetlands (Fig. A.3e). Comparison of the individual sensitivity experiments shows that δTH is relatively weak in the small-lake-extent experiment compared to the maximum-lake-extent experiment. The maximum wetland extent generally causes larger changes in δTH than the maximum lake extent. The changes in δTH relate to the strength of the evaporation increase and, thus, the increase in the specific humidity caused by the prescribed lake and wetland extent in the individual sensitivity experiments.

The dynamic response δDY reveals that the prescribed lakes and wetlands enhance the moisture convergence in the southern west Saharan and the southern Chad region (Fig. A.5a–c). This increased moisture convergence is associated with stronger near-surface monsoon westerlies that enhance the inland moisture transport from the Atlantic Ocean to the North African continent (Fig. A.5a–c). A weakening of the AEJ (Fig. A.6b–c) additionally contributes to this moisture convergence increase by decreasing the moisture export from the North African continent to the Atlantic Ocean. A comparison between the small and large lake experiments shows that the maximum extent of the lakes induces a stronger monsoon westerly wind acceleration that reaches farther to the north (Fig. A.5a–b). Accordingly, the

moisture convergence increases more strongly and reaches higher up north in the maximum-lake experiment (Fig. A.5a–b). Since these differences are particularly strong over the western Sahara, the west Saharan lakes are likely the primary cause for the stronger inland moisture transport seen in the maximum lake extent experiment. Besides, the size of Lake Chad is nearly the same in the small and maximum-lake-extent experiments (Fig. A.1b–c). The dynamic response to the maximum lake and wetland extent shows similar changes in the mean monsoon circulation over the southern Sahara, which results in a similar δDY pattern (Fig. A.4e–f).

The non-linear response, δNL, causes a reversed but less pronounced response pattern compared to the thermodynamic response (Fig. A.7a–c) and is, therefore, overcompensated. The transient eddy response δTE causes a moisture convergence decrease over the west Saharan lakes (around 25 °N) in the maximum-lake and wetland extent experiments (Fig. A.7e–f) but shows only marginal changes in other regions (Fig. A.7d–f). Thus, the total moisture convergence changes primarily emerge from the dynamic and thermodynamic term of the moisture budget equation.

ATMOSPHERIC CIRCULATION RESPONSE

In the sensitivity experiments, the largest precipitation increase occurs in the Chad region and western Sahara. Therefore, we analyze the circulation response to Lake Chad in the small-extent experiment and the circulation response to the west Saharan lakes and wetlands in the maximum-extent experiments.

Lake Chad and the west Saharan lakes and wetlands generally cause a northwards shift of the North African summer monsoon which is associated with enhanced monsoon westerlies and a northward-shifted and weakened AEJ (Fig. A.6a–c). Evaporative cooling above the lakes and wetlands induces a circulation response which is inverse to the one associated with the Saharan heat low (Fig. A.6d–f). A decreased sensible heat flux and increased latent heat flux from the surface to the atmosphere cause descending motions over the cold lakes and wetlands and ascending motions in their warmer vicinity. The resulting overturning circulation response is associated with a near-surface divergence response and a convergence response aloft, in the mid-troposphere. The convergence increase and, thus, low-pressure response in the mid-troposphere induces, by Coriolis force, a westerly wind response to the south and an easterly wind response to the north of the lakes and wetlands at about 700 hPa (Fig. A.6a–c).

The location of this dipole-like zonal wind response depends on the latitudinal position of the lakes and wetlands (Fig. A.6a–c). The existence of Lake Chad leads to a dipolelike zonal wind response around 14 °N, which corresponds to a northward shift of the AEJ. The west Saharan lakes and wetlands induce a dipole-like zonal wind response at around 23 °N, which corresponds primarily to a strong weakening of the AEJ over the western Sahara. Accordingly, lakes located near the AEJ induce a northward shift of the AEJ, while lakes and wetlands located north of the AEJ primarily weaken the AEJ.

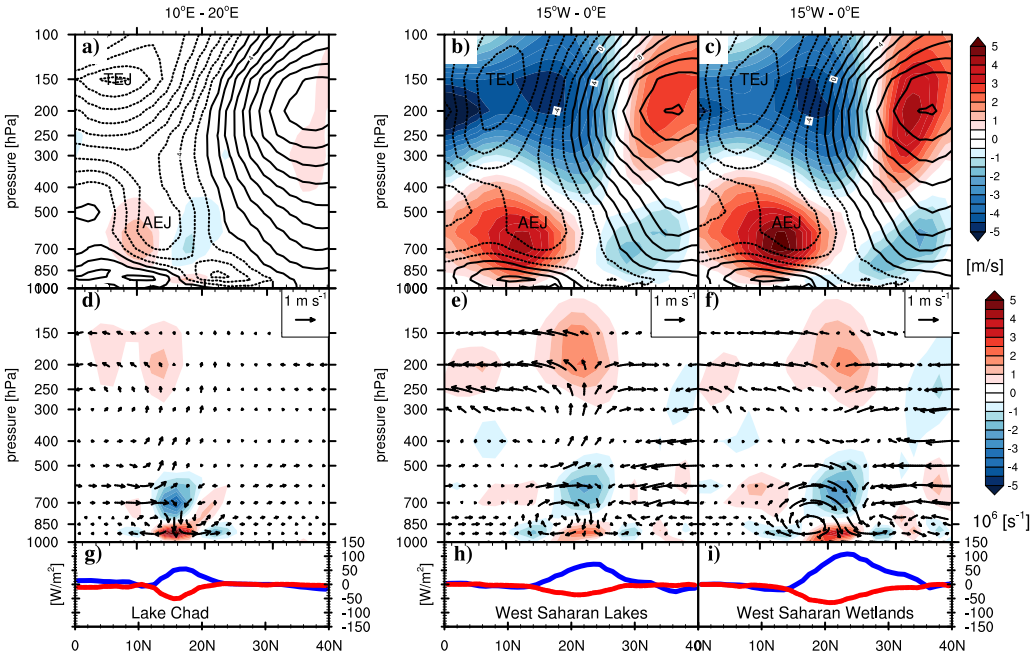

Figure A.6: Mid-Holocene 30-year mean summer (JJAS) circulation response: (a–c) zonal wind response (colored shading), (d–f) divergence response (colored shading) and vertical wind response (black arrows), and (g–i) latent (blue) and sensible (red) heat flux response to the (a, d, g) small lake extent (zonally averaged over the Chad region: 10–20 °E), (b, e, h) the maximum lake extent and (c, f, i) the maximum wetland extent (zonally averaged over the western Sahara: 15 °W–0 °E); (a–c) black contours show the mid-Holocene 30-year mean summer (JJAS) zonal wind climatology zonally averaged over the Chad and west Saharan region.

Beside lower-level circulation changes, lakes and wetlands enhance the convergence of moist air in the mid-troposphere, which favors moist convection in the mid to upper troposphere above the lakes and wetlands (Fig. A.6d–f). The associated upper-level divergence and, thus, high-pressure response lead to an easterly wind acceleration to the south and westerly wind acceleration to the north of the west Saharan lakes and wetlands (Fig. A.6b–c). Accordingly, the TEJ is strengthened in the maximum-lake and wetland experiments. Lake Chad, in contrast, only causes marginal changes in the upper-level mean zonal wind.

Wetlands cause an overturning circulation response that extends higher into the troposphere than the overturning circulation response induced by lakes (Fig. A.6e–f). Accordingly, wetlands cause a higher convection increase than lakes in their vicinity. In contrast, lakes induce a stronger convection increase than wetlands above their water surface in the mid to upper troposphere. The strong convection increase above the lakes and the strong convection increase in the vicinity of the wetlands likely cause the precipitation peak over the prescribed lakes and a rather broad rainfall increase over and around the wetlands (Fig. A.3g).

A.4 DISCUSSION AND CONCLUSIONS

Our study corroborates the results of previous studies, which show that lakes in the Sahara likely enhanced the West African summer monsoon during the mid-Holocene (Krinner et al., 2012). The simulated rain belt northward shift of about 1 ° in the small-lake-extent experiment is relatively large compared to the northward shift simulated by most studies that prescribe a similar small lake extent (Broström et al., 1998; Coe & Bonan, 1997) or an even larger lake extent (Chandan & Peltier, 2020). Only the study by Krinner et al. (2012) shows a northward shift of 1.5 ° in response to this small lake extent. In contrast to other studies, Krinner et al. (2012) use dynamic vegetation that presumably reinforces the precipitation response to the prescribed lakes. Since the vegetation is prescribed in our experiments, the precipitation response to the extended lakes and wetlands in our study can likely be attributed to background and evaporation feedback.

Our results show that the maximum lake extent shifts the isohyets of the mid-Holocene rain belt about 2 to 7 ° farther north than the small lake extent. This difference in the northward shift is mainly caused by the additional lakes over the western Sahara, while the prescribed Lake Chad is nearly the same size in both experiments. The west Saharan lakes strongly affect the monsoon circulation because they lie in a region where the AEJ is strongest and where the Saharan heat low is located. Thus, the location of the prescribed lakes and wetlands likely plays a major role in the northward extent of the African summer monsoon. These findings disagree with the results of Chandan and Peltier (2020), who conducted two mid-Holocene simulations: one with reconstructed lakes and one with a homogeneous lake extent over North African (plus Lake Chad). We suppose that the difference between our simulations results can be attributed to the fact that in their simulation, large lakes over the western Sahara are missing.

Our study also shows that vegetated wetlands cause a stronger precipitation increase than lakes of the same size. This strong precipitation response to vegetated wetlands is likely caused by a high surface roughness which is associated with an enhanced evaporation and surface cooling over the wetlands. Due to this strong surface cooling and, thus, local subsidence, wetlands cause a high precipitation increase in their vicinity. In contrast, lakes show a local precipitation peak above their water surface.

Analysis of the annual course of precipitation shows that the maximum lake and wetland extent over North Africa causes a prolonged rainfall season. This prolonged rainfall season is associated with an earlier onset and later offset of the monsoon season over North Africa. While an enhanced summer monsoon precipitation in the rain belt region occurs in all sensitivity experiments, the maximum lake and wetland extent additionally causes an increased precipitation over the northwestern Sahara during spring and autumn. Precipitation in the northwestern Sahara during fall is presumably associated with the occurrence of rain-bringing tropical plumes. These elongated cloud bands result from extratropical–tropical interaction between an extratropical Atlantic trough and the Saharan heat low. A model study by Skinner and Poulsen (2016) showed that increased moisture availability throughout North Africa during the mid-Holocene enhanced the formation of rainfall-producing

tropical plumes over the northwestern Sahara, which prolongs the rainfall season. Our results indicate that the west Saharan lakes and wetlands provide moisture for the formation of tropical plumes by increasing the local evaporation and by shifting the North African rain belt northward, which likely prolongs the rainfall season.

Analysis of the moisture budget shows that the simulated precipitation increase in the sensitivity experiments is primarily caused by a local evaporation increase in the lakes and wetlands over the northwestern Sahara and by an enhanced moisture convergence over the southern Sahara and Sahel region. The increased precipitation over the southern Sahara is caused by enhanced inland moisture transports and local moisture recycling to the south of the west Saharan lakes and Lake Chad. In contrast, moisture advection by the Harmattan wind transports moisture away from the lakes and wetlands over the northeastern Sahara. This local drying response over the northeastern Sahara indicates why lakes and wetlands do not enhance the local precipitation in this region. The wet-south–dry-north moisture convergence response indicates that lakes and wetlands received excess water primarily from the southern part of their catchment during the summer months. A simulation study by Skinner and Poulsen (2016) and Dallmeyer et al. (2020) showed that the enhanced occurrence of rain-bringing tropical plumes during the mid-Holocene fall season substantially increased the annual precipitation over the western Sahara. Thus, west Saharan lakes and wetlands also might have received excess water during the fall season.

The dynamic response in sensitivity experiments shows that lakes and wetlands cause a circulation response inverse to the one associate with the Saharan heat low. Evaporative cooling causes descending motions above the lakes and wetlands, whereas ascending motions occur in their warmer vicinity. This overturning circulation response causes a convergence increase in the mid-troposphere and, by Coriolis force, a westerly wind response to the south and an easterly wind response to the north of the lakes and wetlands. This dipole-like zonal wind response induces either a northward shift of the AEJ or a weakening of the AEJ depending on the latitudinal position of the lakes and wetlands. For example, Lake Chad causes a northward shift of the AEJ, whereas the west Saharan lakes located higher up north almost cause a strong decay of the AEJ. Along with this shift or weakening of the AEJ the near-surface monsoon westerlies extend farther to the north. These circulation responses indicate that the latitudinal position of the lakes and wetlands strongly affects the monsoon circulation.

Finally, our study shows that the border between savanna and Sahara, the 200 mm yr^{-1} isohyet, is shifted by about 7 ° farther north in the maximum-extent experiment than in the small-extent experiment. This implies that lakes might have had a substantial influence on the vegetation expansion during the mid-Holocene. In this study, we prescribed the vegetation, lakes and wetlands and thus neglect any dynamic feedback. Yet this dynamic interaction might play a key role in understanding the termination of the African Humid Period. Mid-Holocene reconstructions (Lézine et al., 2011; Shanahan et al., 2015) and transient mid-Holocene simulations (Dallmeyer et al., 2020) reveal that the African Humid Period ended earlier in the eastern Sahara than in the west Sahara. This immediately raises questions about the different timescales of vegetation dynamics and lake

dynamics and how they interactively affect the termination of the African Humid Period. Hence in a follow-up study we will explore the effect of dynamic lakes on the African Humid Period and how dynamic lakes and dynamic vegetation interact with each other in this context.

A.5 ADDITIONAL FIGURES

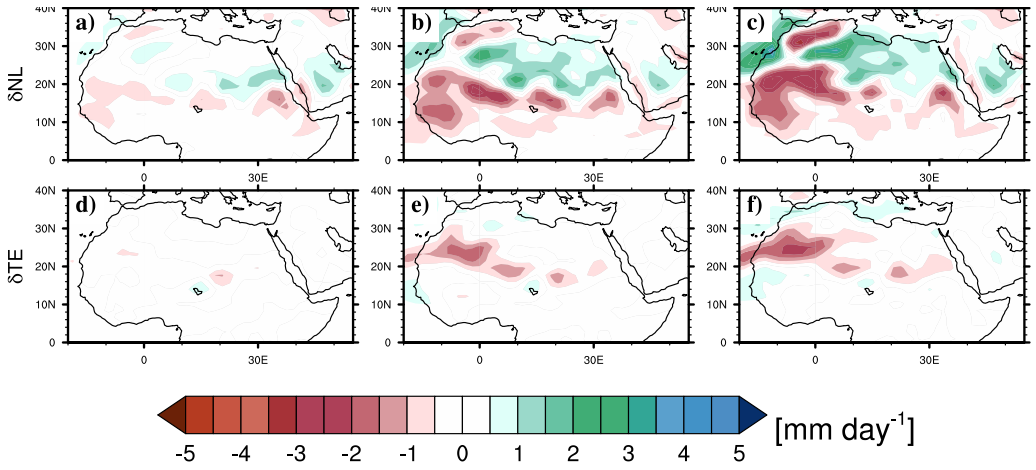

Figure A.7: Mid-Holocene 30-year mean summer (JJAS) (a–c) non-linear and (d–f) transient eddy moisture convergence response to a (a, d) small lake extent, (b, e) maximum lake extent and (c, f) maximum wetland extent.

BIBLIOGRAPHY

Berger, A. (1978). Long-term variations of caloric insolation resulting from the earth's orbital elements. *Quaternary Research*, *9*(2), 139–167. https://doi.org/10.1016/0033-5894(78)90064-9

Brierley, C. M., Zhao, A., Harrison, S. P., Braconnot, P., Williams, C. J. R., Thornalley, D. J. R., Shi, X., Peterschmitt, J.-Y., Ohgaito, R., Kaufman, D. S., Kageyama, M., Hargreaves, J. C., Erb, M. P., Emile-Geay, J., D'Agostino, R., Chandan, D., Carré, M., Bartlein, P. J., Zheng, W., Zhang, Z., Zhang, Q., Yang, H., Volodin, E. M., Tomas, R. A., Routson, C., Peltier, W. R., Otto-Bliesner, B., Morozova, P. A., McKay, N. P., Lohmann, G., Legrande, A. N., Guo, C., Cao, J., Brady, E., Annan, J. D., & Abe-Ouchi, A. (2020). Large-scale features and evaluation of the PMIP4-CMIP6 *midHolocene* simulations. *Climate of the Past*, *16*(5), 1847–1872. https://doi.org/10.5194/cp-16-1847-2020

Broström, A., Coe, M., Harrison, S. P., Gallimore, R., Kutzbach, J. E., Foley, J., Prentice, I. C., & Behling, P. (1998). Land surface feedbacks and palaeomonsoons in northern Africa. *Geophysical Research Letters*, *25*(19), 3615–3618. https://doi.org/10.1029/98GL02804

Brovkin, V., Lorenz, S., Raddatz, T., Ilyina, T., Stemmler, I., Toohey, M., & Claussen, M. (2019). What was the source of the atmospheric CO₂ increase during the Holocene? *Biogeosciences*, *16*(13), 2543–2555. https://doi.org/10.5194/bg-16-2543-2019

Carrington, D. P., Gallimore, R. G., & Kutzbach, J. E. (2001). Climate sensitivity to wetlands and wetland vegetation in mid-Holocene North Africa. *Climate Dynamics*, *17*(2-3), 151–157. https://doi.org/10.1007/s003820000099

Chandan, D., & Peltier, W. R. (2020). African Humid Period Precipitation Sustained by Robust Vegetation, Soil, and Lake Feedbacks. *Geophysical Research Letters*, *47*(21). https://doi.org/10.1029/2020GL088728

Claussen, M., Dallmeyer, A., & Bader, J. (2017). Theory and modeling of the African humid period and the green Sahara. *Oxford Research Encyclopedia of Climate Science*. https://doi.org/10.1093/acrefore/9780190228620.013.532

Claussen, M., & Gayler, V. (1997). The Greening of the Sahara during the Mid-Holocene: Results of an Interactive Atmosphere-Biome Model. *Global Ecology and Biogeography Letters*, *6*(5), 369–377. https://doi.org/10.2307/2997337

Coe, M. T., & Bonan, G. B. (1997). Feedbacks between climate and surface water in northern Africa during the middle Holocene. *Journal of Geophysical Research: Atmospheres*, *102*(D10), 11087–11101. https://doi.org/10.1029/97JD00343

Dallmeyer, A., Claussen, M., Lorenz, S., Sigl, M., Toohey, M., & Herzschuh, U. (2021). Holocene vegetation transitions and their climatic drivers in MPI-ESM1.2. *Climate of the Past*, *17*, 2481–2513. https://doi.org/10.5194/cp-17-2481-2021

Dallmeyer, A., Claussen, M., Lorenz, S. J., & Shanahan, T. (2020). The end of the African humid period as seen by a transient comprehensive Earth system

model simulation of the last 8000 years. *Climate of the Past*, *16*(1), 117–140. https://doi.org/10.5194/cp-16-117-2020

Egerer, S., Claussen, M., & Reick, C. (2018). Rapid increase in simulated North Atlantic dust deposition due to fast change of northwest African landscape during the Holocene. *Climate of the Past*, *14*(7), 1051–1066. https://doi.org/10.5194/cp-14-1051-2018

Giorgetta, M. A., Brokopf, R., Crueger, T., Esch, M., Fiedler, S., Helmert, J., Hohenegger, C., Kornblueh, L., Köhler, M., Manzini, E., Mauritsen, T., Nam, C., Raddatz, T., Rast, S., Reinert, D., Sakradzija, M., Schmidt, H., Schneck, R., Schnur, R., Silvers, L., Wan, H., Zängl, G., & Stevens, B. (2018). ICON-A, the Atmosphere Component of the ICON Earth System Model: I. Model Description. *Journal of Advances in Modeling Earth Systems*, *10*(7), 1613–1637. https://doi.org/10.1029/2017MS001242

Hagos, S. M., & Cook, K. H. (2007). Dynamics of the West African Monsoon Jump. *Journal of Climate*, *20*(21), 5264–5284. https://doi.org/10.1175/2007JCLI1533.1

Hoelzmann, P., Jolly, D., Harrison, S. P., Laarif, F., Bonnefille, R., & Pachur, H.-J. (1998). Mid-Holocene land-surface conditions in northern Africa and the Arabian Peninsula: A data set for the analysis of biogeophysical feedbacks in the climate system. *Global Biogeochemical Cycles*, *12*(1), 35–51. https://doi.org/10.1029/97GB02733

Holmes, J., & Hoelzmann, P. (2017). The Late Pleistocene-Holocene African Humid Period as Evident in Lakes. *Oxford Research Encyclopedia of Climate Science*. https://doi.org/10.1093/acrefore/9780190228620.013.531

Jungclaus, J., Mikolajewicz, U., Kapsch, M.-L., D'Agostino, R., Wieners, K.-H., Giorgetta, M., Reick, C., Esch, M., Bittner, M., Legutke, S., Schupfner, M., Wachsmann, F., Gayler, V., Haak, H., de Vrese, P., Raddatz, T., Mauritsen, T., von Storch, J.-S., Behrens, J., Brovkin, V., Claussen, M., Crueger, T., Fast, I., Fiedler, S., Hagemann, S., Hohenegger, C., Jahns, T., Kloster, S., Kinne, S., Lasslop, G., Kornblueh, L., Marotzke, J., Matei, D., Meraner, K., Modali, K., Müller, W., Nabel, J., Notz, D., Peters-von Gehlen, K., Pincus, R., Pohlmann, H., Pongratz, J., Rast, S., Schmidt, H., Schnur, R., Schulzweida, U., Six, K., Stevens, B., Voigt, A., & Roeckner, E. (2019). CMIP6.PMIP.MPI-M.MPI-ESM1-2-LR.midHolocene. https://doi.org/10.22033/ESGF/CMIP6.6644

Jungclaus, J. H., Lorenz, S. J., Schmidt, H., Gutjahr, O., Haak, H., Mehlmann, C., Mikolajewicz, U., Notz, D., Putrashan, D., von Storch, J.-S., Leonidas, L., Brokvin, V., Chegini, F., Gayler, V., Giorgetta, M. A., Hagemann, S., Ilyina, T., Korn, P., Kröger, J., Müller, W. A., Pohlmann, H., Raddatz, T. J., Ramme, L., Christian, R. H., Schneck, R., Schnur, R., Stevens, B., Ziemen, F. A., Claussen, M., Marotzke, J., Wachsmann, F., Schupfner, M., Riddick, T., Wieners, K.-H., Brueggemann, N., Redler, R., de Vrese, P., Nabel, J. E. M. S., Sam, T., & Hanke, M. (2021). *The ICON Earth System Model Version 1.0* (preprint). Climatology (Global Change). https://doi.org/10.1002/essoar.10507989.1

Kanamitsu, M., Ebisuzaki, W., Woollen, J., Yang, S.-K., Hnilo, J. J., Fiorino, M., & Potter, G. L. (2002). NCEP–DOE AMIP-II Reanalysis (R-2). *Bulletin of the*

American Meteorological Society, *83*(11), 1631–1644. https://doi.org/10.1175/BAMS-83-11-1631

Krinner, G., Lézine, A.-M., Braconnot, P., Sepulchre, P., Ramstein, G., Grenier, C., & Gouttevin, I. (2012). A reassessment of lake and wetland feedbacks on the North African Holocene climate. *Geophysical Research Letters*, *39*(7). https://doi.org/10.1029/2012GL050992

Kutzbach, J. E. (1981). Monsoon Climate of the Early Holocene: Climate Experiment with the Earth's Orbital Parameters for 9000 Years Ago. *Science*, *214*(4516), 59–61. https://doi.org/10.1126/science.214.4516.59

Kutzbach, J. E., & Guetter, P. J. (1986). The Influence of Changing Orbital Parameters and Surface Boundary Conditions on Climate Simulations for the Past 18 000 Years. *Journal of the Atmospheric Sciences*, *43*(16), 1726–1759. https://doi.org/10.1175/1520-0469(1986)043<1726:TIOCOP>2.0.CO;2

Levis, S., Bonan, G. B., & Bonfils, C. (2004). Soil feedback drives the mid-Holocene North African monsoon northward in fully coupled CCSM2 simulations with a dynamic vegetation model. *Climate Dynamics*, *23*(7-8), 791–802. https://doi.org/10.1007/s00382-004-0477-y

Lézine, A.-M., Hély, C., Grenier, C., Braconnot, P., & Krinner, G. (2011). Sahara and Sahel vulnerability to climate changes, lessons from Holocene hydrological data. *Quaternary Science Reviews*, *30*(21), 3001–3012. https://doi.org/10.1016/j.quascirev.2011.07.006

Neupane, N., & Cook, K. H. (2013). A Nonlinear Response of Sahel Rainfall to Atlantic Warming. *Journal of Climate*, *26*(18), 7080–7096. https://doi.org/10.1175/JCLI-D-12-00475.1

Nicholson, S. E. (2009). A revised picture of the structure of the "monsoon" and land ITCZ over West Africa. *Climate Dynamics*, *32*(7-8), 1155–1171. https://doi.org/10.1007/s00382-008-0514-3

Otto, J., Raddatz, T., & Claussen, M. (2011). Strength of forest-albedo feedback in mid-Holocene climate simulations. *Climate of the Past*, *7*(3), 1027–1039. https://doi.org/10.5194/cp-7-1027-2011

Quade, J., Dente, E., Armon, M., Dor, Y. B., Morin, E., Adam, O., & Enzel, Y. (2018). Megalakes in the Sahara? A Review. *Quaternary Research*, *90*(2), 253–275. https://doi.org/10.1017/qua.2018.46

Reick, C. H., Gayler, V., Goll, D., Hagemann, S., Heidkamp, M., Nabel, J. E. M. S., Raddatz, T., Roeckner, E., Schnur, R., & Wilkenskjeld, S. (2021). JSBACH 3 - The land component of the MPI Earth System Model: Documentation of version 3.2. https://doi.org/10.17617/2.3279802

Rodríguez-Fonseca, B., Mohino, E., Mechoso, C. R., Caminade, C., Biasutti, M., Gaetani, M., Garcia-Serrano, J., Vizy, E. K., Cook, K., Xue, Y., Polo, I., Losada, T., Druyan, L., Fontaine, B., Bader, J., Doblas-Reyes, F. J., Goddard, L., Janicot, S., Arribas, A., Lau, W., Colman, A., Vellinga, M., Rowell, D. P., Kucharski, F., & Voldoire, A. (2015). Variability and Predictability of West African Droughts: A Review on the Role of Sea Surface Temperature Anomalies. *Journal of Climate*, *28*(10), 4034–4060. https://doi.org/10.1175/JCLI-D-14-00130.1

Roeckner, E., Bäuml, G., Bonaventura, L., Brokopf, R., Esch, M., Giorgetta, M., Hagemann, S., Kirchner, I., Kornblueh, L., Manzini, E., Rhodin, A., Schlese, U.,

Schulzweida, U., & Tompkins, A. (2003). The atmospheric general circulation model ECHAM 5. PART I: Model description. https://doi.org/10.17617/2.995269

Schneck, R., Gayler, V., Nabel, J. E. M. S., Raddatz, T., Reick, C. H., & Schnur, R. (2022). Assessment of JSBACHv4.30 as land component of ICON-ESM-V1 in comparison to its predecessor JSBACHv3.2 of MPI-ESM1.2. *Geoscientific Model Development Discussions*, 1–45. https://doi.org/10.5194/gmd-2022-74

Seager, R., Naik, N., & Vecchi, G. A. (2010). Thermodynamic and Dynamic Mechanisms for Large-Scale Changes in the Hydrological Cycle in Response to Global Warming. *Journal of Climate*, *23*(17), 4651–4668. https://doi.org/10.1175/2010JCLI3655.1

Shanahan, T. M., McKay, N. P., Hughen, K. A., Overpeck, J. T., Otto-Bliesner, B., Heil, C. W., King, J., Scholz, C. A., & Peck, J. (2015). The time-transgressive termination of the African Humid Period. *Nature Geoscience*, *8*(2), 140–144. https://doi.org/10.1038/ngeo2329

Skinner, C. B., & Poulsen, C. J. (2016). The role of fall season tropical plumes in enhancing Saharan rainfall during the African Humid Period. *Geophysical Research Letters*, *43*(1), 349–358. https://doi.org/10.1002/2015GL066318

Taylor, K., Williamson, D., & Zwiers, F. (2000). AMIP II Sea Surface Temperature and Sea Ice Concentration Boundary Conditions. *PCMDI Rep.*, *60*.

Tegen, I., Harrison, S. P., Kohfeld, K., Prentice, I. C., Coe, M., & Heimann, M. (2002). Impact of vegetation and preferential source areas on global dust aerosol: Results from a model study. *Journal of Geophysical Research: Atmospheres*, *107*(D21). https://doi.org/10.1029/2001JD000963

Vamborg, F. S. E., Brovkin, V., & Claussen, M. (2011). The effect of a dynamic background albedo scheme on Sahel/Sahara precipitation during the mid-Holocene. *Climate of the Past*, *7*(1), 117–131. https://doi.org/10.5194/cp-7-117-2011

Wieners, K.-H., Giorgetta, M., Jungclaus, J., Reick, C., Esch, M., Bittner, M., Legutke, S., Schupfner, M., Wachsmann, F., Gayler, V., Haak, H., de Vrese, P., Raddatz, T., Mauritsen, T., von Storch, J.-S., Behrens, J., Brovkin, V., Claussen, M., Crueger, T., Fast, I., Fiedler, S., Hagemann, S., Hohenegger, C., Jahns, T., Kloster, S., Kinne, S., Lasslop, G., Kornblueh, L., Marotzke, J., Matei, D., Meraner, K., Mikolajewicz, U., Modali, K., Müller, W., Nabel, J., Notz, D., Peters, K., Pincus, R., Pohlmann, H., Pongratz, J., Rast, S., Schmidt, H., Schnur, R., Schulzweida, U., Six, K., Stevens, B., Voigt, A., & Roeckner, E. (2019). CMIP6.CMIP.MPI-M.MPI-ESM1-2-LR.historical. https://doi.org/10.22033/ESGF/CMIP6.6595

Zhao, Y., Braconnot, P., Harrison, S. P., Yiou, P., & Marti, O. (2007). Simulated changes in the relationship between tropical ocean temperatures and the western African monsoon during the mid-Holocene. *Climate Dynamics*, *28*(5), 533–551. https://doi.org/10.1007/s00382-006-0196-7

B

DYNAMIC INTERACTION OF SAHARAN LAKES, CLIMATE AND VEGETATION DURING THE MID-HOLOCENE

The work in this appendix is a manuscript in preparation to be published:

Specht N.F., Claussen C., and Kleinen T. (2023). "Dynamic interaction of Saharan lakes, climate and vegetation during the mid-Holocene." Manuscript in preparation.

AUTHOR CONTRIBUTIONS

NFS and MC planned the study. NFS constructed and implemented the DEL model, ran the simulations and analyzed the results. MC and TK contributed to the discussion of results and the paper.

Dynamic interactions of Saharan lakes, climate and vegetation during the mid-Holocene

Specht Nora Farina [1], **Claussen Martin** [1,2] **and Kleinen Thomas** [1]

[1] Max Planck Institute for Meteorology, Bundesstrasse 53, 20146 Hamburg, Germany

[2] Meteorological Institute, Centrum für Erdsystemforschung und Nachhaltigkeit (CEN), Universität Hamburg, Bundesstrasse 55, 20146 Hamburg, Germany

ABSTRACT

During the early to mid-Holocene, about 11,500 to 5,500 years ago, lakes expanded across the Sahel and Sahara in response to enhanced summer monsoon precipitation. To investigate the effect of these lakes on the West African summer monsoon, previous simulation studies prescribed mid-Holocene lakes from reconstructions. By prescribing mid-Holocene lakes, however, the terrestrial water balance is inconsistent with the size of the lakes. In order to close the terrestrial water cycle, we construct a dynamic endorheic lake (DEL) model and implement it into the atmosphere-land model ICON-JSBACH4. For the first time, this allows us to investigate the dynamic interaction between climate, lakes and vegetation over northern Africa. Additionally, we investigate the effect of lake depth changes on the mid-Holocene precipitation, which was neglected in previous simulation studies.

A pre-industrial control simulation shows that the DEL model realistically simulates the lake extent over northern Africa. The mid-Holocene simulations show several surprising effects. First, a deepening of Lake Chad causes an area-wide precipitation increase over the Sahel and western Sahara. The deepening and, thus, surface cooling of Lake Chad causes an overturning lake-land circulation response that shifts the monsoon system northwards and increases the moisture transport from the tropical Atlantic to the African interior. Second, a dynamic lake extent and a dynamic vegetation expansion individually cause a precipitation increase over northern Africa that is, in the sum, larger than the precipitation increase caused by a combined extent of lakes and vegetation during the mid-Holocene. Thus, the lake-vegetation interaction causes an area-wide drying response over the Sahel and Sahara. The major reason for this drying response is that the vegetation cools the land surface stronger than the simulated mid-Holocene lakes. This causes a circulation and precipitation response reversed to the one associated with a deepening and surface cooling of mid-Holocene lakes. Accordingly, the dynamic lakes and dynamic vegetation together contribute only little to the overall mid-Holocene precipitation increase.

B.1 INTRODUCTION

Climate and environment reconstructions from mid-Holocene sediments show that increased monsoon precipitation over northern Africa caused a widespread expansion of vegetation and lakes over the present-day Sahara, about 11,500 to 5,500 years ago (Hély & Lézine, 2014; Hoelzmann et al., 1998; Holmes & Hoelzmann, 2017; Lézine, 2017). This 'green Sahara' was characterized by a spatially heterogeneous vegetation distribution, reaching from humid forest taxa to wooded grassland taxa (e. g. Hély & Lézine, 2014; Lézine, 2017). Additionally, Mega-lakes Chad (Drake et al., 2022; Hoelzmann et al., 1998; Quade et al., 2018) and Mega-lake Timbuktu (Drake et al., 2022) with an area >25.000 km^2 likely existed in the Sahel. In the Sahara, several smaller, but still substantially lakes formed primarily in regions where the topography is close to the groundwater level (Drake et al., 2022; Holmes & Hoelzmann, 2017; Lézine et al., 2011b). Reconstructions also show that, at the end of this African Humid Period, the transition from a humid to dry climate occurred earlier over the eastern Sahara than over western the Sahara and the drying progressed from the north to the south (Shanahan et al., 2015).

This information is derived from paleo-environmental records that are spatially sparse and often temporally discontinuous (Lézine et al., 2011a). Particularly, the existence of mid-Holocene mega-lakes (Drake et al., 2022; Quade et al., 2018) and the extent of lakes and wetlands over the western Sahara differs strongly between individual reconstruction studies (Chen et al., 2021; Enzel et al., 2017; Hoelzmann et al., 1998). Therefore, previous simulation studies use different lake and wetland reconstructions to investigate the effect of lakes and wetlands on the mid-Holocene climate over northern Africa (Broström et al., 1998; Chandan & Peltier, 2020; Coe & Bonan, 1997; Krinner et al., 2012; Specht et al., 2022).

These simulation studies show that lakes generally cause a precipitation increase over northern Africa. But results differ on whether this precipitation increase is only localized (Broström et al., 1998; Chandan & Peltier, 2020; Coe & Bonan, 1997), or whether lakes cause an area-wide precipitation increase across the Sahel and Sahara (Krinner et al., 2012; Specht et al., 2022). These differences in the precipitation increase might be related to whether vegetation feedback to the extended lakes is considered (Krinner et al., 2012; Specht et al., 2022), or whether a static vegetation is prescribed (Broström et al., 1998; Chandan & Peltier, 2020; Coe & Bonan, 1997). For example, a simulation study by Krinner et al. (2012) that uses a dynamic vegetation model shows that a reconstructed 'small' lake extent over northern Africa induces a northward extent of the African rain belt by about 1.5 ° during the mid-Holocene (Krinner et al., 2012). In contrast, the same lake extent causes only a marginal precipitation increase over the Sahel and Sahara, when the vegetation is prescribed (Broström et al., 1998). Moreover, while some simulation studies use a dynamic vegetation, previous simulation studies all prescribe a static mid-Holocene lake extent over the Sahel and Sahara (Broström et al., 1998; Chandan & Peltier, 2020; Coe & Bonan, 1997; Krinner et al., 2012; Specht et al., 2022).

By prescribing static lakes, the terrestrial water balance is inconsistent with the size of the Saharan lakes. E. g. the lakes might be smaller than prescribed when the evapotranspiration over the lake's catchment is higher than the precipitation or vice

versa. Considering the uncertainties from reconstructions, this raises the question in which region of the Sahel and Sahara lakes would form in the mid-Holocene climate, when dynamically interacting with the atmosphere and the vegetation and how this dynamic interaction between lakes, vegetation and the atmosphere affects the mid-Holocene climate over northern Africa.

To investigate these questions, we simulate the growth and shrink of Saharan lakes and wetlands in interaction with the climate and vegetation over northern Africa under a present-day and mid-Holocene climate. For the purpose of this study, we have constructed and implemented a dynamic endorheic lake model (DEL model) into the hydrological discharge model (HD model) of JSBACH4, the land component of the ICON Earth system model (ICON-ESM). This DEL model interacts with the dynamic vegetation of JSBACH4 and the atmosphere component ICON-A of the ICON-ESM. In the following, we describe the setup of the present-day and mid-Holocene simulations and the concept of the DEL model.

B.2 METHODS

To investigate the dynamic interaction between climate, lakes and vegetation during the mid-Holocene, we conduct a pre-industrial control simulation and a set of mid-Holocene experiments. For the simulations, we use the atmosphere model ICON-A (Giorgetta et al., 2018) and the land model JSBACH4 (Reick et al., 2021; Schneck et al., 2022) at ~160 km horizontal resolution and 47 vertical atmospheric hybrid sigma levels. The atmosphere–land simulations are forced with climatological 0 kyr BP (1850) and 6 kyr BP orbital parameters (Berger, 1978) and greenhouse gas concentrations (GHGs) (Fortunat Joos, personal communication, 2016; see Bader et al., 2020; Brovkin et al., 2019). The pre-industrial (Wieners et al., 2019b) and mid-Holocene (Jungclaus et al., 2019) sea-surface temperatures (SST) and sea-ice concentrations are prescribed from Coupled Model Intercomparison Project 6 (CMIP6) simulations with the Max Planck Institute Earth System Model (MPI-ESM).

Like most Earth system models (Richter & Tokinaga, 2020), the MPI-ESM simulates a too warm SST (>5 K) in the eastern tropical Atlantic (Jungclaus et al., 2013). This promotes a too high precipitation over the Guinea coast (Zhao et al., 2007) and a too southern position of the West African monsoon during the northern hemisphere summer. To simulate a more realistic latitudinal position of the West African summer monsoon, we subtract a monthly climatology of tropical SST biases from the pre-industrial and mid-Holocene MPI-ESM CMIP6 SST. The tropical SST biases are derived from the differences between a historical MPI-ESM CMIP6 simulation (Wieners et al., 2019a) and observation-based Atmospheric Model Intercomparison Project II (AMIP2) SST data (Durack et al., 2022). Finally, the tropical SST biases are smoothed at the 30 °N and 30 °S boundaries to avoid artificial temperatures edges. We only correct the SST in the tropical regions because we assume the influence from the SST biases of higher latitudes to be comparably small.

Furthermore, all simulations are run with a dynamic background albedo scheme as described by Specht et al. (2022). The dynamic background albedo scheme represent changes in the surface albedo due to litter production from vegetation. Vamborg et al. (2011) show that these background albedo changes substantially increase the

mid-Holocene precipitation over northern Africa. This dynamic background albedo is only applied over the northern Africa.

With this setup, we conduct a pre-industrial equilibrium simulation with a dynamic vegetation and dynamic lakes (pidVdL). The mean lake extent of the pidVdL simulation is compared to an observation-based lake map of the HydroLAKES data set (Messager et al., 2016) to evaluate the accuracy of the DEL model in parameterizing the Saharan endorheic lakes.

- pidVdL: dynamic vegetation and dynamic lakes.

In addition, a set of mid-Holocene simulations is conducted to investigate the individual and synergistic effects of vegetation and lake feedback over northern Africa:

- mHdVdL: dynamic vegetation and dynamic lakes.
- mHdV: dynamic vegetation and prescribed pre-industrial lakes from pidVdL.
- mHdL: prescribed pre-industrial vegetation from pidVdL and dynamic lakes.
- mH: prescribed pre-industrial vegetation and lakes from pidVdL.

The prescribed pre-industrial lake and vegetation fractions are derived by averaging the last 150-year of the pidVdL control simulation. Dynamic lakes are considered only for the endorheic catchments over northern Africa. Lakes in other regions are all prescribed from the pidVdL simulation. The individual mid-Holocene simulations are run until the lake and vegetation fraction over northern Africa have reached a close-to-equilibrium state (Fig. B.11). To derive robust results, the individual mid-Holocene simulations have an evaluation period of 100 or 150 years, depending on the variability of the lakes and vegetation in the Sahel and Sahara (Fig. B.11: white part). The individual and synergistic effects of the dynamic lakes and the dynamic vegetation on the precipitation over northern Africa is investigated by applying the following factor analysis:

$$P_{mHdVdL} - P_{mH} = \delta P_{dV} + \delta P_{dL} + \delta P_{syn} \tag{B.1a}$$

$$\delta P_{dV} = P_{mHdV} - P_{mH} \tag{B.1b}$$

$$\delta P_{dL} = P_{mHdL} - P_{mH} \tag{B.1c}$$

$$\delta P_{syn} = P_{mHdVdL} + P_{mH} - P_{mHdV} - P_{mHdL} \tag{B.1d}$$

Where $P_{mHdVdL} - P_{mH}$ is the net precipitation response due to the influence of both, dynamic lakes and vegetation. δP_{dV} and δP_{dL}, respectively, represent the linear precipitation response to dynamic vegetation only (pure vegetation contribution) and dynamic lakes only (pure lake contribution). Finally, δP_{syn} is the non-linear precipitation response due to synergies of the dynamic vegetation and dynamic lakes.

Finally, we take into account that the simulated dynamic lakes change not only in their extent, but also in their depth. Previous simulation studies only focus on

the climate effect from changes in the lake extent and not from changes in the lake depth. Therefore, we conduct an additional mid-Holocene simulation with a prescribed pre-industrial lake and vegetation extent, but a constant 10 m lake depth to investigate the effect of the lake depth changes on the mid-Holocene climate over northern Africa:

- mH10L: prescribed pre-industrial vegetation and prescribed pre-industrial lakes with a constant 10 m lake depth.

In all the described simulations, the lake depth is represented as pure mixed-layer. The simulation with a 10 m lake depth is compared to the mH simulation with an overall small lake depth (taken from the pidVdL reference simulation). In the results, we will show that understanding the effect of lake depth changes, in particular of Lake Chad, is essential to also understand the individual and synergistic effect of the mid-Holocene climate over northern Africa.

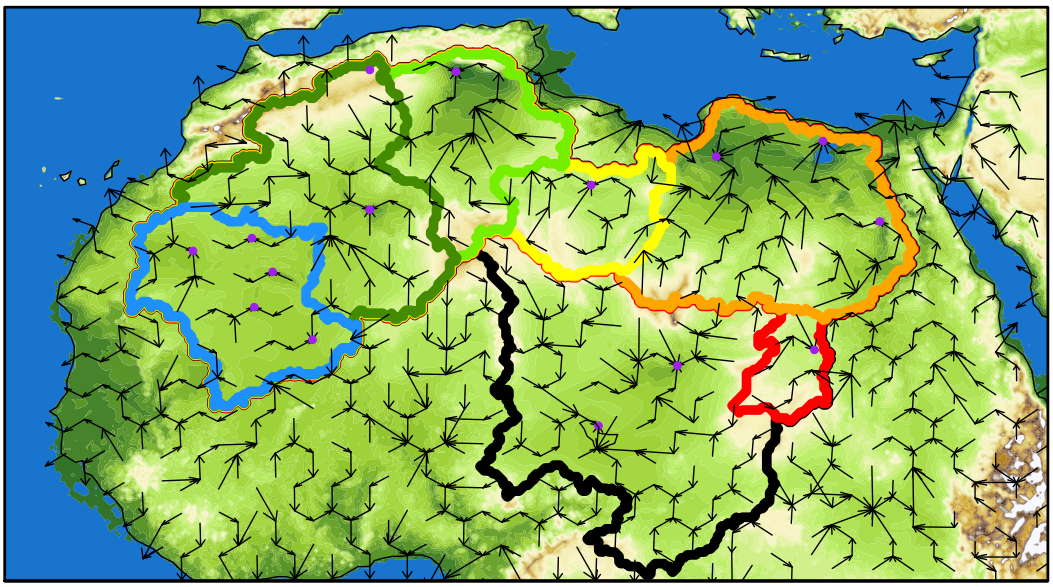

Figure B.1: River flow directions (arrows) used as boundary conditions to simulate the down-slope water transport within each endorheic catchment (colored outlines) to the internal drainage points (purple dots). The digital elevation model represents the topography in the background.

B.2.1 *DYNAMIC ENDORHEIC LAKE MODEL*

The Sahara mainly consists of endorheic catchments, i. e. closed catchments without an outlet (Fig. B.1: colored outlines). Within the endorheic catchment, surface runoff and sub-surface drainage flow down-slope into orographic depressions, hereafter referred to as internal drainage grid cells, at which lakes form (Fig. B.1: symbolized by purple dots). The HD model simulates the down-slope flow to these internal drainage grid cells, and the DEL model is embedded into the HD model

of the ICON-ESM (Hagemann & Duemenil, 1998; Hagemann & Dümenil, 1997; Hagemann & Gates, 2001). The HD model is a river routing model that runs on the same resolution as the land component JSBACH4, which is ~160 km for this study.

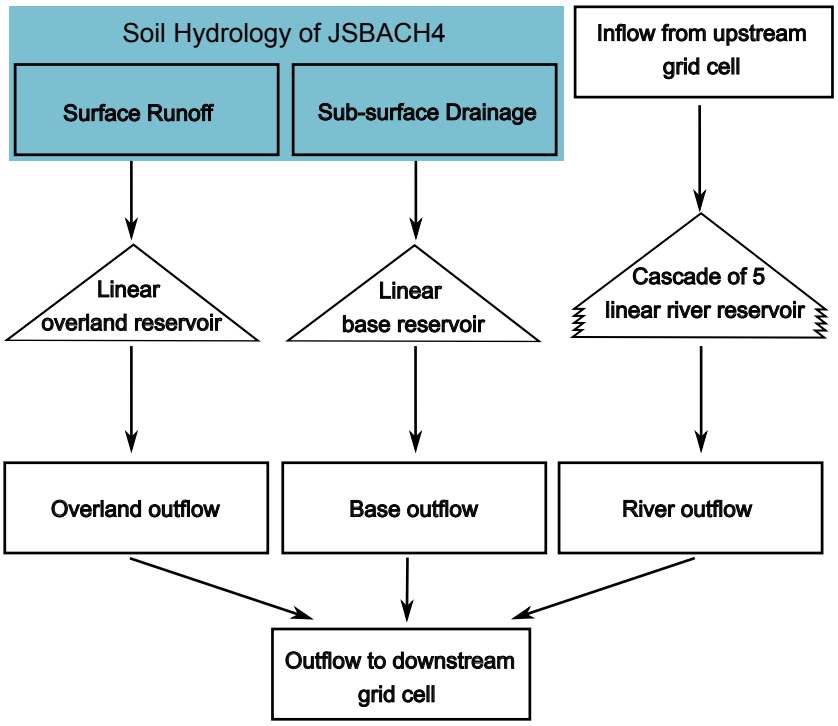

Figure B.2: Structure of the HD model and inputs from the soil hydrology in blue (adapted from Hagemann & Duemenil, 1998).

The HD model includes an overland flow, base flow and river flow (Fig. B.2). These flows are calculated based on the linear reservoir concept, which assumes a time-constant retention time k of water in a reservoir and, thus, a linear relation between the reservoir water storage $S(t)$ and the water outflow $Q(t)$ from that reservoir (e. g. Kang et al., 1998):

$$Q(t) = \frac{S(t)}{k} \tag{B.2}$$

The comparably fast retention time ($k < 1$ day) for the overland flow and the river flow of the HD model is derived from the local slope of the orography. The retention time for the slower base flow is set to a constant value of 300 days.

The water inflow to the HD model is given by the surface runoff for the overland reservoir and by the sub-surface drainage for the base reservoir (Fig. B.2). The k-dependent outflow from the overland and base reservoir is transported to the river reservoir of the neighboring downstream grid cell (Fig. B.2). The river reservoir is a cascade of 5 linear sub-reservoirs that all have the same retention time. After the water has passed the linear river reservoir cascade, the outflow from this reservoir is transported further downstream to the river reservoir of the next neighboring

grid cell. In this way, the discharge water flows down-slope until it reaches either an internal drainage grid cell (Fig. B.1: purple dots) or a coastal grid cell.

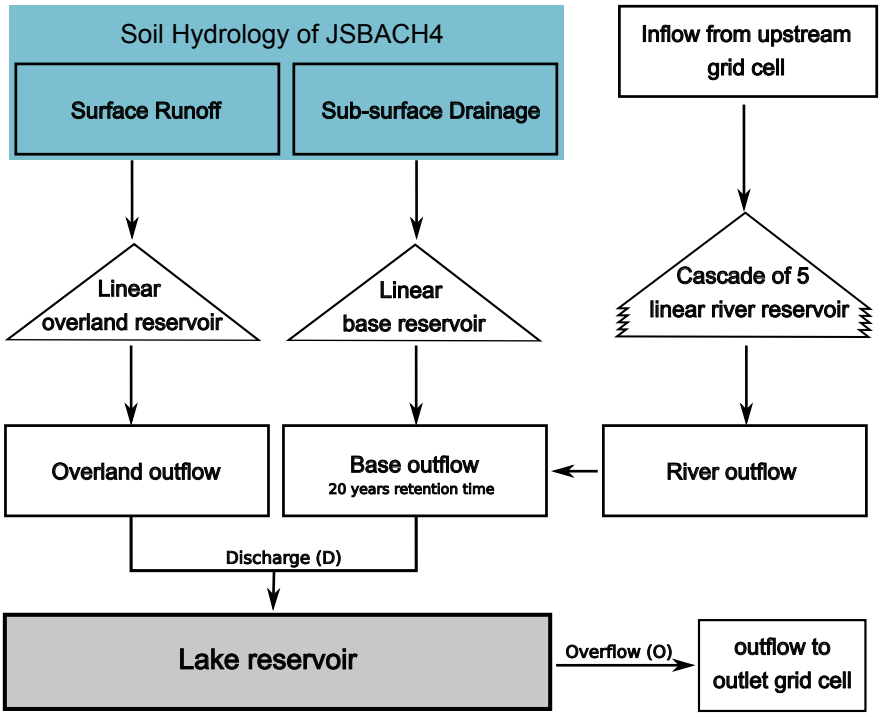

Figure B.3: Structure of the HD model at the internal drainage point and the embedded endorheic lake reservoir with its inflow from and outflow to the HD model (gray box), same as the inputs from the soil hydrology (blue box) (adapted from Hagemann & Duemenil, 1998).

At the internal drainage grid cells, discharge water enters the local lake reservoir (Fig. B.3). In the Sahel and Sahara, most of the discharge water is transported by a sub-surface flow to the groundwater reservoir. E. g. in the Chad watershed, about ~70% of the seasonal discharge contributes to the sub-surface groundwater reservoir (and soil moisture) and less than 30% of the seasonal discharge directly flows into surface storage of the Lake Chad (Pham-Duc et al., 2020). The Quaternary groundwater aquifer and the above surface storage of Lake Chad exchange water on a much longer timescale, i. e. a time period of about 20–40 years is needed to completely replace the water volume of the Chad lake (as before the Sahelian drought in the 1970s) with water from the Quaternary groundwater aquifer (Bouchez et al., 2016). In the HD model, such a groundwater reservoir is missing. First simulations showed that unrealistic high inter-annual fluctuations in the lake extent occur when the discharge from the river reservoir is added directly to the lake reservoir. To avoid these unrealistic high fluctuations, the outflow from the river reservoir is added to the base reservoir at the internal drainage grid cells and the retention time of this base reservoir is set to 20 years (Fig. B.3). This 20-year period mimics the residence time of water in the Quaternary groundwater aquifer before it enters the Lake Chad (Bouchez et al., 2016). We use this 20-year residence time as rough

approximation for all internal drainage grid cells within the Saharan endorheic catchments (see Sec. B.2.1.1).

The lake volume changes ΔV_{lake} of the DEL model are described by:

$$\Delta V_{lake} = (D - O + f_{lake}(P - E_{lake}) + Fin_{lake} - Fout_{lake}) \cdot \Delta t \tag{B.3}$$

D represents the discharge water at the internal drainage grid cell given by the HD model (Fig. B.3). O is the lake water outflow that is returned to the HD model at the outlet point of the respective basin (Fig. B.3). This overflow only occurs when the lake level exceeds the outlet height of the lake basin, that is, when the maximum basin volume $V_{lake,max}$ within a grid cell is exceeded. f_{lake} represents the lake fractions of the grid cell that directly interact with the atmosphere through precipitation P and evaporation E_{lake}. The evaporation over the lake surface is assumed to be equal to the potential evaporation that depend on the surface temperature and surface roughness of the lake. $Fout_{lake}$ and Fin_{lake} describe the lateral lake water flow between neighboring grid cells of the same basin. This lateral lake water flow compensates lake level differences between all grid cells of the same lake basin or sub-basin.

The lateral lake water flow between neighboring grid cells depends on the absolute lake level height H_{dyn} of each grid cell, which is the sum of the orographic minimum elevation or bottom point of a grid cell $H_{oro,min}$ and the lake level H_{lake} above this bottom point:

$$H_{dyn} = H_{oro,min} - H_{lake} \tag{B.4}$$

While $H_{oro,min}$ is given by fixed boundary conditions, H_{lake} is derived by using a lookup table that describe the lake volume-area-height relation for each grid cell at 1 % lake fraction intervals see (Sec. B.2.1.2). The lake level and lake area for a given lake volume is derived by linear interpolation between the intervals of this lookup table. The lookup table intervals are set to 1 % lake fraction intervals to avoid lake fraction errors of >1 % for a given lake volume per ICON grid cell.

To accurately represent the lake water flow between neighboring grid cells with regard to the basin and sub-basin orography, the maximum ridge elevation between each a grid cell and its 3 neighboring lake grid cells ($H_{oro,ridge}$) is required (see Sec. B.2.1.2). $H_{oro,ridge}$ allows the representation of several sub-basins, like the Chad Basin and the Bodélé Depression of the Chad Catchment. E. g. lake water only flows from the present-day Chad lake into the northern Bodélé Depression, when the lake level of the Chad lake exceeds $H_{oro,ridge}$.

Based on H_{dyn} and, $H_{oro,ridge}$ the dynamic flow directions and the flow velocity between grid cells of the same basin are derived. The dynamic flow directions and the corresponding flow velocity depend on the absolute lake level differences, ΔH_{dyn}, between two neighboring lake grid cells:

$$\Delta H_{dyn} = H_{dyn}(up) - H_{dyn}(down) \tag{B.5}$$

$H_{dyn}(up)$ represents the dynamic lake level of the upstream grid cell and $H_{dyn}(down)$ represents the dynamic lake level of the downstream grid cell. ΔH_{dyn} is recalculated at each time step.

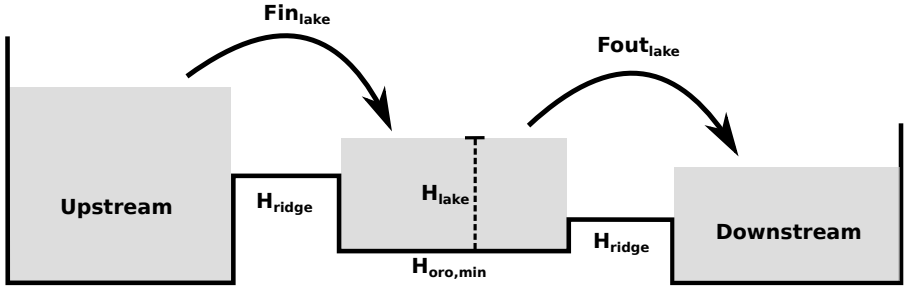

Figure B.4: Structure of the lateral flow of the DEL model.

The flow velocity is derived by using the Manning-Strickler equation, which describes an open channel flow (Strickler, 1981):

$$v_{lake} = k_{st} \cdot \Delta H_{dyn}{}^{2/3} \cdot \left(\frac{\Delta H_{dyn}}{\Delta x}\right)^{0.5} \tag{B.6}$$

$$F_{lake} = \max\left(V_{lake} \cdot \frac{v_{lake}}{\Delta x}, \frac{V_{lake}}{\Delta t}\right) \tag{B.7}$$

v_{lake} is the flow velocity between two neighboring grid cells. k_{st} $[m^{1/3}s^{-1}]$ is the roughness coefficient according to Strickler, which is a measure for the wall roughness of the channel flow (Strickler (1981): page 10-12). k_{st} is set to a constant value of $k_{st} = 100$, which refers to a fast flow over smooth concrete. By setting this high value, we assume that lake level differences between neighboring grid cells are equalized on a short timescale. Δx is the distance between the center points of two neighboring grid cells. V_{lake} is the lake water volume of the upstream grid cell and Δt is the integration time step of the model. The lateral lake flow, F_{lake}, represents the lake water inflow Fin_{lake} of the downstream grid cell and the lake water outflow $Fout_{lake}$ of the upstream grid cell in Eq. B.3.

Finally, the fixed lakes in JSBACH4 are represented by a mixed layer of 10 m depth. The dynamic lakes of the DEL model in JSBACH4 have a dynamic mixed-layer depth equal to the actual lace level H_{lake}, in which a minimum depth of 1 m is applied. This dynamic mixed-layer depth affects the surface temperature of the lakes and, thus, the evaporation over the lake surface.

B.2.1.1 *BOUNDARY CONDITIONS FOR THE HD MODEL*

The flow directions and reservoir retention times for the HD model are generated using the MPI-DynamicHD model version 1.3 (Riddick et al., 2018). The MPI-DynamicHD model requires a 10′ orography and the location of the internal

drainage gird cells as input data. These input data are derived from a 30″ digital elevation model (DEM) and endorheic catchment outlines of the HydroSHEDS data set (Hydrological data and maps based on SHuttle Elevation Derivatives at multiple Scales) that are regridded to a 10′ resolution (Lehner & Grill, 2013).

The internal drainage grid cells are defined as bottom points of a lake basin or sub-basin. To derive these internal grid cells, the local minimum with the lowest elevation within each ICON grid cell is selected using a finer 10′ orography. Subsequently, the basins of these local minima are flooded, starting with the local minimum of the lowest elevation. The orography around the local minimum is flooded until (1) the boundaries of the endorheic catchment is reached or (2) the next downstream lake basin is reached or (3) the flooding height is below the elevation of the respective local minimum. After all local minima and their basins are flooded, only the largest basin and all smaller downstream basins within an endorheic catchment are selected. Additionally, the basin of a local minimum have to be at least 20 % of the area of an ICON grid cell. Since large basins might contain several sub-basins, all local minima within a basin are considered that are at least as large as an ICON grid cell. The minimum basin and sub-basin area is set in a way that the MPI-DynamicHD model generated reasonable flow direction on the coarse R2B4 ICON resolution (˜160 km: Fig. B.1: black arrows).

After processing the flow directions and the retention times with the MPI-DynamicHD model, the retention times of the base flow reservoirs at the internal drainage grid cells are set to 20 year, as mentioned in section B.2.1. This reduces unrealistic high fluctuations in the simulated lake inflow so that the lake size becomes less sensitive to the inter-annual precipitation variability.

B.2.1.2 *BOUNDARY CONDITIONS FOR THE DEL MODEL*

The DEL model requires (1) the minimum geographic height for each grid cell ($H_{oro,min}$), (2) a lake level-area-volume lookup table for each grid cell (H_{lake} and f_{lake}), (3) the minimum ridge height to the 3 neighboring grid cells ($H_{oro,ridge}$) and (4) the maximum lake volume ($V_{lake,max}$) and the lake basin outlet point to simulate the overflow of a flooded basin. All these boundary conditions are derived from a 30″ digital elevation model (DEM) and endorheic catchment outlines of the HydroSHEDS data set that are regridded to a 10′ resolution (Lehner & Grill, 2013).

The minimum geographic height ($H_{oro,min}$) for each grid cell is derived by identifying the minimum elevation within each coarse resolution ICON grid cell using a finer 10′ orography. The lake level-area-volume lookup table is derived by gradually flooding the 10′ orography within each ICON grid cell, starting at the point of minimum geographic height. And the minimum ridge height to the 3 neighboring grid cells ($H_{oro,ridge}$) is derived by flooding the 10′ orography starting at the point of minimum elevation of the current ICON grid cell until the point of minimum elevation of the neighboring ICON grid cell is reached. The maximum elevation point of this flooding process is set as minimum ridge height for the corresponding neighboring grid cell.

The maximum lake volume and lake basin outlet points, used to simulate the overflow of a lake basin, are derived based on the internal drainage grid cells and 10′ orography described in Sec. B.2.1.1. The outlet point of each lake basin is

derived by flooding 10′ orography starting at the internal drainage grid cells. The 10′ orography is flooded until the first ICON grid cell that lies outside the lake basin is reached. This ICON grid cell is set as outlet grid cell. The maximum lake volume for each grid cell is derived from the different between the outlet height and the 10′ orography.

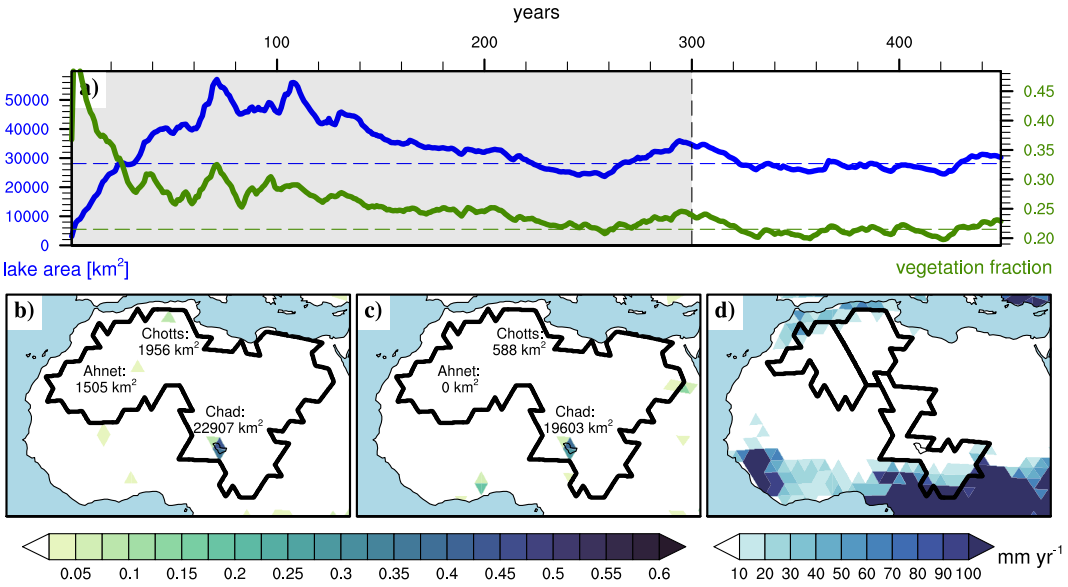

Figure B.5: Time series of the simulated pre-industrial (a: blue line) lake area of the Saharan endorheic catchments and (a: green line) vegetation cover averaged over northern Africa (20 °W-35 °E,10 °N-35 °N). Pre-industrial 150-year mean lake cover fraction of (b) the piVdLd simulation and (c) the observation-based HydroLAKES data (Messager et al., 2016). The simulated pre-industrial (c) mean runoff and drainage shows from which catchment region Lake Chad, Ahnet and Chotts receive most of the discharge water.

B.3 RESULTS

The pidVdL simulation is run for 450 year, in which the lake and vegetation cover over northern Africa reach a close-to-equilibrium state after about 300 years (Fig. B.5a: gray part). The last 150 years of the simulation are used as evaluation period (Fig. B.5a: white part).

The simulated surface area of Lake Chad from pidVdL is about 3.304 km^2 (~16.9%) larger than the observation-based surface area of Lake Chad from the HydroLAKES data (Fig. B.5 b-c). A surface deviation of 16.9% is relatively small, since Lake Chad is characterized by a wide and shallow basin. Accordingly, small changes in the water budget already lead to comparatively large changes in the surface extent. For example, a drought in the 1970s and 1980s reduced the surface area of Lake Chad by about 90% (e. g. Olivry et al., 1996), from about 20.000 km^2 (1950-1972) to less than 2.000 km^2 (1980s) (e. g. Bouchez et al., 2016; Pham-Duc et al., 2020). Considering this large changes in the surface extent, we conclude that

the HD-DEL model properly simulates the pre-industrial equilibrium state of Lake Chad.

The simulated surface area of Lake Ahnet and Lake Chotts from pidVdL is overestimated by about 1.957 km^2 and 2.165 km^2 in comparison to the HydroLAKES data (Fig. B.5 b-c). Both lakes receive most of their water inflow through runoff and drainage from the Atlas Mountains in the northwestern region of Africa (Fig. B.5 d). The overestimated water inflow from the Atlas Mountains is likely due to the coarse resolution of the ICON-JSBACH4 model which causes an inaccurate representation of the catchment's watershed, as well as an inaccurate representation of the small-scale heterogeneous precipitation from orographic updrafts.

Other simulated lakes from pidVdL, that are surrounded by a flatter terrain, are in better agreement with the HydroLAKES data (Fig. B.5 b-c). This includes lakes in the northwestern Sahara, whose surface extent is less than 2.5% of an ICON grid cell (Fig. B.5b). Similarly, simulated lakes that border mountains that render less orographic-forced precipitation are in better agreement with the HydroLAKES data. E. g. Lake Chad mainly receives most of its discharge water from the southern part of the catchment, rather than from the Ahaggar and Tibesti Mountains in the north (Fig. B.5 d). Satellite observations show that >90% of the discharge water of Lake Chad is provided by the Chari/Logone river system in the southern part of the catchment (e. g. Pham-Duc et al., 2020).

Thus, the HD-DEL model accurately simulated the pre-industrial surface extent of Saharan lakes (like Lake Chad), except for lakes adjacent to mountains that receive most of their discharge water from orographic-forced precipitation.

B.3.1 *MID-HOLOCENE PRECIPITATION, LAKE AND VEGETATION CHANGES*

Comparison between mHdVdL and pidVdL show that the mid-Holocene forcing (orbit, GHGs, SST and SIC) and the simulated mid-Holocene lakes and vegetation extent cause a dipole like "wet-north-dry-south" precipitation response around 10 °N (Fig. B.6a). These dipole-like precipitation changes represent a rain belt northward shift of the West African summer monsoon. Along with the precipitation increase north of 10 °N Lake Chad and some smaller Lakes in the western Sahara expand (Fig. B.6b). The vegetation increases mainly over the Sahel (12 °N-18 °N) and over the western Sahara, similar to the pattern of precipitation increase (Fig. B.6a,c).

In general, the ICON-JSBACH4 model underestimates the mid-Holocene precipitation increase and the lake and vegetation extent over northern Africa (Fig. B.6). The precipitation in the mHdVdL simulation increases by about 100-200 mm $year^{-1}$ in the central Sahara (Fig. B.6a: 18 °N-35 °N), while reconstruction suggest an increase of about 200-600 mm $year^{-1}$ (Bartlein et al., 2011; Braconnot et al., 2012). Similarly, the simulated extent of lakes in the Sahel and Sahara (Fig. B.6b) is much smaller than suggested by sediment reconstructions (Drake et al., 2022; Hoelzmann et al., 1998; Quade et al., 2018). For example, Lake Chad extends mainly on its southern side, while only little water overflows into the northern Bodélé Depression, which results in an underestimated northward extension of Lake Chad (Fig. B.6b). The simulated extent of the Saharan vegetation (Fig. B.6c) is underestimated as

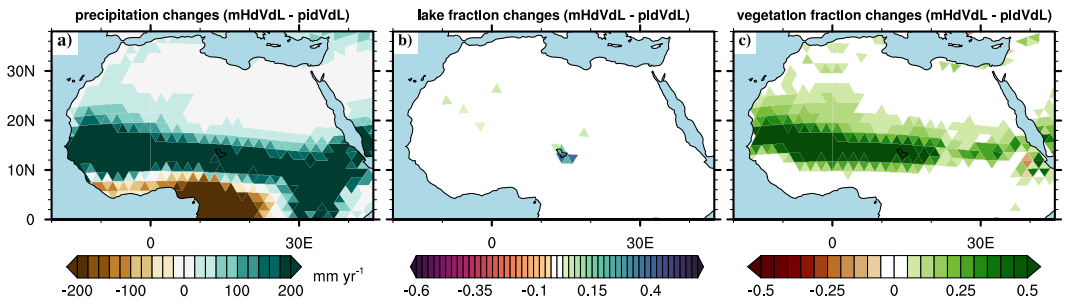

Figure B.6: Simulated mid-Holocene (a) annual precipitation changes, (b) lake fraction changes and (c) vegetation cover changes compared to the pre-industrial simulation (mHdVdL-pidVdL).

well, in comparison to reconstructions (Hély & Lézine, 2014; Hoelzmann et al., 1998; Lézine, 2017) and in comparison to climate models that produce a more humid climate over northern Africa (e. g. Dallmeyer et al., 2021).

The too dry mid-Holocene climate over northern Africa is a known issue of the ICON-JSBACH4 model (Schneck et al., 2022) and some other state-of-the-art climate models (Braconnot et al., 2012). The simulated mid-Holocene lake and vegetation extent likely is much larger in some wetter models, like the MPI-ESM (Max-Planck Institute - Earth System Model) (Dallmeyer et al., 2021). In the ICON-JSBACH4 model, the presence of a dynamic lake does not diminish the dry bias of the model. But to what extent do dynamic lakes contribute to a greener Sahara? In the following, we analyze the individual and synergistic contributions of dynamic lakes and a dynamic vegetation to the mid-Holocene precipitation increase.

B.3.2 *MID-HOLOCENE PRECIPITATION RESPONSE TO DYNAMIC LAKES AND VEGETATION*

The net precipitation changes (mHdVdL-mH) caused by the dynamic interaction between the West African summer monsoon, lakes and vegetation (Fig. B.7a) contributes only little to the overall mid-Holocene precipitation increase over northern Africa (Fig. B.6a). The net precipitation changes show a northward shift of the West African summer monsoon, with a precipitation decrease south of 10 °N and a precipitation increase north of 10 °N (Fig. B.7a). Enhanced precipitation occurs over Lake Chad and in the western Sahel and Sahara.

The factor analysis shows that the dynamic vegetation alone (δP_{dV} pure vegetation contribution) causes a higher precipitation increase over the Sahel and western Sahara (Fig. B.7b) than dynamic lakes and vegetation together, i. e. the net precipitation changes (Fig. B.7a). Similarly, the dynamic lakes alone (δP_{dL} pure lake contribution) cause a precipitation increase over the Chad Lake (Fig. B.7c) that is slightly higher than net precipitation changes (Fig. B.7a). The sum of both, the pure vegetation contribution δP_{dV} and the pure lake contribution δP_{dL}, is higher than the net precipitation changes from dynamic lakes and vegetation together.

Accordingly, the non-linear synergistic contribution (δP_{syn}) shows a negative precipitation response across the Sahel and Sahara (Fig. B.7d). This precipitation

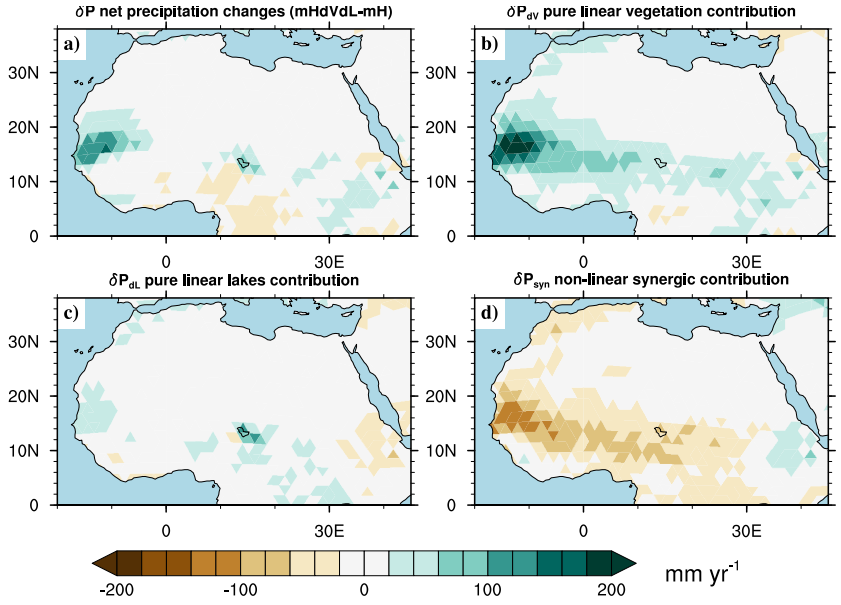

Figure B.7: Simulated mid-Holocene (a) precipitation changes due to the influence of dynamic lakes and dynamic vegetation (δP: mHdVdL-mH). Simulated mid-Holocene precipitation changes caused (b) by dynamic vegetation only (δP_{dV}: mHdV-mH), (c) by dynamic lakes only (δP_{dL}: mHdL-mH), and (d) by vegetation-lake synergies (δP_{syn}: mHdVdL+mH-mHdV-mHdL). The factor analysis of the mid-Holocene precipitation changes due to lakes and vegetation changes is given by: mHdVdL-mH = δP_{dV} + δP_{dL} + δP_{syn}.

decrease is similar in pattern, but opposite in sign, as the precipitation changes δP_{dV} caused by the dynamic vegetation alone (Fig. B.7b). Results show that the dynamic vegetation extent and the dynamic lake extent only differ marginally between the individual mid-Holocene simulations (Fig. B.11). Thus, the area-wide precipitation decrease of the non-linear synergistic contribution must come from some other sources than pure changes in the lake and vegetation extent.

Additional experiments suggest that the major source for the area-wide precipitation decrease from the non-linear synergistic lake-vegetation interaction relates to differences in the surface temperature of Lake Chad relative to its surrounding environment. To explain this mechanism, we first show in an additional experiment how the deepening of Lake Chad induces a lake surface cooling that causes an overturning circulation response above the lake and a large-scale precipitation increase over the Sahel and western Sahara. Thereafter, we show that this circulation and precipitation response is reversed when the vicinity of Lake Chad is widely covered with vegetation (as it is the case in mHdVdL simulation).

To show the influence of a deepening of Lake Chad, we conduct a mid-Holocene simulations similar to mH, but with a deeper 10-m mixed-layer depth. Comparison between the mH10L and mH experiment shows that a deepening of Lake Chad by about 1-5 m (Fig. B.8a) causes an area-wide precipitation increase across northern Africa (Fig. B.8b). This includes a precipitation increase over the Sahel (12 °N-18 °N) and over the western Sahara (Fig. B.8b). A minor drying response is visible at the western coast south of 10 °N Fig. B.8b).

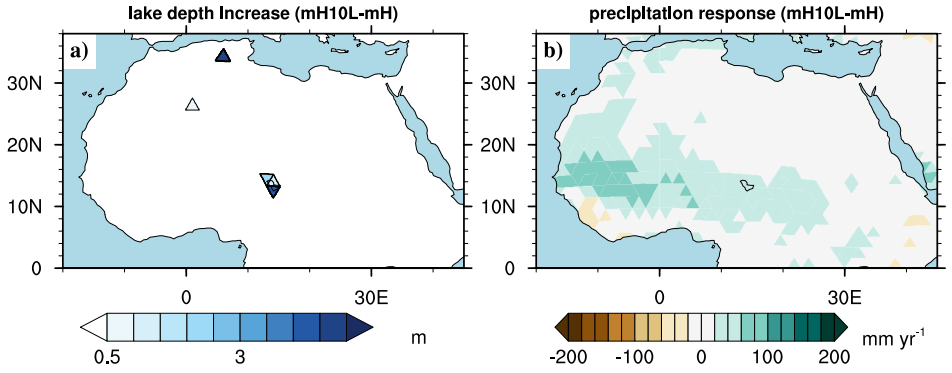

Figure B.8: Differences in the (a) lake depth between the mid-Holocene simulation with a constant 10 m mixed-layer lake depth and the simulation with a mixed-layer lake depth as simulated in the pre-industrial reference simulation (mH10L - mH). Simulated (b) precipitation response to the increased mixed-layer lake depth.

The precipitation changes from the deepening of Lake Chad are primarily caused by a decrease in the lake surface temperature (Fig. B.9e). In the ICON-JSBACH4 model, lakes are represented as a mixed layer with a constant surface albedo of 0.07. By increasing the lake depth, the heat capacity of Lake Chad increases, which lowers the surface temperature of the lake relative to its surrounding environment (Fig. B.9e).

The decrease in surface temperature causes an overturning circulation response above Lake Chad in the lower to mid-troposphere (Fig. B.9c: 1000-600 hPa). The surface cooling leads to descending motions and to a near surface divergence above Lake Chad (Fig. B.9c). In the warmer vicinity north (20 °N) and south (8 °N) of Lake Chad, the moist air rises and converges again into a low pressure response above Lake Chad (Fig. B.9c). This overturning circulation causes a near-surface divergence and, thus, a near-surface high pressure response and a mid-troposphere convergence and, thus, mid-troposphere low pressure response above Lake Chad (Fig. B.9c).

The mid-troposphere low pressure response causes, by Coriolis force, a westerly wind acceleration south and an easterly wind acceleration north of Lake Chad (Fig. B.9a). This dipole response is associated with a northward shift of the African Easterly Jet (AEJ) and, thus, northward extent of the monsoon rain belt. Along with the monsoon northward shift, increased convection occurs at the southern side of Lake Chad (Fig. B.9c). This increased convection is likely caused by enhanced near-surface moisture convergence at 8 °N (south of Lake Chad) where the monsoon southwesterly wind (Fig. B.10a: 10 °N) and lake-induced northerly winds meet (Fig. B.9c): 10 °N). The near-surface moisture convergence and convection aloft cause the release of latent heat, which causes deep convection through the whole troposphere to the south of Lake Chad (Fig. B.9c).

The increased convection south of Lake Chad enhances the moisture flux of the near-surface southwesterly monsoon winds (Fig. B.10). The near-surface southwesterly winds of the monsoon system transport moisture from the Atlantic Ocean

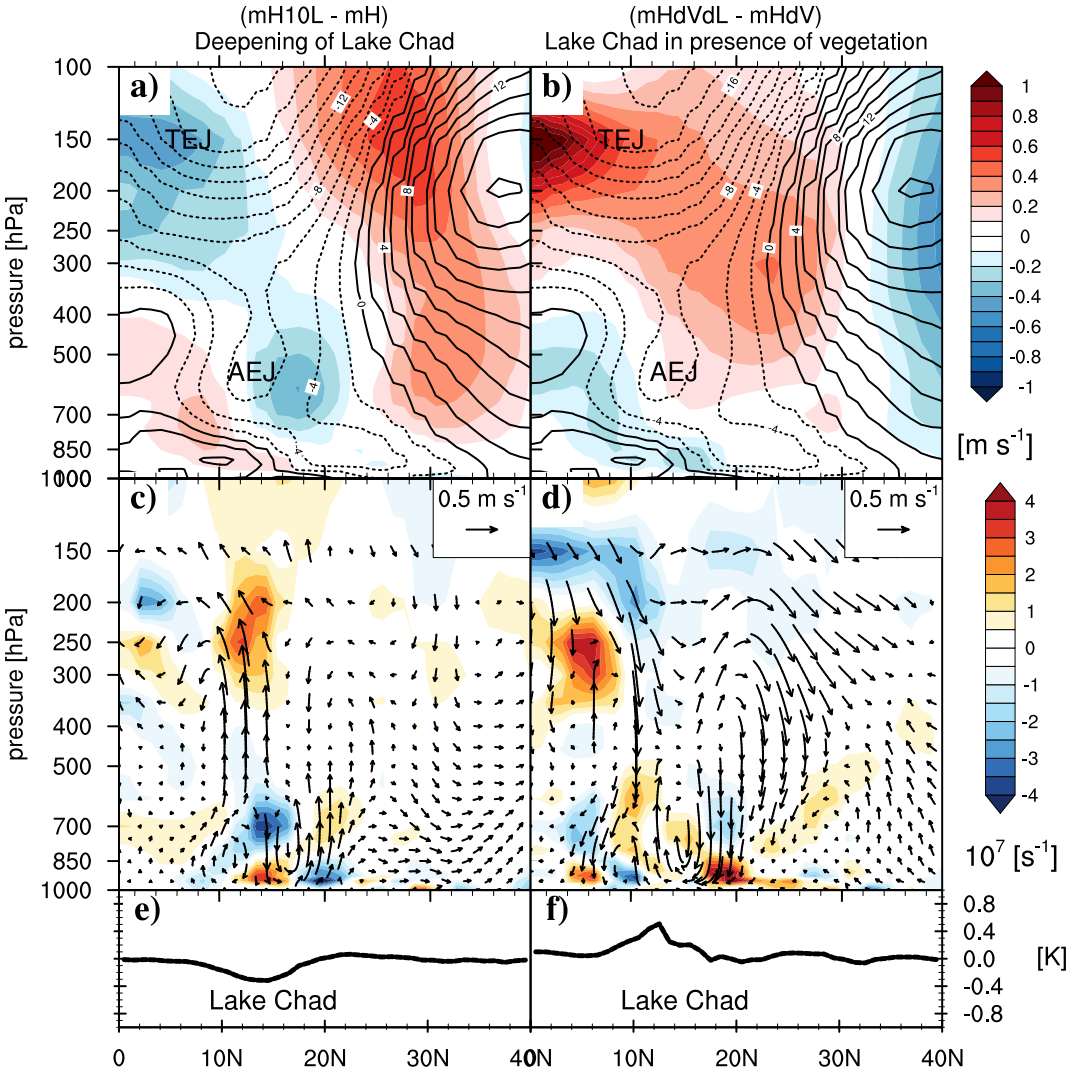

Figure B.9: Mid-Holocene summer (JJAS) circulation response zonally averaged over 10 °N-20 °N (left panel) to a pure deepening of Lake Chad as shown in Fig. B.9a and (right panel) to a deepening (and extent) of Lake Chad in the presence of vegetation as shown in Fig. B.6b-c. The upper panel (a,b) shows the zonal wind response to the lake changes (colored shades) and the zonal wind climatology of the respective reference simulation (mH, mHdV: black contours). The middle panel (c,d) shows the vertical and meridional wind response (arrows) and divergence response (colored shades) to the lake changes. The vertical wind component was re-scaled (multiplied by 1000) for visibility reasons. The lower panel (e,f) shows the surface temperature response to the lake changes.

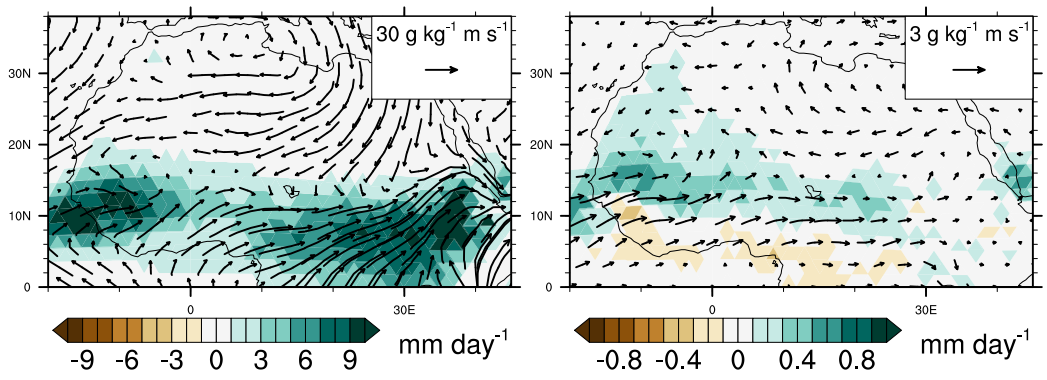

Figure B.10: Mid-Holocene summer (JJAS) (a) moisture flux (arrows) and precipitation (colored shades) of the mH simulation and (b) the moisture flux and precipitation response to a deepening of Lake Chad (mH10L-mH).

to the African continent during the summer months (Fig. B.10a). The convection increase south of Lake Chad enhances the moisture flux of the near-surface southwesterly monsoon winds (Fig. B.10b). Particularly, the westerly wind component shows an increased moisture flux south of Lake Chad and upstream in the western Sahel and Sahara. This upstream increase of the westerly moisture flux explains the area-wide precipitation increase across the Sahel and western Sahara induced by the deepening of Lake Chad.

This precipitation response and the circulation response to a deepening and surface expansion of Lake Chad is reversed, though, when the Sahel is widely covered with vegetation (Fig. B.9: right). The major reason for this is that the vegetation cools the land surface stronger than Lake Chad (Fig. B.9f). Accordingly, the overturning circulation response is reversed (Fig. B.9d) and the West African summer monsoon is shifted to the South (Fig. B.9b). The reversal of the surface temperature response due to the presence of vegetation and the associated reversal of the circulation response likely is the primary reason for the negative non-linear synergistic precipitation contribution in the factor analysis (Fig. B.7d).

B.4 CONCLUSIONS AND DISCUSSION

Our results show that the DEL model realistically simulates the pre-industrial extent of Lake Chad and the presence of some dry basins over northern Africa. Only the extent of Lake Ahnet and Lake Chotts, which receive most of their discharge from the Atlas Mountains, is overestimated by about 1.957 km^2 and 2.165 km^2. The overestimated lake extent of both lakes likely is caused by the coarse resolution of the simulation. The coarse resolution limits the accurate representation of the catchment boundaries and the accurate representation of the small-scale heterogeneous precipitation from orographic updrafts, as it occurs in the Atlas Mountains.

Additionally, the DEL model only mimics the effect of an aquifer reservoir to avoid unrealistic high inter-annual fluctuations in the lake depth and lake

extent. In the HD model, though, a comprehensive aquifer model that interact with the overlying dynamic lakes is missing. Yet, reconstructions indicate a complex interaction between endorheic lakes and the underlying aquifer reservoirs (Lézine et al., 2011a). This interaction causes, for example, a 3000-year time-lag between the orbital-forced summer insolation maximum and the maximum lake extent, because the aquifers over northern Africa filled during the early Holocene and recharged the overlying lakes during the mid-Holocene and towards the end of the African Humid Period (Lézine et al., 2011a). This interaction is not explicitly simulated by the DEL and HD model. Therefore, we assume that the DEL model is likely not suitable for transitional simulations, like the simulation of the delayed lake decline over northern Africa at the End of the African Humid Period. But our results indicate that the DEL model realistically simulates the mean state of the endorheic lakes over northern Africa with regard to the terrestrial water balance.

In the mid-Holocene simulation, the lake extent over northern Africa is generally underestimated. For example, the simulated Lake Chad expands primarily on its southern side, while too little overflow into the Bodélé Depression results in a too small northward expansion of Lake Chad compared to sediment-based reconstructions (Drake et al., 2018; Hoelzmann et al., 1998; Quade et al., 2018). The underestimated mid-Holocene lake extent mainly relates to a known dry bias over northern Africa simulated by the ICON-ESM (Schneck et al., 2022). Climate models that produce a more humid mid-Holocene climate over northern Africa, like the MPI-ESM (e. g. Dallmeyer et al., 2021), potentially simulate a much larger vegetation and lake extent over northern Africa, and along with that a stronger deepening of the mid-Holocene lakes. The underestimated northward extent and deepening of the simulated mid-Holocene lakes by the ICON-JSBACH4 model likely affect the simulated precipitation response over the Sahel and Sahara.

An idealized mid-Holocene simulation reveals that a pure deepening of Lake Chad by about 1-5 m causes an area-wide precipitation increase across the Sahel and western Sahara. Enhancing the depth of Lake Chad increases the heat capacity of the lake, which leads to a surface cooling. The surface cooling induces an overturning lake-land circulation response that shifts the West African summer monsoon northward and that increases the moisture flux from the tropical Atlantic to the dry African interior. This sensitivity of the monsoon system to changes in the lake depth was neglected by previous simulation studies, which only consider changes in the lake extent (Broström et al., 1998; Carrington et al., 2001; Chandan & Peltier, 2020; Coe & Bonan, 1997; Krinner et al., 2012). The mid-Holocene lake depth increase and corresponding surface cooling likely play an important role in the interaction between the West African summer monsoon, lakes and vegetation.

A factor analysis shows that the mid-Holocene interaction between the West African summer monsoon, lakes and the vegetation contributes only little to the overall mid-Holocene precipitation increase over the Sahel and western Sahara. The mid-Holocene vegetation expansion and the mid-Holocene lake expansion individually cause a precipitation increase over northern Africa. The individual precipitation increase from a dynamic vegetation alone and from dynamic lakes alone is, in the sum, higher than the precipitation increase caused by a combined expansion of dynamic lakes and a dynamic vegetation. Accordingly, the synergistic

vegetation-lake effect during the mid-Holocene causes a broad drying response over the Sahel and western Sahara. The major reason for the drying response is that the vegetation cools the land surface stronger than the simulated mid-Holocene lakes, mainly Lake Chad. This causes a circulation and precipitation response reversed to the one associated with a deepening and surface cooling of mid-Holocene lakes. The drying response from the lake-vegetation interaction is strong enough to almost compensate the precipitation increase caused by the mid-Holocene vegetation expansion alone.

In contrast to previous simulation studies (Krinner et al., 2012), our results suggest that the mid-Holocene lake extent does not cause a positive vegetation feedback over northern Africa. In our simulations, though, the extent and deepening of mid-Holocene lakes is underestimated compared to reconstructions (Drake et al., 2022; Hoelzmann et al., 1998; Quade et al., 2018). Therefore, the surface cooling by the simulated mid-Holocene lakes is likely underestimated, too. A larger lake extent and lake deepening over northern Africa, as it presumably is simulated by some wetter climate models, might cause a positive vegetation feedback if these simulated lakes cool the land surface stronger than the simulated vegetation in the vicinity of these lakes.

In our study, the effect of wetlands and endorheic lakes, like Mega-lake Timbuktu in the Niger River Inland Delta (Drake et al., 2022), is neglected in our study. Wetlands might cause a relatively high evaporation and surface cooling, because this land surface type combines the high surface roughness of the vegetation with the moisture saturated surface of lakes. Thus, a strong cooling effect presumably occurs in the region where wetlands formed, like in the vicinity of Mega-Lake Chad (Hoelzmann et al., 1998). But to gain a more comprehensive understanding on the effect of dynamic wetlands, more research is needed.

In summary, our results show that the accurate simulation of the lake surface temperature and the surface temperature of the surrounding vegetated land plays an essential role in the dynamic interaction between the West African summer monsoon, lakes and vegetation during the mid-Holocene over northern Africa. The surface temperature of the lakes is sensitively influenced by the lake depth. Since the surface temperature of the simulated mid-Holocene lakes in our simulations is higher than the surface temperature of the simulated mid-Holocene vegetation, the dynamic interaction between the atmosphere, lakes and vegetation contribute only little to the overall mid-Holocene precipitation increase.

B.5 ADDITIONAL FIGURES

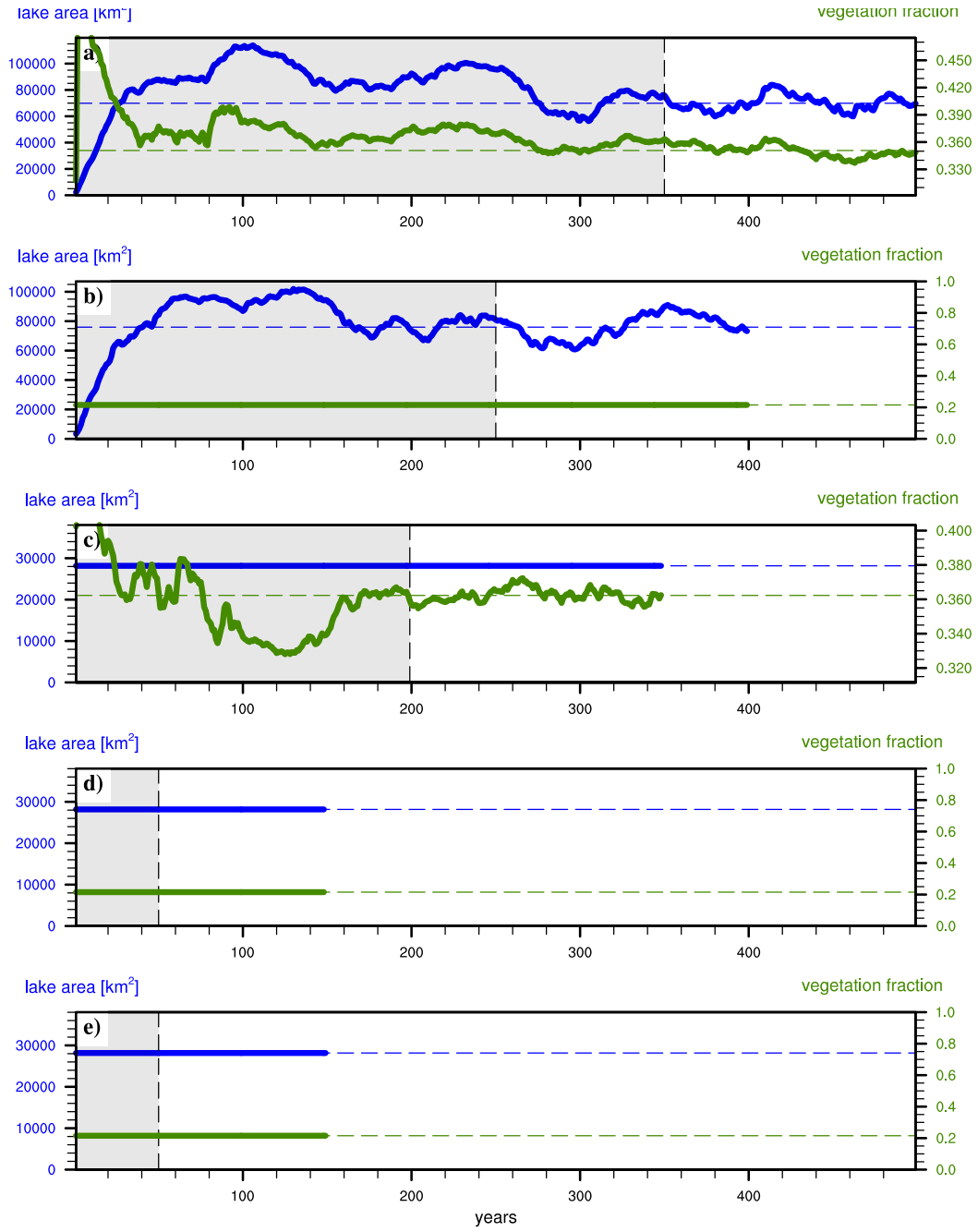

Figure B.11: Time series of mid-Holocene simulation (a) mHdVdL, (b) mHdL, (c) mHdV, (d) mH, and (e) mHL10. The blue line shows the lake area within the endorheic catchments of North Africa and the green line shows the vegetation cover averages over the Sahel and Sahara (20 °E-35 °W,10 °N-35 °N). The time series section with the white background part shows the evaluation period used for the analysis. Depending on the variability of the lake area and vegetation cover, the evaluation period is 100 or 150 year long.

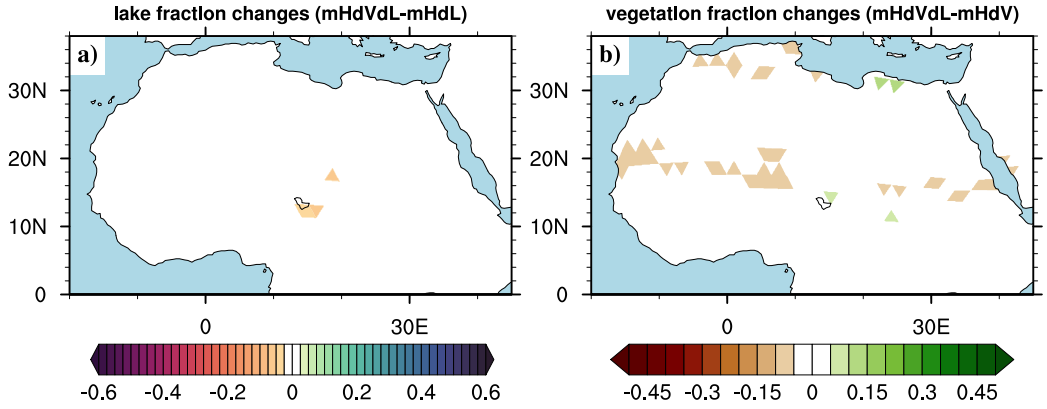

Figure B.12: Simulated (a) mid-Holocene changes of the lake extent due to mid-Holocene changes in vegetation cover (mHdVdL-mHdL) and simulated (b) mid-Holocene changes of in vegetation cover due to mid-Holocene changes in lake extent (mHdVdL-mHdV).

BIBLIOGRAPHY

Bader, J., Jungclaus, J., Krivova, N., Lorenz, S., Maycock, A., Raddatz, T., Schmidt, H., Toohey, M., Wu, C.-J., & Claussen, M. (2020). Global temperature modes shed light on the Holocene temperature conundrum. *Nature Communications*, *11*(1), 4726. https://doi.org/10.1038/s41467-020-18478-6

Bartlein, P. J., Harrison, S. P., Brewer, S., Connor, S., Davis, B. A. S., Gajewski, K., Guiot, J., Harrison-Prentice, T. I., Henderson, A., Peyron, O., Prentice, I. C., Scholze, M., Seppä, H., Shuman, B., Sugita, S., Thompson, R. S., Viau, A. E., Williams, J., & Wu, H. (2011). Pollen-based continental climate reconstructions at 6 and 21 ka: A global synthesis. *Climate Dynamics*, *37*(3-4), 775–802. https://doi.org/10.1007/s00382-010-0904-1

Berger, A. (1978). Long-term variations of caloric insolation resulting from the earth's orbital elements. *Quaternary Research*, *9*(2), 139–167. https://doi.org/10.1016/0033-5894(78)90064-9

Bouchez, C., Goncalves, J., Deschamps, P., Vallet-Coulomb, C., Hamelin, B., Doumnang, J.-C., & Sylvestre, F. (2016). Hydrological, chemical, and isotopic budgets of Lake Chad: A quantitative assessment of evaporation, transpiration and infiltration fluxes. *Hydrology and Earth System Sciences*, *20*(4), 1599–1619. https://doi.org/10.5194/hess-20-1599-2016

Braconnot, P., Harrison, S. P., Kageyama, M., Bartlein, P. J., Masson-Delmotte, V., Abe-Ouchi, A., Otto-Bliesner, B., & Zhao, Y. (2012). Evaluation of climate models using palaeoclimatic data. *Nature Climate Change*, *2*(6), 417–424. https://doi.org/10.1038/nclimate1456

Broström, A., Coe, M., Harrison, S. P., Gallimore, R., Kutzbach, J. E., Foley, J., Prentice, I. C., & Behling, P. (1998). Land surface feedbacks and palaeomonsoons in northern Africa. *Geophysical Research Letters*, *25*(19), 3615–3618. https://doi.org/10.1029/98GL02804

Brovkin, V., Lorenz, S., Raddatz, T., Ilyina, T., Stemmler, I., Toohey, M., & Claussen, M. (2019). What was the source of the atmospheric CO₂ increase during the Holocene? *Biogeosciences*, *16*(13), 2543–2555. https://doi.org/10.5194/bg-16-2543-2019

Carrington, D. P., Gallimore, R. G., & Kutzbach, J. E. (2001). Climate sensitivity to wetlands and wetland vegetation in mid-Holocene North Africa. *Climate Dynamics*, *17*(2-3), 151–157. https://doi.org/10.1007/s003820000099

Chandan, D., & Peltier, W. R. (2020). African Humid Period Precipitation Sustained by Robust Vegetation, Soil, and Lake Feedbacks. *Geophysical Research Letters*, *47*(21). https://doi.org/10.1029/2020GL088728

Chen, W., Ciais, P., Qiu, C., Ducharne, A., Zhu, D., Peng, S., Braconnot, P., & Huang, C. (2021). Wetlands of North Africa During the Mid-Holocene Were at Least Five Times the Area Today. *Geophysical Research Letters*, *48*(20), e2021GL094194. https://doi.org/10.1029/2021GL094194 e2021GL094194 2021GL094194

Coe, M. T., & Bonan, G. B. (1997). Feedbacks between climate and surface water in northern Africa during the middle Holocene. *Journal of Geophysical Research: Atmospheres*, *102*(D10), 11087–11101. https://doi.org/10.1029/97JD00343

Dallmeyer, A., Claussen, M., Lorenz, S., Sigl, M., Toohey, M., & Herzschuh, U. (2021). Holocene vegetation transitions and their climatic drivers in MPI-ESM1.2. *Climate of the Past*, *17*, 2481–2513. https://doi.org/10.5194/cp-17-2481-2021

Drake, N. A., Candy, I., Breeze, P., Armitage, S. J., Gasmi, N., Schwenninger, J. L., Peat, D., & Manning, K. (2022). Sedimentary and geomorphic evidence of Saharan megalakes: A synthesis. *Quaternary Science Reviews*, *276*, 107318. https://doi.org/10.1016/j.quascirev.2021.107318

Drake, N. A., Lem, R. E., Armitage, S. J., Breeze, P., Francke, J., El-Hawat, A. S., Salem, M. J., Hounslow, M. W., & White, K. (2018). Reconstructing palaeo-climate and hydrological fluctuations in the Fezzan Basin (southern Libya) since 130 ka: A catchment-based approach. *Quaternary Science Reviews*, *200*, 376–394. https://doi.org/10.1016/j.quascirev.2018.09.042

Durack, P. J., Taylor, K. E., Ames, S., Po-Chedley, S., & Mauzey, C. (2022). PCMDI AMIP SST and sea-ice boundary conditions version 1.1.7. https://doi.org/10.22033/ESGF/input4MIPs.16485

Enzel, Y., Quade, J., & Kushnir, Y. (2017). Response to Engel et al. (in press): Lakes or wetlands? A comment on "The middle Holocene climatic records from Arabia: Reassessing lacustrine environments, shift of ITCZ in Arabian Sea, and impacts of the southwest Indian and African monsoons" by Enzel et al. (2015). *Global and Planetary Change*, *148*, 268–271. https://doi.org/10.1016/j.gloplacha.2016.11.003

Giorgetta, M. A., Brokopf, R., Crueger, T., Esch, M., Fiedler, S., Helmert, J., Hohenegger, C., Kornblueh, L., Köhler, M., Manzini, E., Mauritsen, T., Nam, C., Raddatz, T., Rast, S., Reinert, D., Sakradzija, M., Schmidt, H., Schneck, R., Schnur, R., Silvers, L., Wan, H., Zängl, G., & Stevens, B. (2018). ICON-A, the Atmosphere Component of the ICON Earth System Model: I. Model Description. *Journal of Advances in Modeling Earth Systems*, *10*(7), 1613–1637. https://doi.org/10.1029/2017MS001242

Hagemann, S., & Duemenil, L. (1998). Documentation for the hydrological discharge model.

Hagemann, S., & Dümenil, L. (1997). A parametrization of the lateral waterflow for the global scale. *Climate Dynamics*, *14*(1), 17–31. https://doi.org/10.1007/s003820050205

Hagemann, S., & Gates, L. D. (2001). Validation of the hydrological cycle of ECMWF and NCEP reanalyses using the MPI hydrological discharge model. *Journal of Geophysical Research: Atmospheres*, *106*(D2), 1503–1510. https://doi.org/10.1029/2000JD900568

Hély, C., & Lézine, A.-M. (2014). Holocene changes in African vegetation: Tradeoff between climate and water availability. *Clim. Past*, *7*.

Hoelzmann, P., Jolly, D., Harrison, S. P., Laarif, F., Bonnefille, R., & Pachur, H.-J. (1998). Mid-Holocene land-surface conditions in northern Africa and the Arabian Peninsula: A data set for the analysis of biogeophysical feedbacks

in the climate system. *Global Biogeochemical Cycles*, *12*(1), 35–51. https://doi.org/10.1029/97GB02733

Holmes, J., & Hoelzmann, P. (2017). The Late Pleistocene-Holocene African Humid Period as Evident in Lakes. *Oxford Research Encyclopedia of Climate Science*. https://doi.org/10.1093/acrefore/9780190228620.013.531

Jungclaus, J. H., Fischer, N., Haak, H., Lohmann, K., Marotzke, J., Matei, D., Mikolajewicz, U., Notz, D., & von Storch, J. S. (2013). Characteristics of the ocean simulations in the Max Planck Institute Ocean Model (MPIOM) the ocean component of the MPI-Earth system model. *Journal of Advances in Modeling Earth Systems*, *5*(2), 422–446. https://doi.org/10.1002/jame.20023

Jungclaus, J., Mikolajewicz, U., Kapsch, M.-L., D'Agostino, R., Wieners, K.-H., Giorgetta, M., Reick, C., Esch, M., Bittner, M., Legutke, S., Schupfner, M., Wachsmann, F., Gayler, V., Haak, H., de Vrese, P., Raddatz, T., Mauritsen, T., von Storch, J.-S., Behrens, J., Brovkin, V., Claussen, M., Crueger, T., Fast, I., Fiedler, S., Hagemann, S., Hohenegger, C., Jahns, T., Kloster, S., Kinne, S., Lasslop, G., Kornblueh, L., Marotzke, J., Matei, D., Meraner, K., Modali, K., Müller, W., Nabel, J., Notz, D., Peters-von Gehlen, K., Pincus, R., Pohlmann, H., Pongratz, J., Rast, S., Schmidt, H., Schnur, R., Schulzweida, U., Six, K., Stevens, B., Voigt, A., & Roeckner, E. (2019). MPI-M MPI-ESM1.2-LR model output prepared for CMIP6 PMIP midHolocene. https://doi.org/10.22033/ESGF/CMIP6.6644

Kang, I. S., Park, J. I., & Singh, V. P. (1998). Effect of urbanization on runoff characteristics of the On-Cheon Stream watershed in Pusan, Korea. *Hydrological Processes*, *12*(2), 351–363. https://doi.org/10.1002/(SICI)1099-1085(199802)12:2<351::AID-HYP569>3.0.CO;2-O

Krinner, G., Lézine, A.-M., Braconnot, P., Sepulchre, P., Ramstein, G., Grenier, C., & Gouttevin, I. (2012). A reassessment of lake and wetland feedbacks on the North African Holocene climate. *Geophysical Research Letters*, *39*(7). https://doi.org/10.1029/2012GL050992

Lehner, B., & Grill, G. (2013). Global river hydrography and network routing: Baseline data and new approaches to study the world's large river systems. *Hydrological Processes*, *27*(15), 2171–2186. https://doi.org/10.1002/hyp.9740

Lézine, A.-M., Zheng, W., Braconnot, P., & Krinner, G. (2011a). Late Holocene plant and climate evolution at Lake Yoa, northern Chad: Pollen data and climate simulations. *Climate of the Past*, *7*(4), 1351–1362. https://doi.org/10.5194/cp-7-1351-2011

Lézine, A.-M. (2017). Vegetation at the Time of the African Humid Period. *Oxford Research Encyclopedia of Climate Science*. https://doi.org/10.1093/acrefore/9780190228620.013.530

Lézine, A.-M., Hély, C., Grenier, C., Braconnot, P., & Krinner, G. (2011b). Sahara and Sahel vulnerability to climate changes, lessons from Holocene hydrological data. *Quaternary Science Reviews*, *30*(21), 3001–3012. https://doi.org/10.1016/j.quascirev.2011.07.006

Messager, M., Lehner, B., Grill, G., Nedeva, I., & Schmitt, O. (2016). Estimating the volume and age of water stored in global lakes using a geo-statistical

approach. *Nature Communications*, *7*, 13603. https://doi.org/10.1038/ncomms13603

Olivry, J.-C., Chouret, A., Vuillaume, G., Lemoalle, J., & Bricquet, J.-P. (1996). *Hydrologie Du Lac Tchad* (Vol. 12). Orstom.

Pham-Duc, B., Sylvestre, F., Papa, F., Frappart, F., Bouchez, C., & Crétaux, J.-F. (2020). The Lake Chad hydrology under current climate change. *Scientific Reports*, *10*(1), 5498. https://doi.org/10.1038/s41598-020-62417-w

Quade, J., Dente, E., Armon, M., Dor, Y. B., Morin, E., Adam, O., & Enzel, Y. (2018). Megalakes in the Sahara? A Review. *Quaternary Research*, *90*(2), 253–275. https://doi.org/10.1017/qua.2018.46

Reick, C. H., Gayler, V., Goll, D., Hagemann, S., Heidkamp, M., Nabel, J. E. M. S., Raddatz, T., Roeckner, E., Schnur, R., & Wilkenskjeld, S. (2021). JSBACH 3 - The land component of the MPI Earth System Model: Documentation of version 3.2. https://doi.org/10.17617/2.3279802

Richter, I., & Tokinaga, H. (2020). An overview of the performance of CMIP6 models in the tropical Atlantic: Mean state, variability, and remote impacts. *Climate Dynamics*, *55*(9/10), 2579–2601. https://doi.org/10.1007/s00382-020-05409-w

Riddick, T., Brovkin, V., Hagemann, S., & Mikolajewicz, U. (2018). Dynamic hydrological discharge modelling for coupled climate model simulations of the last glacial cycle: The MPI-DynamicHD model version 3.0. *Geoscientific Model Development*, *11*(10), 4291–4316. https://doi.org/10.5194/gmd-11-4291-2018

Schneck, R., Gayler, V., Nabel, J. E. M. S., Raddatz, T., Reick, C. H., & Schnur, R. (2022). Assessment of JSBACHv4.30 as land component of ICON-ESM-V1 in comparison to its predecessor JSBACHv3.2 of MPI-ESM1.2. *Geoscientific Model Development Discussions*, 1–45. https://doi.org/10.5194/gmd-2022-74

Shanahan, T. M., McKay, N. P., Hughen, K. A., Overpeck, J. T., Otto-Bliesner, B., Heil, C. W., King, J., Scholz, C. A., & Peck, J. (2015). The time-transgressive termination of the African Humid Period. *Nature Geoscience*, *8*(2), 140–144. https://doi.org/10.1038/ngeo2329

Specht, N. F., Claussen, M., & Kleinen, T. (2022). Simulated range of mid-Holocene precipitation changes from extended lakes and wetlands over North Africa. *Climate of the Past*, *18*(5), 1035–1046. https://doi.org/10.5194/cp-18-1035-2022

Strickler, D. A. (1981). Contributions to the Question of a Velocity Formula and Roughness Data for Streams, Channels and Closed Pipelines, 112.

Vamborg, F. S. E., Brovkin, V., & Claussen, M. (2011). The effect of a dynamic background albedo scheme on Sahel/Sahara precipitation during the mid-Holocene. *Climate of the Past*, *7*(1), 117–131. https://doi.org/10.5194/cp-7-117-2011

Wieners, K.-H., Giorgetta, M., Jungclaus, J., Reick, C., Esch, M., Bittner, M., Legutke, S., Schupfner, M., Wachsmann, F., Gayler, V., Haak, H., de Vrese, P., Raddatz, T., Mauritsen, T., von Storch, J.-S., Behrens, J., Brovkin, V., Claussen, M., Crueger, T., Fast, I., Fiedler, S., Hagemann, S., Hohenegger, C., Jahns, T., Kloster, S., Kinne, S., Lasslop, G., Kornblueh, L., Marotzke, J., Matei, D., Meraner, K., Mikolajewicz, U., Modali, K., Müller, W., Nabel, J., Notz,

D., Peters-von Gehlen, K., Pincus, R., Pohlmann, H., Pongratz, J., Rast, S., Schmidt, H., Schnur, R., Schulzweida, U., Six, K., Stevens, B., Voigt, A., & Roeckner, E. (2019a). MPI-M MPI-ESM1.2-LR model output prepared for CMIP6 CMIP historical. https://doi.org/10.22033/ESGF/CMIP6.6595

Wieners, K.-H., Giorgetta, M., Jungclaus, J., Reick, C., Esch, M., Bittner, M., Legutke, S., Schupfner, M., Wachsmann, F., Gayler, V., Haak, H., de Vrese, P., Raddatz, T., Mauritsen, T., von Storch, J.-S., Behrens, J., Brovkin, V., Claussen, M., Crueger, T., Fast, I., Fiedler, S., Hagemann, S., Hohenegger, C., Jahns, T., Kloster, S., Kinne, S., Lasslop, G., Kornblueh, L., Marotzke, J., Matei, D., Meraner, K., Mikolajewicz, U., Modali, K., Müller, W., Nabel, J., Notz, D., Peters-von Gehlen, K., Pincus, R., Pohlmann, H., Pongratz, J., Rast, S., Schmidt, H., Schnur, R., Schulzweida, U., Six, K., Stevens, B., Voigt, A., & Roeckner, E. (2019b). MPI-M MPI-ESM1.2-LR model output prepared for CMIP6 CMIP piControl. https://doi.org/10.22033/ESGF/CMIP6.6675

Zhao, Y., Braconnot, P., Harrison, S. P., Yiou, P., & Marti, O. (2007). Simulated changes in the relationship between tropical ocean temperatures and the western African monsoon during the mid-Holocene. *Climate Dynamics*, *28*(5), 533–551. https://doi.org/10.1007/s00382-006-0196-7

EIDESSTATTLICHE VERSICHERUNG

DECLARATION ON OATH

Hiermit erkläre ich an Eides statt, dass ich die vorliegende Dissertationsschrift selbst verfasst und keine anderen als die angegebenen Quellen und Hilfsmittel benutzt habe.

I hereby declare upon oath that I have written the present dissertation independently and have not used further resources and aids than those stated.

Hamburg, den 4. April 2023

Nora Farina Specht